Norwegian University
of Life Sciences

Master's Thesis 2023 60 ECTS
Faculty of Biosciences

Supercooling as an Alternative to Chemical Cryopreservation and Implications for Nuclear bodies

Magnus Barnholt Skulberg
M.Sc. Genome Science

Abstract

Most of the assays used today to study the genome and its physical topography, cannot identify the spatiotemporal genomic regions associated with the majority of different nuclear bodies. This is because the experimental conditions commonly used in these assays alter the chemical or physical environment around the genome and influence the closely linked and sensitive structure of nuclear bodies. This thesis explores whether supercooling without ice formation could preserve the structural integrity of isolated nuclei from Atlantic salmon (*Salmo salar*) hepatocytes, and a nuclear body contained within them, the nucleolus. The findings reported in this thesis suggests that supercooling can be used to store high-quality nuclei without additional cryoprotectants down to −15.3°C, with unnoticeable deterioration after >2 weeks storage. Several other observations during this work could form the basis for new scientific enquiries. The most notable being the possible observation of a supercooling-induced transition of nucleoli from an environmental sensitive structure to a largely insensitive structure. If the supercooling-induced effect, which needs to be confirmed in further studies, represent a general phenomenon for structures enriched in intrinsically disordered proteins, this would likely have implications for the study of other nuclear bodies.

Sammendrag

De fleste analyser som benyttes i dag for å studere genomet og dets romlige organisering er ikke i stand til å identifisere genomiske områder som er midlertidig forbundet med en cellekjernes kjernelegemer i rom og tid. Dette skyldes at de eksperimentelle forholdene som blir brukt endrer det kjemiske eller fysiske miljøet i eller rundt genomet og påvirker den nært forbundne og følsomme strukturen til kjernelegemene. Denne avhandlingen undersøker om dyp underkjøling uten isdannelse kan bevare den strukturelle integriteten til isolerte hepatocytt-cellekjerner fra atlanterhavslaks (*Salmo salar*), og et kjernelegeme til stede i dem kalt nukleolus. Funnene rapportert i denne avhandlingen antyder at dyp underkjøling kan brukes til å lagre cellekjerner av høy kvalitet uten ekstra kryobeskyttelse ned til −15.3°C, uten observerbar forringelse etter >2 ukers lagring. Flere andre observasjoner gjort i forbindelse med dette arbeidet kan danne grunnlaget for videre vitenskapelige undersøkelser. Av dem er det verdt å bemerke en mulig observasjon av en underkjøling-fremkalt overgang for nukleolus, fra en miljøfølsom struktur, til en struktur som reagerer lite på ytre påvirkning. Hvis denne underkjøling-fremkalte effekten, som må bekreftes i andre studier, representerer et generelt fenomen for strukturer beriket med proteiner uten veldefinert struktur, vil dette trolig ha implikasjoner for studiet av også andre kjernelegemer.

Table of Contents

LIST OF ABBREVIATIONS

RNA = ribonucleic acids

DNA = deoxyribonucleic acid

IDP = intrinsically disordered protein

IDR = intrinsically disordered region

LCD = low-complexity domain

SE = super-enhancer

TF = transcription factor

LLPS = liquid-liquid phase separation

MLO = membraneless organelle

PML = promyelocytic leukemia

pI = isoelectric point

FIB1 = fibrillarin

DFC = dense fibrillar component

NPM1 = nucleophosmin

GC = granular component region

NOR = nucleolar organizer region

rRNA = pre-ribosomal RNA

RRM = RNA-recognition motifs

RNP = ribonucleoprotein

ATP = adenosine triphosphate

PIC = protease inhibitor cOmplete

PFA = paraformaldehyde

Immuno-FISH = immunofluorescence microscopy with fluorescence *in situ* hybridization

ChIP = chromatin immunoprecipitation

SPRITE = split-pool recognition of interactions by tag extension

MAR = matrix attachment region

HRS = high-salt recovered sequence

IF = immunofluorescence

T_{cd} = cold-denaturation temperature

SA (HSA/BSA) = serum albumin, human/bovine

PTM = Post-translational modification

MPDS = mean predicted disorder score

MO (LMO/HMO) = mineral oil, light/heavy

CBB = coomassie brilliant blue G250

HRF = hydroxyl radical footprinting

SDS-PAGE = sodium dodecyl-sulfate polyacrylamide gel electrophoresis

BN-AGE = blue native agarose gel electrophoresis

βMe = β-mercaptoethanol

GSH = glutathione (reduced)

PVDF = polyvinylidene difluoride

1. INTRODUCTION AND LITERATURE REVIEW

1.1 NUCLEAR BODIES

1.1.1 Intrinsic disorder in biomolecular condensates

Cells utilizes different tools to regulate the rate and direction of biochemical reactions to meet physiological needs.

The nucleus contains thousands of different biomolecules (e.g., proteins and ribonucleic acids (RNAs)) important for the cell to function properly, and to do this efficiently they cannot execute their function everywhere. Many proteins have evolved independently folding, well-structured (ordered), domains giving them high-affinity for certain targets, enabling the formation of specific complexes with other proteins, deoxyribonucleic acid (DNA) or RNA. However, some proteins lack a well-defined three-dimensional structure (conformation) under physiological conditions, being intrinsically disordered proteins (IDPs) containing both ordered domains and intrinsically disordered regions (IDRs), less structured low-complexity domains (LCDs) and IDRs, or only IDRs. It has been shown that IDPs are not uniformly distributed in the cell, but significantly enriched in the nucleus, with main functions involving interactions with proteins and nucleic acids, such as activating transcription factor binding (Zhao et al., 2020).

Genes with important roles in development (Vicioso-Mantis et al., 2022), health and disease are often controlled by clusters of special gene regulatory elements called enhancers. Such clusters or “hubs” can form super-enhancers (SEs) by being available for the binding of special transcription factors (TFs), “master” TFs, with both a structured DNA-binding domain and an intrinsically disordered transcriptional activation domain (Sabari et al., 2018).

IDRs and LCDs can engage in low-affinity interactions that by themselves are weak, but also less specific, enabling associations between multiple simultaneously accessible binding sites (valency) on IDRs and LCDs in interacting molecules. Such multivalent and cooperative associations are strong enough to maintain protein- and RNA-factors concentrated to a higher concentration relative to their surrounding milieu, forming co-existing liquid sub-mixtures (phases) of varying densities. The disordered activation domains of the master TFs can recruit higher densities of IDR-enriched components of the transcriptional machinery by forming such phase-separated multimolecular assemblies (biomolecular condensates)(Sabari et al., 2018). Such condensates can potentially pull (Quail et al., 2021) enhancer elements into

proximity in the denser condensed phase forming SEs and ensure robust gene expression (Sabari et al., 2018; Vicioso-Mantis et al., 2022). A general SE is illustrated in **Figure 1.**

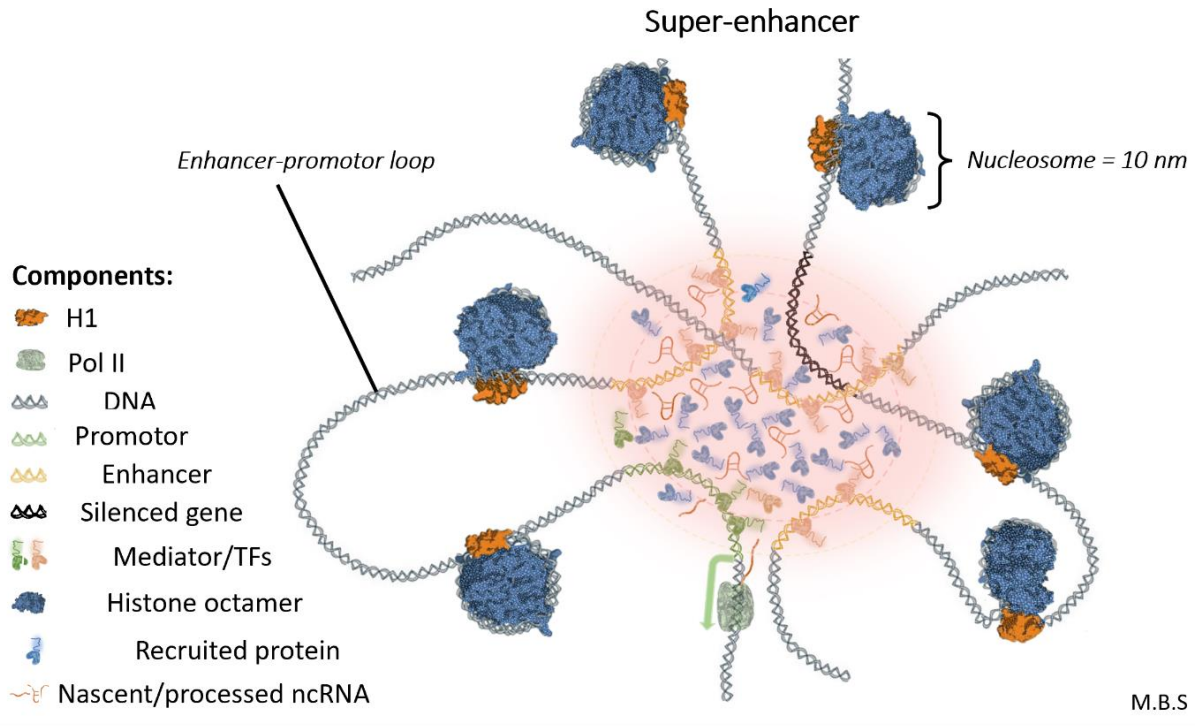

Figure 1 | Biomolecular condensate forming a super-enhancer hub. *Low compaction chromatin loops with distinctive regulatory elements are seen interacting via high local concentrations of intrinsically disordered proteins and RNA, forming a super-enhancer hub. Polymerase II (Pol II) produce RNA that favors heterotypic interactions and recruits proteins (e.g. RNA-binding and RNA processing proteins), into a transcriptional active condensate scaffolded by nascent and processed RNA. As shown in black, a gene can be recruited into the condensate which, by lacking specific factors for its transcription, would render it silenced.*

Besides functioning as a regulator for specific transcription, biomolecular condensates can help the cell utilize limited resources by compartmentalizing rare components, to achieve higher concentrations and reaction rates at specific genomic loci where they are most needed. This can drive higher levels of transcription (Sabari et al., 2018), in addition to activating various signaling processes (e.g., in differentiation; Vicioso-Mantis et al., 2022). Compartmentalization also reduces the need to have the same concentration of components everywhere, limiting the availability of different components where they are not needed, slowing or inhibiting damaging signal transduction/enzymatic processes (exemplified by the formation of stress granules; An et al., 2021).

In summary, the sequestration of different components recruited into a dense phase, whereas others distribute in the dilute phase (Deviri & Safran, 2021), can regulate the rate and direction of biochemical reactions both inside and outside biomolecular condensates. In

addition, it works in concert with the spatial distribution of the genetic information, and its level of availability, to meet physiological needs.

1.1.2 Nuclear bodies contribute to stable function

Random variations in the interactions between molecules involved in gene expression and translation can generate fluctuations in the abundance of expressed or translated molecules (stochasticity). This produces substantial biological noise and even in genetically identical cell populations the total concentration of certain protein- and RNA-types changes constantly (Deviri & Safran, 2021). The cells need to be robust against such noise to provide precise spatial and temporal functions.

In the nucleus, the spontaneous demixing of a solution into two or more phases known as liquid-liquid phase separation (LLPS) frequently occur around or near DNA to form complex biomolecular condensates - membraneless organelles (MLOs) - termed *nuclear bodies* (An et al., 2021). Different nuclear bodies located in a genome setting are visualized in **Figure 2**.

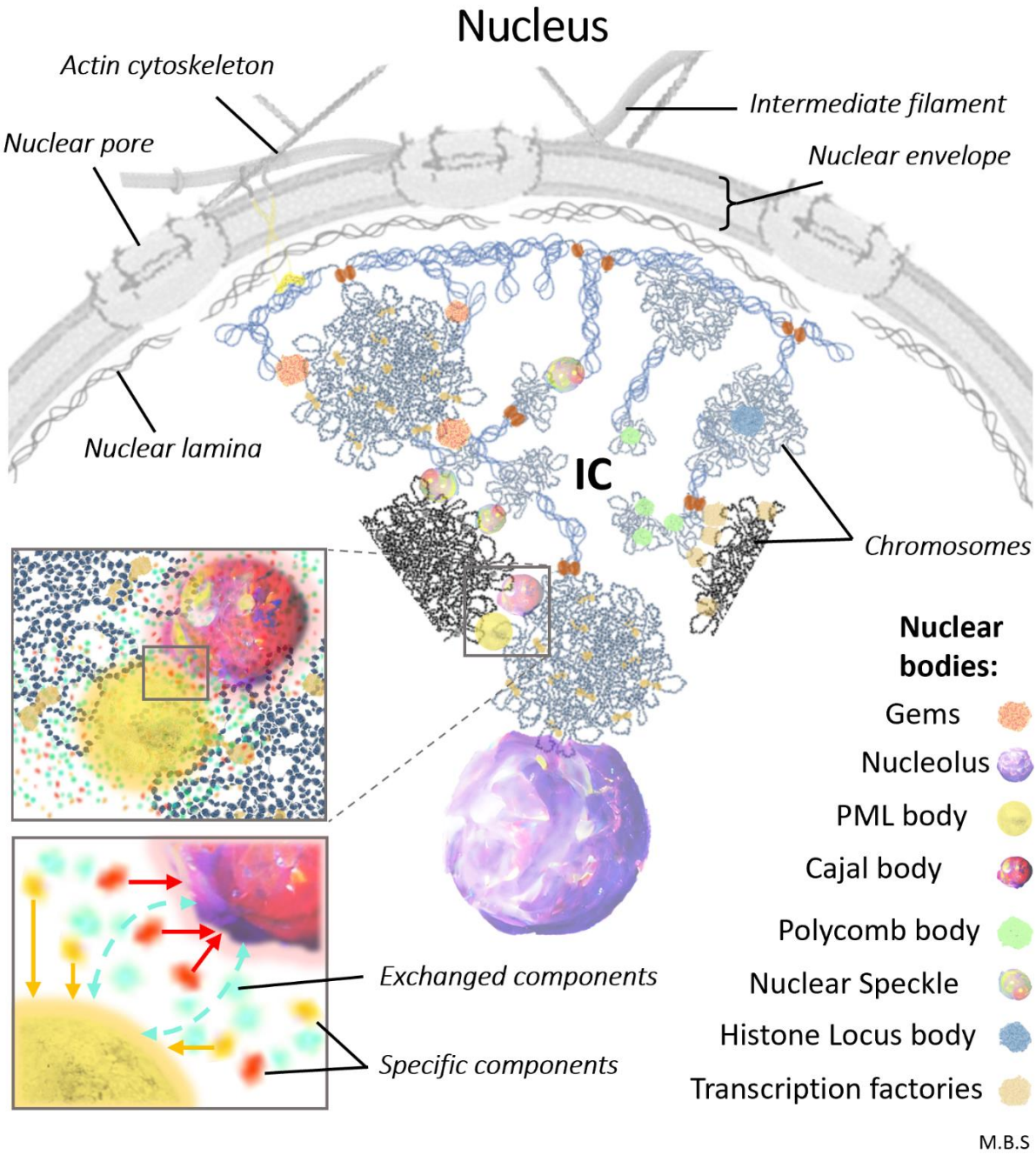

***Figure 2 | Nucleus with nuclear bodies bridging genomic regions. IC**=Interchromatin compartment (RNP-containing channels). Chromosomes can be seen intermingling (overlapping) at the border between different chromosomes (black/blue) via nuclear body-associated loop-structures. The genome is more compact and overlapping than visualized here.*

Nuclear bodies such as the Nucleolus, Cajal bodies, Promyelocytic leukemia (PML) bodies and Nuclear speckles shown in **Fig. 2** are composed of multiple RNA types and enriched in IDPs (Meng et al., 2015) involved in different biochemical reactions. Nuclear bodies can exchange components (**Fig. 2**) like in a network resulting in compositional overlap (Meng et al., 2015; An et al., 2021). However, compared to liquid droplets readily fusing when they

come into contact, the borders between even physically interacting nuclear bodies do not become blurred (Görisch et al., 2004; An et al., 2021). Indeed, not all components are shared (An et al., 2021) as shown in **Fig. 2**. Both the primary amino acid sequence (Miyagi et al., 2022) and conformation of the involved IDPs/RNAs (Garaizar et al., 2020; Paloni et al., 2021), influences chemical features and affinity for the other proteins or nucleic acids, deciding the recruitment of disordered proteins (Meng et al., 2015), RNA and DNA to nuclear bodies.

Many IDPs have sequences carrying charges of both signs (polyampholytes)(Chen et al., 2015), and the arrangement of charged amino acids (charge patterning) appears to be important for correct localization to the target nuclear body (Miyagi et al., 2022). An advantage of electrostatic interactions is that they do not require any specific three-dimensional (stereospecific) arrangement between interacting sites (although might benefit from it; Paloni et al., 2021) and only require a few amino acids. As long as they are not shielded by proximal opposite-charges (e.g., from scrambling; Miyagi et al., 2022), or clustered together, they are anticipated to occur between an IDR and many other cellular proteins (promiscuous). Why some components can be found in several nuclear bodies while some is more frequent in specific nuclear bodies can be attributed to a balance in interaction partners. A special condensation mechanism known as electrostatic complex coacervation (Henninger et al., 2020) can be used as a general example of the importance of such balance.

Coacervation can arise from favorable interactions occurring between molecules of different types (heterotypic interactions) with opposite charges. An example of this is between IDRs rich in positive charges that can bind to negatively charged RNA (RNA-binding proteins). Nascent RNAs produced from an activated promoter during the early steps of transcription-initiation can stimulate condensate formation this way by recruiting more TFs with IDRs that can facilitate LLPS via multivalent interaction sites (motifs). However, the promotional effects on this type of LLPS persist only up to a certain (balanced) concentration or threshold RNA-to-protein molar ratio, beyond which one type of charged species becomes dominant. Such dominance give rise to increasing electrostatic repulsion which disrupt the bonding networks. This is believed to occur during mammalian transcription considering that the duration of “bursts” of transcription from genes are typically shorter than the half-lives of mRNA and proteins within a condensate (Henninger et al., 2020). This would help avoid excessive transcription and serve as an “over-flow drainer”, as occasional extreme transcriptional responses from individual genes will be short-lived.

For nuclear bodies with multiple different interaction partners, the balance in interactions is more complex and follows thermodynamic laws which constrain the concentrations inside and outside these condensates (Deviri & Safran, 2021). This gives nuclear bodies a thermodynamic self-regulating ability (Henninger et al., 2020; An et al., 2021). If stress from various external and internal stimuli increase production of some LLPS-prone proteins (An et al., 2021), nuclear bodies can rapidly adjust their distribution of sizes and momentary numbers to keep the concentration outside of them insensitive to such fluctuations (Riback et al., 2020; Deviri & Safran, 2021), and also buffer other proteins prone to aggregate to reduce aggregation rates (Küffner et al., 2021) to levels that the cell can handle. This self-maintaining equilibrium of phase-separating molecules have several implications.

One implication is that molecules necessary for initiating condensates can be lost without dissolving the LLPS (exemplified by the long non-coding RNA Xist that initiates X-chromosome inactivation; Pandya-Jones et al., 2020). Another implication is related to the underlying chromatin. The formation and growth (Shin et al., 2018) of nuclear bodies in proximity to some target sites can be strongly dependent on the underlying sequence-tension in associated chromatin (Naughton et al., 2013; Shin et al., 2018; Quail et al., 2021). However, when formed, the dynamic self-regulating nature of nuclear bodies enables individual loci to rearrange within the structure without disrupting it, accommodating the constrained diffusion of chromatin (observed as nuclear bodies being mobile; Görisch et al., 2004) important for consistent transcription.

Another aspect of this is that nuclear bodies can be located near or at the border between regions that can share specific resources needed for their expression (co-regulated). This forms nuclear compartments where multiple loci both from the same chromosome (cis) and/or different chromosomes (trans) can converge for gene activation. One example is loci found in spatial association with each other, and with the PML body, sharing commonality among the transcription factor binding sites enriched in them (Anchel et al., 2016).

In summary, by compartmentalizing components in a space- (tension dependent) and time-(thermodynamic dependent) regulated manner in nuclear bodies, cells establish a buffering capacity against biological noise (and stress) to average stochastic gene expression over the lifetime of a cell (Deviri & Safran, 2021). Nuclear bodies contribute to stable functions by rapidly change size or spontaneously form or dissolve on altered ratios of specific functional

“building blocks” required in different nuclear bodies (An et al., 2021) (and/or changes in local tension).

1.1.3 Nuclear bodies contribute to adaptive function

Cells need plasticity to cope with changing environments (such as elevated carbon dioxide, salinity, temperature and physical obstacles (exercise) for Atlantic salmon; Byrne et al., 1972; Mota et al., 2020), being able to alter their expression profiles rapidly to respond to environmental stimuli and protect cells from damaging conditions.

An example is the cells in the Atlantic salmon (*Salmo salar*) liver (hepar)(Amin, 1991, p. 96, 112-113) that receive blood with varying amounts of nutrients based on their location in relation to the supplying blood vessels, and whether they are of the arterial (oxygen-rich) or venous (oxygen-poor) type, via the hepatic artery or portal vein, respectively. The liver cells (hepatocytes) making up most of the cells in the liver are polygonal and have a clear central nucleus with strongly colored chromatin along the nuclear membrane and a clearly visible nuclear body, the nucleolus (Amin, 1991, p. 96, 114-115). Normal hepatocytes have eosinophilic cytoplasm containing glycogen and fat, reflecting the liver cells’ function, which is to reabsorb nutrients from the intestine, as well as "purify" the blood by breaking down waste substances, toxins etc. The hepatocytes that are further away from the sinusoidal blood supply will receive blood with the least nutrition, and this also means that if the liver's blood supply is compromised, it first affects these hepatocytes. If, on the other hand, there is a toxic effect, the cells closest to the blood supply will be affected by the highest toxin concentration. Differences in the surrounding (extracellular) environment will therefore create a not insignificant fluctuation in functional burden during the life cycle of individual (single) cells, but also across the cell population (organ). In the case of toxins, one can imagine that it will require rapid and different gene expression at the single-cell level to counter such fluctuations in the extracellular environment to prevent deleterious effects.

It is consensus that only a few specific DNA regions are left accessible (at any given moment) to interact with transcription factors in some cell types and cell cycle stages, to influence the transcriptional profiles, while most of the genome is tightly wound into nucleosomes. Large changes in transcriptional output are often reflected by broad changes in the accessibility (i.e. the positioning and density of nucleosomes) of several loci in the surrounding chromatin, which is assumed to be mediated by the change in some transcription factor activity (although not always; Kiani et al., 2022). However, sometimes cells might need to respond to fast

physical cues directly (biophysical pathways) or converted into biochemical signals (mechanotransduction pathways), quicker than histone modifications can alter accessibility (Roy et al., 2018; Stephens et al., 2019; Nava et al., 2020), to change transcription (Deviri & Safran, 2021).

Considering the surprisingly similar accessibility between euchromatin and heterochromatin (Mansisidor & Risca, 2022), reports of active genes located in compact regions, with inactive genes located in open regions (Naughton et al., 2013) and promoter accessibility observed also in inactive genes, this suggest that many small enzymes can access their binding sites on DNA unaffected by accessibility. Nevertheless, a system in which enhancer-promoter contacts are in more or less static configurations and it is mainly the accessibility status and/or factor activity that changes, would not be able to respond sufficiently quickly to some external stimuli to prevent deleterious effects due to long assemble or disassemble time.

In comparison, the dynamic nature of nuclear bodies enables them to respond sufficiently rapid (from seconds to minutes; Henninger et al., 2020) to physiochemically activated mechanotransduction or biophysical pathways, by providing buffering (Deviri & Safran, 2021), disassemble or exchange of components (An et al., 2021; Meng et al., 2015) and thus provide a quicker regulation to alter expression than changes in accessibility. By being adaptive (plastic) to changes in the environment, this spatiotemporal regulation contributes to functional equivalence among cells independent of functional load in a tissue, such as liver, providing stable phenotypes.

1.2 FACTORS INFLUENCING NUCLEAR BODIES

Several environmental factors including solvent ion-composition, pH, crowding, molarity and other abundant cellular metabolites are critical for the *in situ* integrity of dynamic nuclear bodies and needs to be considered when investigating them.

The sequences of IDPs remain particularly soluble in very polar environments (Riback et al., 2017) such as the nucleus, with large numbers of charges from DNA and to a lesser extent counterions (Sasmal et al., 2013). This can be attributed to the abundance of highly soluble (polar) residues (Nomoto et al., 2021) and the scarcity of aromatic and hydrophobic (nonpolar) residues (Zhao & Kurgan, 2022). In other words, a high water preference over other amino acids and aromatic rings.

When reducing the net charge and increasing hydrophobicity to be more similar to ordered proteins, IDPs still resist a folded structure, instead maintaining more expanded states in water compared to ordered proteins (Riback et al., 2017). This is an important feature of IDPs as the extended IDRs can establish a larger density of molecular connections within a condensed liquid phase, while the more compact and structured globular states (such as after a disorder-to-order transition; Garaizar et al., 2020) limit the valency and thus hinders LLPS. Thus, the number of inter-molecular contacts (liquid-network connectivity) that an IDR can establish to stabilize the condensed liquid phase is directly regulated by the conformational ensemble (Garaizar et al., 2020).

IDRs disfavor the stable (native) intrachain interactions common for globular proteins, and instead favors transient (nonnative) interactions (Chen et al., 2015), allowing IDPs to exhibit dynamic ensembles of interconverting conformations (Zhao et al., 2020). This means that a specific IDP can exhibit both the extended and cooperatively folded states simultaneously, involving both cooperative folding and unfolding events (Kurzbach et al., 2013). While it is the primary amino acid sequence of IDPs that makes certain conformations possible (Garaizar et al., 2020), the physical-chemical characteristics of their surroundings determines if the conformational ensemble remain highly expanded in water, or collapses like structured proteins (Riback et al., 2017).

In other words, as IDPs expose a greater area of their sequence to the surrounding solution, all residues in IDRs are to some extent solvent exposed (Moses et al., 2020). This makes IDR ensembles carry an inherent, sequence-encoded sensitivity to their chemical environment, which could in turn influence their chemical features and conformations, changing their affinity for the other proteins or nucleic acids important for LLPS.

1.2.1 Solvent ion-compostion

Charged residues are among the highly soluble residues enriched in IDPs (Tedeschi et al., 2017). This enrichment makes nuclear bodies extremely susceptible to changes in ion concentrations, as ions can screen charge attraction between protein residues or nucleic acids (Mitrea et al., 2018), reducing multivalency important for initiating LLPS and maintaining condensates.

The intracellular chemical environment can fluctuate in response to extracellular cues, such as changes in extracellular blood plasma electrolytic concentrations. Exemplified for Atlantic

salmon, this can arise following different exposures such as elevated carbon dioxide, salinity, temperature and exercise (Byrne et al., 1972; Mota et al., 2020). Such physiochemical changes can act upon the nuclear envelope via internal macromolecular structures (mechanotransduction pathways) used by the cells to "sense" their environment (e.g., cytoskeleton; Engler et al., 2006; via SUN dimer/Nesprin; Hoffman et al., 2020). This can result in transient calcium influx (via activation of various mechanotransduction-activated ion channels from endoplasmic reticulum; Nava et al., 2020) and has been shown to change nuclear morphology resulting in genome reorganization (Stephens et al., 2019) and change in gene expression (Hoffman et al., 2020). Although only trace amounts of calcium have been reported in the nucleus (Nolin et al., 2013), because calcium is a very effective charge shielder (exemplified for chromatin; Phengchat et al., 2016) one must emphasize that such fluctuations can have potentially large effects on proteins relying on charge in their interactions. This includes IDPs targeting nuclear bodies via charge patterning (Miyagi et al., 2022) or driving LLPS with RNA (Henninger et al., 2020). This means that the ion-composition of the solvent needs to be considered as a potential influence on nuclear bodies.

1.2.2 pH

The isoelectric point (pI) distribution of human cellular proteins localized in the same subcellular compartment, are strongly correlated with the local pH, with a large overweight of proteins at either side of this value in the nucleus (Kurotani et al., 2019). It is thus possible that there is a close relationship between the local pH and the pI of IDPs to maintain solubility.

Net charge and charge pattern along the protein sequence determines the conformational dimension of IDP polyampholytes (Chen et al., 2015), and thus their solubility. The amphoteric polyelectrolytes are ionizable with both acid and base characteristics (Tedeschi et al., 2017). pH can thus influence their compactness (by enabling salt bridges and hydrogen bonding), as even small changes in the net charge per residues can lead to transitions from more expanded to collapsed conformations (Garaizar et al., 2020). Such conformational switching will influence the accommodation of multivalent interactions of elements within some IDRs or LCDs, and multiple weakly adhesive sequence elements in modular (structural) interaction domains also able to drive phase separation (Mitrea et al., 2018). This means that the pH needs to be considered as a potential influence on nuclear bodies.

1.2.3 Crowding

In addition to the direct influence on the primary amino acid sequence from the chemical environment, the presence of other macromolecules with high-volume occupancy can also influence the multivalency and conformational landscape. Large molecules that due to their size reduces the volume of accessible solvent is called crowding agents or “crowders”.

In the nucleus, the concentration of macromolecules differs between 75 mg/ml in the nucleoplasm and 400 mg/ml in condensed chromatin (Nolin et al., 2013), and many native macromolecules can serve as crowders. The general effects of crowding is best described with artificial molecules that does not usually have attraction for droplet-forming components and does not partition in the dense droplet phase. Such molecules preferentially partition in the dilute dispersed phase. If other macromolecular components, e.g., another protein or RNA, with only a mild attraction to the droplet phase are present, crowders can promote LLPS by displacing proteins into the droplet phase to strengthen bonding networks there (Hancock, 2004).

In addition, the dimensions of IDPs relatively extended conformations are also expected to be reduced in environments with a high concentration of other macromolecules. However, along the IDP chain the modulation of conformation is not uniform, but allows certain target-binding motifs to be selectively stabilized (Chen et al., 2015). Together with the exclusion from the space occupied by the crowding agents (excluded volume effect), this greatly enhances intramolecular associations and the rates of protein–protein, protein–DNA, and protein–RNA interactions (Riback et al., 2020). This allows interactions to proceed efficiently with fewer members of each species compared to dilute conditions. In other words, it increases the thermodynamic activity of each component.

It is estimated that the concentration of macromolecules within the nuclear body nucleolus is ~200 mg/mL, and that this crowding is important for IDR compaction and non-covalent inter-IDR interactions (Mitrea et al., 2018). The inheritably strong crowding in nuclear bodies suggests that IDPs involved in LLPS both tolerate the forces created from this strong crowding, but also relies on it, meaning that a change in crowding is likely to influence the maintenance and function of nuclear bodies *in vivo* (Hancock, 2004). For native macromolecules the effect can be complex but can be exemplified with the electrostatic complex coacervation (section 1.1.2; Henninger et al., 2020). For example, by modulating conformation like induce weakening of secondary structures and strengthening of tertiary

structures as for RNA (Leamy et al., 2017), this could remove favorable heterotypic interactions occurring specifically with unfolded RNA (exemplified in nucleoli; Riback et al., 2020) in coacervates.

In summary, the presence of native macromolecules in the droplet phase could serve to either disrupt or strengthen the bonding networks of IDPs/RNAs in nuclear bodies, if the macromolecule-IDP/RNA attraction is weaker/stronger than the IDP/RNA-IDP attraction (Mitrea et al., 2018). In other words, suppress or promote LLPS depending on the composition of nuclear bodies. In addition, a lack of crowding is likely to also have an effect, as it would reduce the physiological thermodynamic activity of different components. Together this means that the crowding (or lack of it) needs to be considered as a potential influence on nuclear bodies.

1.2.4 Specific example: Nucleoli

The effects of crowding and charge balance in a complex environment, and the sensitivity condensates have to such conditions, is exemplified with the nuclear body nucleoli.

In nucleoli three coexisting liquid phases form in a “core-shell” fashion depending on the independent ability of nucleolar proteins to undergo LLPS, such as Fibrillarin (FIB1) in the dense fibrillar component (DFC) needed for pre-ribosomal RNA (rRNA) processing, and Nucleophosmin (NPM1) in the surrounding granular component region (GC) where the ribosome assembly occurs (Feric et al., 2016).

In many cases nuclear bodies form around some genomic regions, in the case of nucleoli this is tandem rDNA gene repeats known as nucleolar organizer regions (NORs) (Feric et al., 2016; Quinodoz et al., 2018). These regions can adopt an underwound configuration (Naughton et al., 2013) because of the recruitment of a multi-protein complex RNA polymerase. This complex generates both positive (overwound) and negative (underwound) supercoils ahead of and behind it as it bidirectionally transcribe small short-lived noncoding RNAs. This creates a favorable environment for a stable initiation complex and condensate formation (Henninger et al., 2020; Vicioso-Mantis et al., 2022), like the small pre-nucleolar bodies eventually fusing to form the nucleolus.

After the initiation of transcription, polymerases and other proteins (e.g., topoisomerases and helicases) might collaborate to maintain the supercoiling, where the transmission of tension to adjacent gene regions might influence the supercoiling of surrounding regions, and their

tension-dependent incorporation into the condensate. This is likely an evolutionary constraint for clustering or separating genes with certain tension properties to avoid encapsuling untargeted genomic regions as condensates grow large (Naughton et al., 2013; Shin et al., 2018), which in the context of nucleoli could contribute to cluster NORs for efficient gene expression (and cancel transcription of other neighboring genes). Continuous transcription of rRNA transcripts within the Fibrillar center (FC) causes the need for a radial flux of rRNA through the DFC into the GC and finally into the nucleoplasm (Feric et al., 2016), as illustrated in **Figure 3**. Otherwise, the accumulation of RNA would dissolve the LLPSs (Henninger et al., 2020).

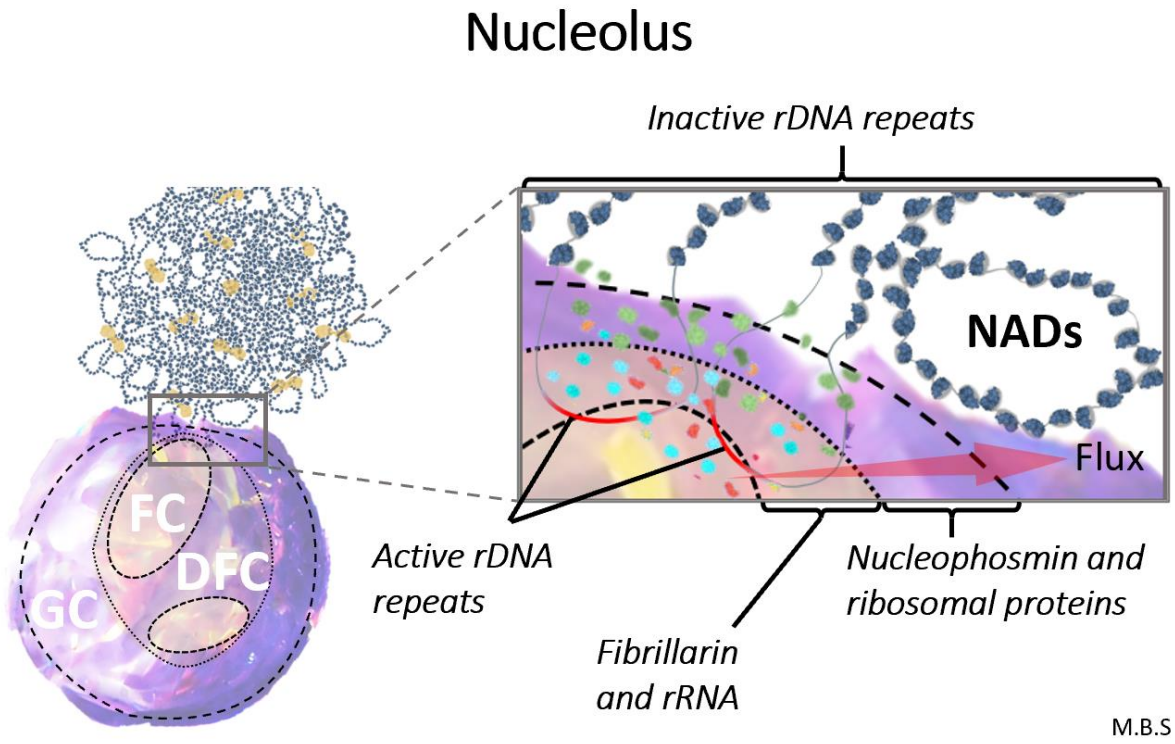

Figure 3 | Nucleoli and associated genomic regions. ***FC****=fibrillar center.* ***DFC****=dense fibrillar component.* ***GC****=Granular component.* ***NADs****=Nucleoli-associated domains. A flux can be seen radiating from the inner FC, through the middle DFC and the outer GC, into the surrounding nucleoplasm.*

The flux is achieved via the compositional features of the FIB1-rich DFC and NPM1-rich GC (**Fig. 3**) that tune this vectorial transport via sequential processing steps of rRNA into mature pre-ribosomal particles (Feric et al., 2016). rRNA transcripts can engage in more interactions with NPM1 and other scaffolding components in the GC (Mitrea et al., 2018), retaining them here while being processed and folded. The folding reduces electrostatic interactions (Leamy et al., 2017) and thus its retention in the GC layer and displaces it from this droplet phase into the next layer.

The interactions driving phase separation of rRNA with the nucleolar scaffold becomes progressively less energetically favorable in each layer (as components mature into fully assembled ribosomal subunits). This thermodynamically driven flux (Riback et al., 2020) effectively prevent premature exit of subunits out of the nucleolus before they are correctly folded, and also selectively exclude partial or fully assembled pre-ribosomal particles from entering and interfering (Feric et al., 2016). Both heterotypic and homotypic LLPS mechanisms contributes to this, with the NPM1-rich GC playing a potential buffering role during ribosomal subunit assembly (Mitrea et al., 2018).

As the accessibility of NPM1 for interactions with ribosomal proteins and RNA can be tuned by crowding (and/or slight changes in salt; Mitrea et al., 2018), changes in the physiological state can potentially disrupt this flux with detrimental effects, which underlines the importance of the sensitivity condensates have to such conditions, enabling them to rapidly dissolve.

1.2.5 Molarity

Both short and long-term exposure to external mechanical stimuli can change the volume of a cell and result in alterations in the availability of chromatin (Roy et al., 2018; Hoffman et al., 2020) and thus transcription factor localization and gene expression (Hoffman et al., 2020). This can have a large effect on the biomolecular condensates and nuclear bodies in light of what we know about their tension-sensitive mechanisms of formation (Naughton et al., 2013; Shin et al., 2018; Quail et al., 2021), mobility and co-localization (Görisch et al., 2004).

The concentration of osmotically active solutes in the plasma (osmolality) of Atlantic salmon can vary on scales (Byrne et al., 1972) where the mechanical stiffness of most cell membranes (excluding the rigid membranes of plants) are insignificant. This means that changes in extracellular osmolality can alter the cells volume similar to mechanical stimuli, with cells experiencing swelling when extracellular osmolality falls (hypo-osmotic) and shrinking when extracellular osmolality rises (hyper-osmotic) due to dehydration.

When nuclei expand, both reduced intracellular macromolecule concentration below a critical concentration (Mitrea et al., 2018; Henninger et al., 2020) and therefore reduced crowding (discussed previously), in addition to changes in chromatin tension (Naughton et al., 2013; Quail et al., 2021) is likely to dissolve nuclear bodies. Both nucleoli and PML bodies have been found to completely dissolve in hypo-osmotic nuclei following low-molarity conditions

(Hancock, 2004). This is not linked to reduced charge screening and consequent increased mutual repulsion of the negatively charged chromatin, because under the same hypo-osmotic conditions, both physical restrictions to swell, or restoring the normal intranuclear concentration of macromolecules by inert crowders, maintains nuclear bodies (Hancock, 2004).

In comparison, under high-molarity (hyper-osmotic) conditions, shrinkage of nuclei have been linked to permanent changes to chromatin condensation (Irianto et al., 2013), which can affect the spatial organization in the nucleus. This change in chromatin accessibility (not driven by histone rearrangement but biophysically) is likely to influence nuclear bodies as it may promote tension-dependent dissolving by trapping them in condensed regions. The increased intracellular macromolecule concentration from shrinkage could also lead to increased crowding conditions, where the conformation of components can change and effect multivalency (exemplified by RNA; Leamy et al., 2017), important for balancing phase separation. In addition, hyper-osmotic conditions can also change the hydration of macromolecules. Hydration is important for sequence recognition by proteins (Nolin et al., 2013), and IDPs often have one or more separate RNA-binding domains, such as RNA-recognition motifs (RRMs), giving them RNA-binding ability to form ribonucleoprotein (RNP) particles involved in nuclear bodies (An et al., 2021). It could therefore influence the balance in interaction partners important for LLPS. This means that molarity needs to be considered as a potential influence on nuclear bodies.

1.2.6 Abundant cellular metabolites

In living cells, the environment around condensate-forming proteins can expose them to high, millimolar concentrations of cellular metabolites. Given the promiscuous nature of many IDR interactions, that would make them susceptible to other highly abundant molecules *in vivo*, this can have potentially high influence on their function. Among the most highly abundant cellular metabolites (except nucleotides), adenosine triphosphate (ATP) is the only that has been found to inhibit RNA-driven LLPS by binding to RNA-recognition motifs (Zhou et al., 2021). This important energy source shares some of the basic features of nucleotides and thus its specific binding to these motifs (Zhou et al., 2021), however ATP has a lower binding affinity than nucleic acids, and high ATP concentrations are necessary to prevent phase separation in the presence of RNA (Song, 2021).

While many proteins have been shown to have the intrinsic ability to phase separate, only limited cellular MLOs have been identified in cells. It could be that cells maintain a high ATP concentration to inhibit the potentially pathological phase separation of IDR-rich proteins in the absence of nucleic acids. This means that too high ATP concentrations also needs to be avoided, in line with findings that high concentrations (6-10 mM) of ATP dissolves LLPS (Kang et al., 2018). The ionic effect of the triphosphate group is likely what might suppress phase separation, while controlled nucleotide production/consumption (turnover) might be required for disassembly of existing condensates (Begovich & Wilhelm 2020). Any depletion of ATP could therefore decrease both effects, effectively enhance phase separation and produce artefacts. Indeed, low concentrations around 1-2 mM significantly enhance LLPS (Kang et al., 2018). This means that ATP needs to be considered as a potential influence on nuclear bodies.

1.2.7 Concluding point

Different fast and slow mechanotransducive, physiochemical, or osmotic cues from the extracellular environment of cells can influence intracellular solvent conditions - environmental parameters - such as local ion and pH, and internal parameters such as metabolite concentrations (crowding), as well as charge patterning (valencies). When performing lab work aimed to study nuclear bodies it is important to be aware of the conditions used, as the factors mentioned above and the interplay between them (exemplified for nucleoli) can easily remodel the valency and interaction strength of disordered proteins and interaction partners. This can modulate the process of LLPS, and thereby influence nuclear bodies, perturbing them or introduce artefacts.

1.2.8 Implications: Nuclei isolation with an established lab-protocol

Optimally, a protocol for isolation of nuclei for examining chromatin 3D structure and/or nuclear bodies would satisfy three goals (1) the nuclei are anatomically identical to those of the whole cell, (2) the contents of the nuclei as they exist in the cell are all present in the isolated product, and (3) the isolated nuclei do not contain cytoplasmic constituents (Busch, 1967). In other words the *in vitro* conditions used during nuclei isolation must ensure the integrity of nuclear membranes and stability of nuclei throughout the isolation, if not severe effects can include rupture, leakage and/or clumping of nuclei, in addition to extensive debris making it difficult to evaluate nuclei.

Currently, to the best of my knowledge, no procedures used for the isolation of nuclei fulfill objective 1. However, electron microscopy and phase microscopy of cell cultures or smears, have established that the appearance of nucleoli can be used as a measure of the nuclei "nativeness" (Busch, 1967). When an optimized nuclei extraction is performed correctly, one can expect to observe one or a few nucleoli in several nuclei (depending on the cells ribosomal demands; Meng et al., 2015) under a single viewing pane, and either the absence or loss of nucleoli speaks against a satisfactory nuclear product from a given preparation (Busch, 1967).

In Atlantic salmon hepatocytes, nucleoli are visible as round spots with a dark-shaded color (Amin, p. 96, 114-115), possibly with a similar size range of 0.5-5 µm as in other eukaryotic cells (Lyon & Lamond, 2000). Because of the tight link between the nucleoplasm and cytosol *in vivo* (Nolin et al., 2013), reagents and buffers used during cell manipulation prior to nuclei isolation have the potential to change the conditions in the nucleus with potential effects on nuclear bodies like the nucleolus. An established lab protocol (AquaFaang, n.d.), adapted from the supplementing protocol of Corces et al., 2017, for hepatocyte nuclei isolation from Atlantic salmon can provide examples of possible unsuitable conditions.

pH

In the lab protocol, an organic buffer, Tris-HCl (pH 7.8), were used to stabilize the pH in the homogenization buffer to 7.4. While the pH in mammalian nuclei have been found to be 7.2, pH 7.4 is close to the average isoelectric points (pI) of proteins predicted to localize to the nucleus (7.54; Kurotani et al., 2019). Some proteins show significantly reduced solubility and even precipitation at their pI (Tedeschi et al., 2017). Thus, the number of proteins with a pI at this average value is low in the nucleus, with a large overweight of proteins at either side of this value with the largest fraction below 7 towards 6 (Kurotani et al., 2019). Evaluation of homogenization medium for the isolation of rat brain nuclei have previously shown that in the pH range 5.2-6.2, notable contamination of the nuclear suspension is observed (Lovtrup-rein & McEwen, 1966). However at pH 6.8-8.0, the gelation increase (related to leakage of DNA/RNA) explained by nuclear membranes showing a greater tendency to rupture at pH values above 6.8 (Lovtrup-rein & McEwen, 1966). As high solubility is a characteristic for IDPs (Riback et al., 2017) it is possible that pH 7.4 used in the lab protocol is sub-optimal for maintaining nuclear bodies and that a lower (more acidic) pH closer to the range between 6.2

and 6.8 could be tested (less clumping of brain nuclei observed in this range; Lovtrup-rein & McEwen, 1966).

Crowding

The mild detergent NP40 were used in the lab protocol to help weaken/lyse the cell membrane. NP40 contains bulky nonpolar head groups that can compromise the integrity of cell membranes by strongly bind lipids breaking lipid-interactions. The use of such mild detergents in nuclei isolation could result in highly mobile nuclear proteins to diffuse out of the nucleus (exemplified with HMGB1; Herrmann et al., 2017) reducing crowding. Although the head groups are not able to penetrate into water-soluble proteins such as the lamins, leaving these structures intact, it could target the nuclear membrane and potentially activate mechanotransductive responses (Stephens et al., 2019; Hoffman et al., 2020) with effects on nuclear bodies. Thus, omitting it could be tested.

Abundant cellular metabolites

When isolating nuclei with dilute homogenization buffers, one can expect that the replacement of cytoplasm with buffer removes much of the ATP pool, in addition to the possibility that ATP diffuses out from the nuclei when local perinuclear concentrations are no longer maintained (compared to whole cells) (Eckmann et al., 2019). This could enhance phase separation and give rise to artefactual appearance of nuclear bodies. However, it is also possible that nuclear bodies dissolves at low ATP concentrations as ATP depletion is observed to condense chromatin (Görisch et al., 2004) likely changing the internal spatial organization of chromatin, such as weak three-dimensional folding interactions (Mansisidor & Risca, 2022). This could have complex effects on the accessibility and dynamics of the chromatin environment around nuclear bodies sensitive to it (section 1.1.2). The addition of ATP could be tested.

Molarity

The relative high density of mammalian nuclei ($_{\varrho}$ >1.30 g/cm^3) (Graham, 1993), usually requires hyperosmotic solutions to generate banding densities for nuclei, when density-based centrifugation techniques is used to separate nuclei from debris. Sucrose gradients is one example, where the high concentration necessary for isolating nuclei leads to significant collapse of nuclei during their passage through the sucrose barrier, before they swell back when resuspended in an iso-osmotic medium at about 8.5% sucrose (0.25 M or 248

mOsmol/kg) (Graham, 1993), i.e., possess solute concentrations comparable to the outside of living (mammalian) cells.

The use of hyperosmotic sucrose gradients has been shown to result in loss of nuclear material and enzyme activity compared to iodinated density gradient media (media combined with iodine or a compound of iodine) at similar densities, such as metrizamide (Mathias & Wynter, 1973). Considering the permanent changes in the chromatin condensation observed for live cells (Irianto et al., 2013), it is likely that high concentration of sucrose or other hyperosmotic media can disturb the chromatin organization of nuclei if used as a separation solution, attributed to reduced hydration (of RNA, DNA and proteins; Nolin et al., 2013). As iodinated density gradient media such as metrizamide and Nycodenze, forming iso-osmotic solutions only at 37 and 30 w/v% with equivalent densities of $_{0}$= 1.192 and 1.159 g/cm^3, respectively (Ford et al., 1994), this means that these also requires hyperosmotic solutions to generate banding densities for nuclei.

The lab protocol utilizes discontinuous gradients containing another iodinated density gradient media instead called Iodixanol, with no osmotic activity itself, and can be adjusted to iso-osmoticity up to a density of 1.32 g/cm^3 (Ford et al., 1994). However, to maintain the solution close to iso-osmotic, and possibly stabilize the nuclear membranes, 0.32M of the organic agent sucrose were used in the lab protocol's homogenization buffer and subsequently mixed with Iodixanol supplied with 0.16M sucrose, before density centrifugation. It has been found that sucrose up to 400 mM show increasingly purer nuclear suspensions, i.e., with less cytoplasmic contamination and residues from damaged nuclei (Lovtrup-rein & McEwen, 1966). However, this is above the iso-osmotic concentration at 0.25M and could be adjusted to avoid potential detrimental effects on nuclear bodies.

Solvent ion-composition

In addition to a serine (and cysteine) protease inhibitor (serine hydrolase inactivator) called PMSF (Roche Diagnostics, 2004), a solution of a Protease Inhibitor cOmplete (PIC) EDTA-free Tablet were used in the lab protocol to inhibit a broader spectrum of serine, cysteine, and metalloproteases, as well as calpains, containing both irreversible and reversible protease inhibitors (Roche Diagnostics, 2004). In addition, 0.1mM EDTA was added, which is a metal chelator for many divalent cations such as magnesium, which are cofactors of enzymes such as DNAses and proteases. EDTA was likely added in the lab protocol due to the use of EDTA-free PIC (no other chelating agent present either), as the presence of divalent cations like

Ca^{2+}, Mg^{2+}, or Mn^{2+} could result in incomplete inhibition of metalloproteases. By chelating the co-factors of these enzymes, the activity of the enzyme decreases, as they will be unavailable for the reaction. Nevertheless, divalent cations from 5mM $CaCl_2$ and 3mM $Mg(Ac)_2$, 0.5mM spermine and 0.15mM spermidine (polyamines), were also used in the homogenization buffer. This is consistent with the paper by Graham (1993) pointing out that it is customary to include a number of ions, exemplified by the divalent cations Ca^{2+} and Mg^{2+} at concentrations of 1-5 mM and the monovalent K^+ at 10-25 mM in the homogenization medium to stabilize nuclei.

It could be that the available ion concentrations are reduced following EDTA (which has a high affinity for chelating Mg^{2+} ions) in line with the report that phosphate and Mg^{2+} ion contents higher than 1.5 mM cause precipitation of the nucleoplasm, while concentrations of 1.5 mM or less give satisfactory results (Lovtrup-rein & McEwen, 1966). However, the calcium levels are much higher than the trace amounts reported *in vivo* (Nolin et al., 2013). Omitting EDTA and reduce the addition of cations could be tested due to possible charge screening of nuclear chromatin (Phengchat et al., 2016) and envelope, to avoid aggregation of nuclei from leakage or lysis.

Synergistic/crossover effects

The combination of the individual effects from pH, crowding and molarity could induce synergistic effects (greater combined effect) or crossover effects (influence each other) in the lab protocol. It has been shown that HeLa cells contain at least 5 mM magnesium, 7 mM chloride, 70 mM potassium, 50 mM phosporus (mostly in nucleic acids and nucleotides), and 21 mM sulphur (mostly in glutathione (GSH) discussed later) in the nucleoplasm with similar values in the surrounding cytosol (Nolin et al., 2013). However, it seems like a slight acidic pH is more effective in preventing clumping of nuclei than an increased concentration of other elements (when looking at the synergistic effects) proposed by Lovtrup-rein & McEwen, 1966, reporting a final homogenization solution containing 320 mM sucrose, only 1 mM MgCl2 and 1 mM potassium phosphate, adjusted to pH 6.5. Considering the theory for solubility of proteins, with a tendency of nuclear proteins to prefer a slightly acidic pH below their pI values (Kurotani et al., 2019), it could be tested to see if the combined effect of pH and other compounds applies to Atlantic salmon cells.

1.3 LIMITATIONS WITH HOW NUCLEAR BODIES ARE INVESTIGATED TODAY

Many assays used today give only clues on what genomic loci might be converging on nuclear bodies as they use experimental conditions, such as chemical fixation or high salt concentrations, that disturb the *in vivo* organization and distribution of nuclear bodies.

1.3.1 Chemical fixation

Paraformaldehyde (PFA), a powder dissolved in hot water to become a formaldehyde solution, can non-selectively cross-link or 'fix' biomolecules in proximity, such as proteins and nucleic acids, to enable characterization of their interactions. It has been shown that PFA fails to capture DNA–protein interactions, such as the binding of transcription factors, which take place faster than the several minutes it takes the fixative agents to move through and immobilize the molecules in the cell (due to their small size limiting the fixation distance) (Irgen-Gioro et al., 2022). Chemical fixation may therefore not provide an instantaneous snapshot and may miss interactions that happen at or faster than the timescale of fixation, underrepresenting more transient or weaker contacts associated with nuclear bodies.

In addition, the reactivity and reaction rates of PFA can vary by orders of magnitude depending on amino acid sequences and tertiary structures of the protein substrates (Irgen-Gioro et al., 2022). This influences how quickly the proteins stop moving once exposed to the fixative, with some still diffusing 1 hour after fixation (Mansisidor & Risca, 2022). If the exchange rate of components within condensates is higher compared to the fixation rates, this can strongly alter LLPS with condensates increasing or decreasing in size, or even appear or disappear after fixation (Irgen-Gioro et al., 2022) depending on whether molecules outside or inside these structures are fixed first. In other words, chemical fixation can stimulate artifacts, with growing or multiplying condensates occurring when the internal proteins are fixed in place while the ones outside are still able to move freely and enter, but not leave. Conversely, shrinkage or disappearing of condensates occur when the internal proteins can move freely and leave, but not enter it. For the highly dynamic nuclear bodies where exchange rates are high, PFA may thus be ill-suited to preserve them (Irgen-Gioro et al., 2022).

1.3.2 Specific examples: Assays relying on crosslinking

Microscopy methods involving *in situ* imaging of a small number of DNA, RNA and proteins within the nucleus have shown that specific genomic regions can organize around nuclear bodies, exemplified with the rDNA genes (discussed in section 1.2.4) encoded on several

different chromosomes but localizing to the same nucleolus (Feric et al., 2016; Quinodoz et al., 2018). Such methods usually rely on *a priori* basis for selecting a candidate genomic locus of interest for i*n situ* labelling, such as with "immunofluorescence microscopy with fluorescence *in situ* hybridization" (Immuno-FISH), alternatively, prior knowledge of a constituent protein of the nuclear body being chemically cross-linked to DNA with PFA, followed by precipitation in a biochemical pulldown like with "Chromatin immunoprecipitation" (ChIP), or a combination (e.g. to study PML-bodies; Gialitakis et al., 2010). Novel associations between specific genes in nuclear bodies where the constituent protein is not known or dispersed throughout the nucleoplasm, cannot be discovered with these established methods (Anchel et al., 2016).

Current methods to study 3D structure of genomes without *a priori* knowledge, such as chromosome conformation capture techniques for genome-wide mapping (e.g., Hi-C), works by crosslinking nuclei with formaldehyde before DNA is digested with a restriction enzyme, leaving ends that can be modified to ligate to other ends in close proximity. In other words, ligating the ends of DNA regions that are able to frequently form a ligation junction due to a close spatial proximity in the nucleus, which can be mapped by sequencing (Quinodoz et al., 2018). In theory, promotors may encounter cooperative regulatory elements to initiate transcription several times during the life cycle of the cell via temporal nuclear bodies. Their interaction frequency and average spatial distance is then expected to remain stable at the cell population level, which can be captured by proximity-ligation methods applied to bulk cells. However, such methods fail to identify even known DNA regions associated with specific nuclear bodies, as they are too far apart due to the large, sometimes micrometer size, of the nuclear bodies (Quinodoz et al., 2018). This is illustrated in **Figure 4**.

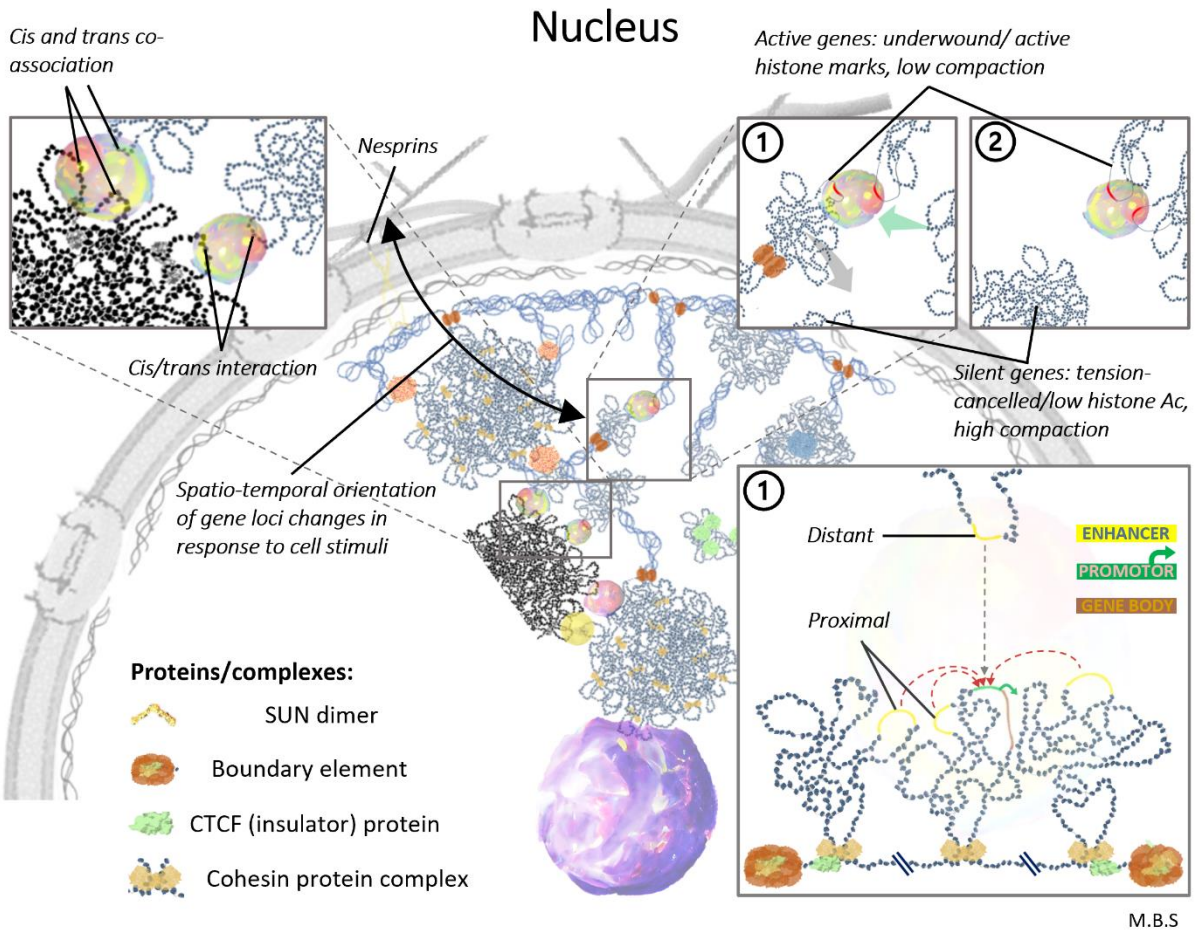

Figure 4 | Nucleus with DNA regions associated with nuclear bodies. *Multiple proximal or distant loci both from the same chromosome (cis) and/or different chromosomes (trans) can be seen converging in nuclear bodies for gene activation. While the formation of nuclear bodies in proximity to some target sites can be dependent on the underlying sequence-tension, once formed, loci can shift in and out of association without disrupting the nuclear body following mechanotransductive cell stimuli.*

As visualized in **Figure 4**, box 1, some genomic regions within an individual chromosome are in close proximity and can be captured by proximity-ligation methods. However, others are much further apart, and in addition, the regions can loose (or gain) association with a nuclear body upon cell stimuli regardless of the distance between the loci (**Fig. 4**, box 2).

Due to these limitations, it is challenging to generate comprehensive maps of genome structure that can address which DNA regions organize simultaneously around the same nuclear body, and how DNA is organized in the nucleus relative to multiple nuclear bodies (Quinodoz et al., 2018). A method known as “split-pool recognition of interactions by tag extension” (SPRITE) have overcome some of these limitations. By not relying only on proximity ligation, SPRITE have shown that inter-chromosomal interactions within nuclear bodies can shape the global genome organization in the nucleus (Quinodoz et al., 2018). This

is consistent with the phase separation of proteins, and tension-dependent formation of spatially distinct condensates, appearing to promote the maintenance of underwound domains (transcriptionally permissive) (Naughton et al., 2013) on their own (Quail et al., 2021), bringing some loci together by tethering them to the same condensate (**Fig. 4**, box 1 & 2).

Although SPRITE, as well as Hi-C and many other techniques are providing comprehensive models of genome organization, most suffer from relying on crosslinking of cells or nuclei using formaldehyde solutions. If condensates are able to pull (Quail et al., 2021) enhancers into proximity (as with SEs; Sabari et al., 2018; Vicioso-Mantis et al., 2022), their dissolving by chemical fixation is likely to revert this (losing proximity). As the numbers and positions of some nuclear bodies (where some loci can converge) constantly change to average stochastic gene expression (discussed in section 1.1.2), the relatively large three-dimensional distance between two potential chromatin loci, forming interaction partners, varies in individual cells by their dynamic movement (**Fig. 4**, box 1 → 2). In cases where low-frequency interactions rather than pervasive (relatively) are the ones that shape gene expression patterns, such as with fluctuations in the extracellular environment, the study of genomic regions temporarily converging at nuclear bodies become inheritable difficult with the assays commonly used today.

1.3.3 Permeabilization

Many assays involve permeabilizing cells, incubating nuclei with enzymes, and then halting the reactions after a specified amount of time that can vary widely between experiments (Mansisidor & Risca, 2022). Although it is well established that chromosomes and proteins are kept largely within the nuclei, because enzymes can move into the nuclei, it is equally likely that many small molecules of the nucleoplasm get released under such conditions (exemplified with the mild detergent NP40; Herrmann et al., 2017). This could potentially reduce crowding and disrupt native conformations and chromatin activities relying on them.

1.3.4 High salt concentrations

Many proteins experience a significant drop in solubility upon the addition of high concentrations of salt. Salt precipitation or “salting-out effect” is likely connected to strong ionic (electrostatic) interactions becoming negligible (Krainer et al., 2020) as they are screened by ions associating with opposite charges within the protein moiety, in addition to inherently weaker hydrophobic (and to a lesser extent nonionic) interactions becoming dominant (Krainer et al., 2020). The dominance of the hydrophobic interactions arise from

ions compressing the solvation layer around proteins, resulting in fewer water molecules available to hydrate the amino acid sequence/protein surface, i.e., most of the local/bulk water becomes associated with the salt ions as the salt is dissolved. Initial folding of ordered proteins bury many hydrophobic residues due to a thermodynamic benefit that prevents them from being exposed at the surface, known as the hydrophobic effect. High salt concentrations weaken the stabilization of such folded structures, in addition to making it thermodynamically favorable for proteins to shift folding, to engage in hydrophobic protein–protein interactions, to expose less surface due to limited hydration. In other words, high salt concentrations trigger unfolded structures more prone to aggregate and precipitate.

The less structured IDPs are naturally depleted of hydrophobic patches, which is linked to their high solubility and interconverting conformations in polar environments. Both Aspartate (-) and Lysine (+) are among the most disorder-promoting residues enriched in IDPs (Zhao & Kurgan, 2022) and even though the electrostatic repulsion between the charged residues is reduced with increasing salt, it is not able to stabilize expanded conformations enabling IDPs to aggregate by salt alone (up to 4M; Kurzback et al., 2013). A possible reason for why IDPs have proven to be less prone to aggregation, is because not only does IDPs have high solubility themselves (less hydrophobic attraction), but due to their lack of strict spatial constraints (likely due to disorder-promoting residues) they are hypothesized to act as solubility enhancers by sweeping the space around them, acting as “entropic bristles” that prevent large molecules to participate in aggregation (Tedeschi et al., 2017).

A large contribution to the high (51-60%) average disorder score of proteins in chromatin is the intrinsically disordered nature of the “tail” domains of histone proteins (Frege & Uversky, 2015), the major proteins involved in the hierarchical packaging of genomic DNA forming nucleosomes (fundamental repeating units of chromatin). In the presence of salt, these IDPs acquire a fold similar to renatured (i.e., refolded) unfolded globular proteins (Frege & Uversky, 2015). In other words, they are not expanded to engage in aggregation, however some DNA binding proteins with less disorder are. This discrepancy has been utilized to deplete chromatin of histones following treatment with 2M salt concentrations. An observation following this is that DNA strands loop out of (and possibly between) the many nuclear pore complexes left attached to the nuclear lamina (a supportive fibrous meshwork of lamins and other proteins that connects with the cytoskeleton underlying the inner nuclear membrane). This resembles a “halo” of DNA surrounding an insoluble skeletal framework (or “nuclear matrix”) of the remaining salt-aggregated proteins (Vogelstein et al., 1980).

An implication of depleting chromatin of nucleosomes is that it becomes negatively supercoiled (Vogelstein et al., 1980). This does not allow transmission of the tension associated with maintenance of phase separation (Naughton et al., 2013; Quail et al., 2021). Still, 20-40% of known components of the Cajal body, nuclear speckle, and the PML body, have been found retained in the nuclear matrix following different extraction procedures including high salt concentrations (Engelke et al., 2014). This is interesting considering that the average disorder score of Cajal body, nuclear speckle, and the PML body have been found to be 54%, 65%, and 37%, respectively (Frege & Uversky, 2015). In other words, the disorder content is not very different from the histones, not aggregating, indicating that some proteins might be contributing more to the average disorder score than others and that at least some less disordered proteins in these nuclear bodies can be expected to aggregate.

1.3.5 Specific examples: Assays relying on permeabilization and high-salt

A method known as HRS-seq (Baudement et al., 2018) have taken advantage of salt-induced precipitation by cutting around DNA attached to the salt-insolubilized nuclear matrix known as Matrix Attachment Regions (MARs)(Weber et al., 2003) illustrated in **Figure 5**, and sequence it, obtaining High-salt Recovered Sequences (HRS)(Braem et al., 2008) along with the cut DNA fragments (Baudement et al., 2018) from the “halo”.

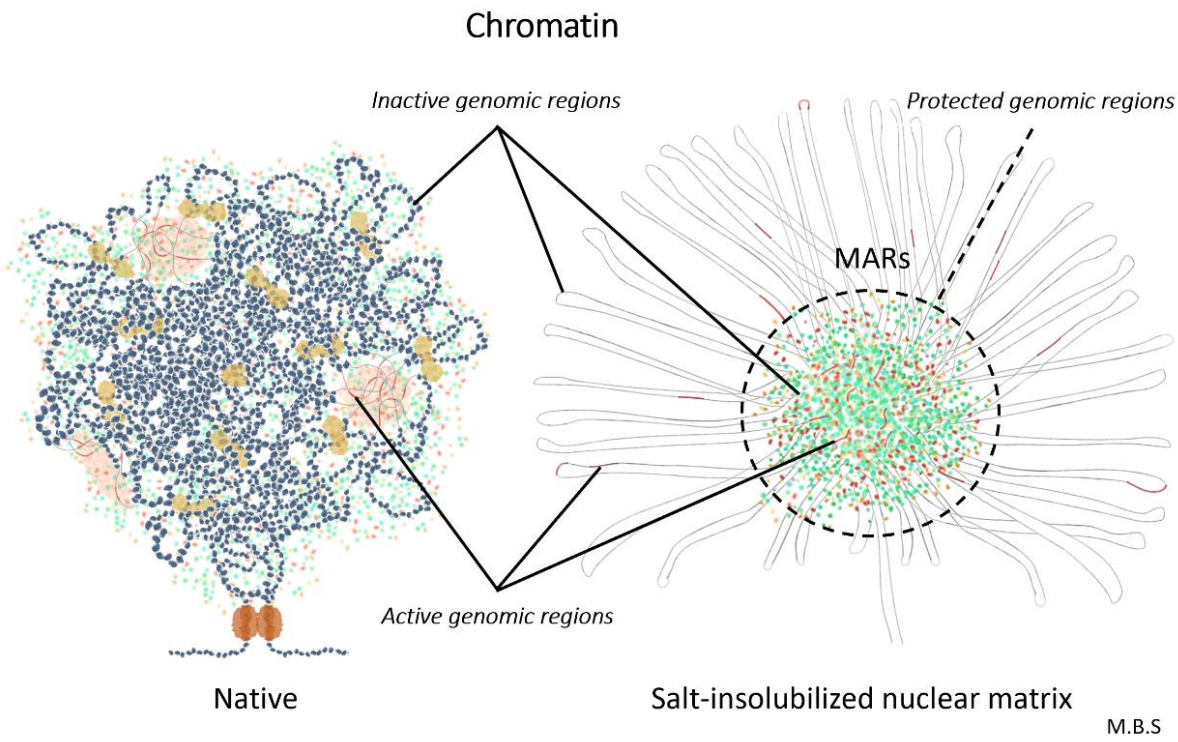

Figure 5 | Chromatin with nucleosomes and depleted of nucleosomes following high salt concentrations. ***MARs****= Matrix Attachment Regions. Compared to the more dispersed proteins seen around chromatin in its*

native state, precipitated proteins can be seen shielding some genomic regions following high salt concentrations, enabling enzymes to cut around them.

It was found that highly expressed genes were overrepresented (enriched) in the protected fraction (HRSs) compared to the cut fraction, and considering that the average disorder score of the RNA polymerase II transcription machinery have been found to be 27% (Frege & Uversky, 2015), it is likely that these sequences correspond to RNA polymerase II foci (Baudement et al., 2018) being aggregated near DNA or exhibit salt-resistant binding to it.

In addition, it was suggested that HRSs could represent genomic regions associated with nuclear bodies/large RNP complexes associated with RNA polymerase II (Baudement et al., 2018). The rationale for this was that immunofluorescence (IF) microscopy experiments on the nuclear halos indicated that the experimental conditions made proteins known to associate with nuclear bodies appear in close proximity to DNA, that in turn could be obtained as HRSs with the protocol. However, before imaging with immunofluorescence, or cutting of DNA with enzymes for sequencing, the nuclear halos were washed several times before staining/digestion (Baudement et al., 2018). Washing with such dilute buffers have been found to eliminate protein binding to histone-depleted chromatin, following high-salt treatment, for almost all nuclear proteins except lamina proteins (Lebkowski & Laemmli, 1982A) associated with both transcriptionally inactive, but also active genes (Kumaran & Spector, 2008). In addition, as only one specific marker protein was targeted in each IF experiment, able to exchange extensively between nuclear bodies (An et al., 2021), it can be argued if PML bodies as well as nuclear bodies of the Cajal body family (Histone Locus Bodies, gems, or Cajal bodies) are truly retained as reported under the experimental conditions.

One main concern for preparing nuclear matrices with high salt conditions is that the use of non-physiological extraction procedures might induce rearrangement and artificial formation of macromolecular complexes (Engelke et al., 2014), such as nonspecific protein precipitations that can adhere to chromatin. High salt conditions were used by Baudement et al., 2018, specifing that the sample must be very dilute to prevent digested “loop” DNA to falsely bind to the insoluble material in the solution. Baudement et al., 2018, filtered permeabilized nuclei in suspension were filtered before subjecting them directly to 2M NaCl (following Weber et al., 2003). This is expected to wash away less of the nuclear proteins after permeabilization, compared to dipping nuclei in increasingly higher salt concentrations to gradually deplete chromatin of histones and other proteins as in the procedure by Vogelstein et

al., 1980 for obtaining nuclear halos with proteins involved in DNA replication attached. It is therefore possible that proteins not binding to DNA *in vivo* is retained within the confinements of the permeabilized nuclei, and could become part of the insoluble material by salt precipitation *in vitro*, which means that DNA could become falsely attached as well.

Baudement et al., 2018 reported enrichment in HRSs for only the Histone Locus body-associated sequences, and only one spec from the IF microscopy experiments, for a protein known to localize to Histone Locus Bodies and Cajal bodies (Baudement et al., 2018), were observable although expected to be more numerous (Meng et al., 2015; Frege & Uversky, 2015). Considering the above points, it is possible that the experimental conditions have distorted at least most of the nuclear bodies.

1.3.6 Concluding point

In conclusion, chemical fixation used in ChiP, Hi-C and SPRITE, or high-salt treatment used in HRS-seq, alone or together with permeabilization, are examples of experimental conditions believed to disturb dynamically forming nuclear bodies. These assays are therefore to a certain degree incapable of easily extracting the temporarily genomic regions associated with nuclear bodies. An alternative approach is therefore necessary.

1.4 NON-BIOCHEMICAL ALTERNATIVE TO HOW NUCLEAR BODIES CAN BE INVESTIGATED

1.4.1. Main pitfall

Many approaches have been used to gain the knowledge we have on nuclear bodies today. They have been able to reveal a few sets of gene loci either in *trans*, or separated by large regions on the same chromosome (*cis*), that converge at a shared nuclear body enriched for their cognate regulatory factors, acting as a “gene hub” for their potential co-regulation (exemplified by Anchel et al., 2016). However, there is a knowledge gap from the current assays deployed today to study nuclear bodies, and alternative approaches that could provide more knowledge should be evaluated. It seems like the largest pitfall with current assays is that they disturb the LLPS that form nuclear bodies to the point where they disassemble, loosing information about DNA-protein interactions. One example is non-specific chemical fixation such as PFA, targeting the entire nuclei. PFA can only preserve the condensate structure if the molecules are fixed 'instantaneously' before they have a chance to leave or enter the condensate (Irgen-Giori et al., 2022). This raised the question about whether a non-

biochemical approach could be used, in which the native chemical environment remain unaltered.

1.4.2. Ordered and disordered proteins behave differently at high temperatures

Temperature can be controlled rapidly for a given space and the objects within, without the need for chemicals. Temperature studies on proteins have shown that at sufficiently high temperatures (e.g., 70ºC; Szyperski et al., 2006), ordered proteins can unfold, referred to as "heat denaturation". This exposes hydrophobic patches able to drive aggregation via hydrophobic interactions, similar to the salting-out effect (discussed in section 1.3.4).

Water molecules order themselves around protein molecules (hydrating them) depending on the hydrophilicity of the surface, where hydrophobic patches generate highly ordered water shells to accommodate the hydrophobicity, and consequently they have less entropy (i.e., freedom to arrange) than free water molecules. If these hydrophobic surfaces can coalesce, they expose less surface and thus exclude water, i.e., the ordered water molecules become disordered and return to the bulk solvent. This thermodynamic benefit is what drives intramolecular folding of primary amino acid sequences into proteins *in vivo*. In folding, the polypeptide chain also loses entropy (although less than the gain from freed water molecules) as it adopts a single conformation burying its hydrophobic side chains. In other words, there is a balance between the loss and gain that can be shifted. Because the thickness of the hydration shell (and thus the thermodynamic benefit) is related to the number of radial hydrogen bonds formed, which depends on the temperature of the solution (Li et al., 2008), we can understand that temperature can control this shift and the dimensions of proteins.

For the non-polar and hydrophobic amino acids whose hydration is normally unfavorable, i.e., the solvation entropy is unfavorable, the turnover in solvation free energy they exhibit (energy difference between solvated and unsolvated) thus become less unfavorable with increasing temperature. In contrast, the polar and charged residues, which IDPs are enriched in, show large variations in solvation free energy, decreasing with temperature (Wuttke et al., 2014). Although IDPs remain largely unstructured under all physiological conditions compared to other polypeptides, when comparing IDPs with varying average hydrophobicities, they all undergo compaction at increasingly higher temperatures, with more compaction the less hydrophobic (more hydrophilic) they are (Wuttke et al., 2014). For a chain with overall repulsive interactions (exemplified by ProTα; Wuttke et al., 2014), as the variation in configurational entropy for a reduction in chain dimensions is much smaller than that for

folding, the chain continues to collapse, otherwise one would expect a slight expansion for the hydrophilic ones at some point due to the contributions from electrostatic repulsion increasing with compaction.

Considering the paper by Li et al., 2008, this means that as the temperature increases, hydrogen bonds are broken around hydrophilic polar and charged residues as water molecules become further apart, and this limits the number of hydrating water molecules to such an extent that the chain collapses to reduce its surface (similar to the hydrophobic effect). In other words, only the excluded volume part of the interactions for IDPs remains important at high temperatures where the effect of temperature-dependent solvation free energy will be amplified.

1.4.3. Difference between heat denaturation and cold denaturation

Ordered proteins generally function optimally at the physiological temperature range in which they retain their native fold (and function), and the stability of the fold depends on a complex balance of mutually competing stabilizing and destabilizing forces. The thermodynamic stability of folded species of many proteins is only slightly higher than that of the corresponding unfolded species. This implicates that they are only marginally stable towards environmental factors such as extreme temperatures where they can experience reduced stability (Li et al., 2008). Similar to heat denaturation, proteins are expected (on thermodynamic grounds) to be able to cold denature, however the cold denaturation temperature (T_{cd}) for most proteins is well below the freezing point of aqueous solutions, and because unfolding kinetics is quite slow at such temperatures, freezing of the solvent happens faster and makes it difficult to study this phenomenon (Davidovic et al., 2009).

Previous studies have shown that without adding chemicals or applying high pressure, the use of capillary tubes makes it possible to maintain aqueous solutions at temperatures down to −15ºC, without freezing, for long periods of time (Szyperski et al., 2006). Water survives in a metastable state at subzero temperatures because of the absence of templates for heterogeneous ice nucleation, and the limited rate (high barrier) of homogeneous ice nucleation (Davidovic et al., 2009). The process to achieve this sub-zero non-frozen state is known as supercooling.

Although it is possible to keep some ordered proteins under supercooled conditions (−12ºC; Szyperski et al., 2006), the limiting temperature for the capillaries at −15°C prevents the study

of most native (wild type) proteins as they cold-denature at even lower temperatures. To observe cold denaturation, it is therefore necessary to destabilize ordered proteins through mutations (Szyperski et al., 2006) and/or addition of denaturants (e.g., urea; Davidovic et al., 2009), to raise the temperature of cold denaturation (Davidovic et al., 2009). In other words, the more destabilized the protein is, the higher is the cold denaturation temperature (easier to achieve).

A reconciling explanation for this is that some secondary structures remain largely intact in cold-denatured proteins (Davidovic et al., 2009) compared to heat denaturation. In other words, cold denaturation does not occur with full cooperativity, i.e., a two-state equilibrium between a single native conformation and a denatured state (Szyperski et al., 2006). In contrast to increasing temperatures where the number of hydrogen bonds decrease due to the thermal energy of water breaking them, resulting in a thin water shell, a thicker water shell may arise at low temperatures due to the enthalpy (internal energy) of the formation of hydrogen bonds exceeding the thermal energy of water (Li et al., 2008). An implication of this is that the repulsive interactions between nonpolar residues and water is weaker, decreasing the strength of hydrophobic interactions and increase hydration of nonpolar groups (Davidovic et al., 2009). At a sufficiently low temperature, exposing internal nonpolar sidechains to the solvent becomes thermodynamically favorable. This increases in magnitude at decreasing temperatures, accommodating the disruption of the protein's hydrophobic core as the polypeptide chain partly unfolds. Thus, above and below the cold denaturation temperature a shift occurs where it becomes thermodynamically favored for water to penetrate the hydrophobic core (Davidovic et al., 2009). In other words, an already destabilized structure would likely enable this disruption of the core at a higher temperature.

The reduced strength of hydrophobic interactions at low temperatures may reduce the likelihood to encounter aggregation, compared to heat denaturation, contributing to cold denaturation of destabilized ordered proteins being largely reversible (~93%; Szyperski et al., 2006) in contrast to heat denaturation, which is a large advantage for studying cold denaturation transitions of ordered proteins (Szyperski et al., 2006).

1.4.4. Ordered and disordered proteins behave differently at low temperatures

The point that cold denaturation does not occur with full cooperativity is important considering that IDPs usually exhibit both the extended and cooperatively folded states simultaneously, involving both cooperative folding and unfolding events (Kurzbach et al.,

2013). Due to the behavior as “entropic bristles” (Tedeschi et al., 2017), IDPs can avoid certain protein-protein associations that could otherwise lead to deleterious aggregation at physiological temperatures. In addition, relative to ordered proteins, IDPs can also avoid this at higher temperatures by a more collapsed state (Li et al., 2008; Wuttke et al., 2014). However, as cold denaturation does not follow the normal transitions, it could be that the conformational ensemble of IDPs become restricted at extremely low temperatures, and possibly to conformations able to aggregate.

Recapitulating the previous sections, we have that heat denaturation of ordered proteins is entropically driven, as it is mainly dictated by the increase in conformational entropy associated with protein unfolding. In contrast, cold denaturation of ordered proteins is enthalpically driven, because the mechanism of cold denaturation of ordered proteins is likely to involve temperature-dependent interactions of nonpolar groups with water. Neither of these driving forces apply to largely disordered proteins with already high freedom and lacking nonpolar groups. Instead, the solvation free energy becomes monotonically less favorable with increasing temperature (collapsing IDP conformations) for the normally favorable hydrated hydrophilic amino acids enriched in IDPs. Similarly, the solvent also plays a large role at low temperatures.

At very low temperatures, a shift occurs where it becomes thermodynamically favorable for more water molecules to become buried in protein cavities, than interacting with the external surface of the protein (Davidovic et al., 2009). One can from the thermodynamic and kinetic properties of water at low temperatures (Li et al., 2008) assume that the confinement (entrapment) within a limited space between two protein segments (similar to a cavity) in supercooled conditions contribute to a conformational preference for a slight collapse of structure. Considering an initially lower packing density (less dense) due to disorder from destabilization, it is interesting that a moderately destabilized protein has been found to exhibit a relatively compact structure at low temperatures like predicted above, compared to its native state (Davidovic et al., 2009).

This behavior can be attributed to several small cavities (exemplified by the heme cavity for apomyoglobin; Davidovic et al., 2009) still large enough to contain relative mobile hydrating water molecules, compared to internal water molecules trapped in even smaller cavities. Cold denaturation could cause these larger cavities to collapse, effectively reducing the solvent-exposed surface area of the protein.

At the same time, other water molecules could become internally trapped in the collapsed cavities or penetrate the structurally destabilized protein. The cold-denatured state of a moderately destabilized protein can thus be better described as solvent-penetrated, than unfolded (Davidovic et al., 2009). This can be understood as water molecules can bridge nearby polypeptide segments and become more strongly dynamically perturbed (rotational motion is slowed down) compared to most water molecules in the hydration layer of native proteins (Davidovic et al., 2009).

For a disordered protein containing similar regions where water molecules bridge polypeptide segments with relatively slow dynamics, strings and sheets of such bridging water with strong conformational preferences, interacting strongly (Davidovic et al., 2009) within the disordered protein, could provide extensive hydrogen bonding functioning as a glue that favors a collapsed state, i.e. a more compact cold-denatured state. One can imagine that this would reduce the "entropic bristle" behavior that helps IDPs avoid aggregation, in addition to weakening repulsion between charged surfaces, and instead favoring bridging water sheets.

This raise the question, while the ordered proteins remain incapable of aggregation following unfolding by cold denaturation, is it possible that the disordered proteins, collapsing at sufficiently low temperatures, acquire this ability instead as illustrated in **Figure 6**?

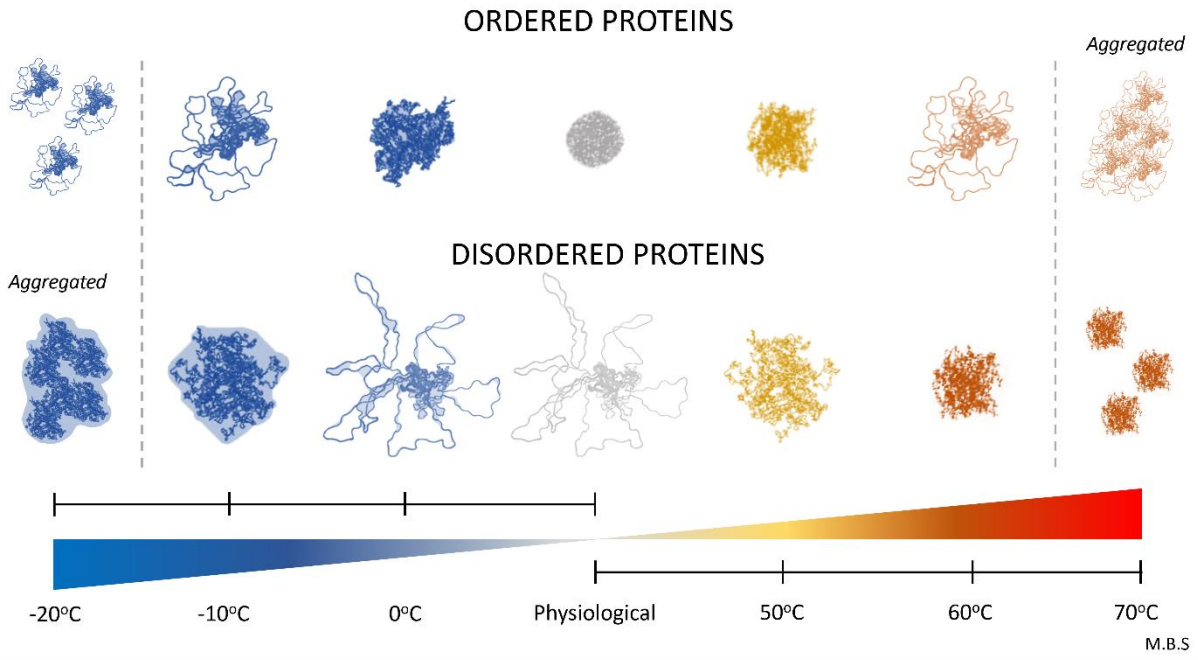

Figure 6 | Proteins on opposite scales of order behaving differently under very low or very high temperatures. ***ORDERED PROTEINS****: A temperature-dependent globule-to-coil transition via "molten" globule states can be seen for ordered proteins, being an irreversible process at high temperatures but not at low.* ***DISORDERED***

***PROTEINS**: A temperature-dependent extended(random coil)-to-compact coil transition can be seen for disordered proteins via a more open "crumpled" coil or more collapsed molten globule-like state, hypothesized to be an irreversible process at low temperatures. The difference between the crumpled coil state at low temperature compared to the molten globule-like state at high temperatures can be attributed to the formation of intra-chain water structures (shown in light-blue), where the intra-chain hydrogen bonding favors the collapsed state. Similar inter-chain water hydrogen bonding is hypothesized to drive aggregation at low temperatures.*

1.4.5. Specific example – Disordered albumin at low temperatures

Some biologically active proteins do not have a fully defined 3D structure, as they are hybrid proteins having a certain structure in only some of their parts, i.e., containing ordered domains in addition to IDRs. The human and bovine serum albumin (HSA/BSA) proteins serve as good examples of this (Litus et al., 2018). Although serum albumins (SAs) are predicted to be mostly ordered, when consensus per-residue disorder predictions for HSA is mapped onto its tertiary structure, it shows that HSA is largely dominated by either intrinsic disorder or high flexibility (Litus et al., 2018). This can be explained by the low tryptophan, methionine and isoleucine content in SAs, combined with the high content of charged amino acids, such as lysine, in agreement with these amino acids' roles in disordered regions (discussed in sections 1.2 & 1.3).

Due to the extended states of these disordered or flexible regions, residues are highly accessible for a range of modifying enzymes or reactions, providing "display sites" for residues amenable to modifications called post-translational modifications (PTMs). One such PTM is glycation, a non-enzymatic condensation reaction between nucleophilic groups (of the biomolecule and sugar), more specifically a carbonyl compound and an amino (-NH2) group, leading to the formation of a Schiff's base. Among the identified glycation modification sites in HSA, there is 24 arginine and 59 lysine residues, and all of these residues are characterized by rather high mean predicted disorder scores (MPDSs) (Litus et al., 2018) with many of them expected to be most frequently located in solvent exposed IDRs, i.e. accessible. However, sometimes residues with glycation rates faster than other glycation sites is predicted to have low accessibility although high MPDS values (e.g., Lys525; Litus et al., 2018). This can be explained as one effect from glycation is to "soften" the protein fold by reducing the α-helical content (often containing lysine), which increases the intrinsic flexibility of domains and secondary structure elements, which in turn could make certain parts more accessible.

The above point is important considering a paper by Öner & Groves, 1993, examining conditions needed to form human albumin microparticles by glutaraldehyde cross-linking.

The chemical fixative glutaraldehyde has previously been found to insolubilize proteins (Avrameas & Ternynck, 1969). This can be understood considering the high affinity of glutaraldehyde reported towards the charged amino acid lysine, and disorder-promoting glycine possessing a free amino group (Avrameas & Ternynck, 1969). As the amino groups of lysine residues are among the principal sites of glycation of proteins (in addition to the guanidine groups of arginine residues and the N-terminal amino group), it is likely that a "softening" of the protein fold (Litus et al., 2018) also occur following fixation with glutaraldehyde. This could contribute to the observed insolubilization by exposing additional hydrophobic sites on the protein surface.

Several methods involving suspensions and emulsions have been reported in the literature for the preparation of albumin microspheres. However the key factor that makes the approach by Öner & Groves, 1993, different from the others is the use of low temperatures (−15ºC) to form such particles very rapidly over a short time scale with low concentrations of cross-linking reagent. Starting from a 1w/w% HSA solution dripped into chilled (−15ºC) anhydrous (absolute) ethanol under stirring (200 rpm) with glutaraldehyde, Öner & Groves, 1993, report the formation of particles with mean particle diameters of 2 µm after 10 hours, of which only the first hour were in actively maintained supercooled conditions. In contrast, particles formed under similar mixing (200 rpm, 95% ethanol), but in room temperature and with a more concentrated HSA solution (10%), have been reported with a the mean particle diameter of just 500 nm after 12 hours (von Storp et al., 2012).

Both supercooling (Öner & Groves, 1993) and room temperature (von Storp et al., 2012) approaches to form albumin particles, likely involves precipitation of albumin as water surrounding the albumin molecules is removed by the anhydrous ethanol (referred to as a desolvation process where the desolvating agent is ethanol), i.e., the albumin sample is dried out in the ethanol solution. We can understand that hydrophobic interactions are strong drivers to increase the size of aggregates at moderate temperatures, however this effect is likely weakened at the supercooled temperatures (discussed in the previous sections) the solutions are kept in while adding the glutaraldehyde. It is thus tempting to ascribe the more rapid formation of larger albumin microspheres for Öner & Groves, 1993, by an initial supercooled-induced aggregation of relatively disordered albumin, acting as the nucleation site for further cross-linking. Interestingly, a response-surface diagram for the mean particle diameter of albumin microparticles by duration of the cross-linking reaction, show the most rapid increase in size at the 10 h mark (no measurements before this), slowing down between 10 and 45 h

(Öner & Groves, 1993), i.e., when the temperature has increased to the point where the hydrophobic effect becomes dominant again.

Cross-linking likely changes the molecular structure of albumin (Öner & Groves, 1993). This is consistent with the "softening" of the structure described by Litus et al., 2018, to reveal more Schiff's-base forming residues and additional hydrophobic-binding sites, to increase intra-molecular contacts at moderate temperatures. The same exposure of hydrophobic residues become thermodynamically favored at low temperatures (Davidovic et al., 2009). However, a partial unfolding of the structured domains would probably not reveal enough residues that could explain the difference between supercooling and room temperature, as most of the target residues for glutaraldehyde are already solvent exposed being in disordered regions. However, due to the large disorder content of albumin (Litus et al., 2018), it could be that the remaining hydrophilic sequences instead collapse the protein into a water-perturbed compact state during supercooling (Davidovic et al., 2009). This could form inter-chain water hydrogen bonding (**Fig. 6**), that could drive aggregation more rapidly than glutaraldehyde on its own.

1.4.6. Concluding point

In conclusion, the abovementioned papers provide some hints about the role that supercooling could play in the aggregation of disordered proteins. Due to the different responses of disordered and ordered proteins at such temperatures, with ordered proteins unable to irreversibly aggregate, if some proteins are found to aggregate at the most easily achieved supercooled conditions (−15ºC), it is likely disordered proteins with inheritably higher T_{CD}. This makes supercooling an interesting non-biochemical alternative worth to explore for the study of biomolecular condensates, such as nuclear bodies, naturally rich in disorder by their mechanism of formation (discussed in section 1.1).

1.5 GOALS OF THE THESIS

Most of the assays used today to study the genome and its physical topography (e.g., Hi-C, ChiP + Immuno-FISH, HRS-seq, etc.), cannot identify the spatiotemporal genomic regions associated with the majority of different nuclear bodies. Some mayor pitfalls are that they rely on formaldehyde fixation, chemical permeabilization, structure altering modifications like osmotic compression, and/or enzymatic cleavage, all of which alter the physical topography

of the genome and in turn the highly dynamic, tension- and crowding-sensitive nuclear bodies.

As described in the background theory presented above, there is some evidence pointing to supercooling having different effects on disordered proteins (enriched in nuclear bodies) compared to structured proteins. Supercooling is largely incapable of irreversibly aggregating structured proteins. Instead, supercooling is believed to aggregate disordered proteins, which is enriched in nuclear bodies. Based on this differential effect, this thesis seek to answer whether supercooling can avoid some of the most common pitfalls with current assays by answering two research questions: (1) does supercooling preserve structural integrity of nuclei?, and (2) does supercooling influence nuclear bodies?.

The first goal of this master project was to *establish supercooling in the lab and identify if the overall structure of the nucleus is influenced by supercooling*. A general change would be indicative of a non-specific effect similar to a chemical fixative. A part of this goal was isolation of high-quality nuclei from the species of interest in the lab, Atlantic salmon. High quality nuclei could also allow the observation of one nuclear body, the nucleolus, which can be used for the second goal to *establish conditions to evaluate the effect of supercooling on nuclear bodies*.

2 Materials and Methods

2.1 SAMPLES

Liver tissue collected from two commercial strain Atlantic salmon (*Salmo salar*), identified as J11 and J7, were made available to me for this thesis. Details regarding sample collection and storage is included in **Appendix A**. The whole sample J11 and half of the sample J7 were used for the initial testing and optimalization of the experimental protocol for nuclei isolation. The remaining half of J7 were used to perform the final nuclei isolation protocol (**Appendix D**), obtaining nuclei used in all downstream tests allowing direct comparison.

2.2 REAGENTS AND SOLUTIONS

Details about commercial reagents used directly (ready-to-use) are included in **Appendix B**.

The following stock solutions were prepared as described in **Appendix C**: 0.5M Adenosine 5′-triphosphate, 0.001M Calcium Chloride, 10% (w/v) Coomassie® Brilliant blue G 250,

0.5M Disodium Ethylene Diamine Tetra-Acetate, 0.5M Ethylene Glycol Tetra-Acetic Acid, 30mM Fe(II)-EDTA, 0.5M L-Glutathione, 50v/v% Glycerol, 2M Glycine, 0.5M Magnesium Chloride, 0.5M Magnesium Sulfate, 1M Potassium Chloride, 5M Potassium hydroxide, 0.5M Potassium phosphate, 5M Sodium Chloride, 2.5M Sucrose, 2M Tris base, 1M Tris-HCl pH 7.2, 1M Spermidine, 1M Spermine.

2.3 LABORATORY WORK

2.3.1 Isolate nuclei

Isolation of nuclei with high quality was necessary to evaluate the effects from supercooling on chromatin 3D structure.

Nuclei isolation was achieved using the protocol described in AquaFaang, n.d., with modifications to the homogenization buffer to account for possible effects on nuclear bodies (discussed in section 1.2.8). The modifications included a lower pH, the addition of Sodium and Potassium, the omitting of Spermine, Spermidine, EDTA, NP40, PMSF and β-mercaptoethanol, the changing of acetate to chloride and sulphate and Tris-HCl to HEPES, and the adjustment of sucrose, magnesium and calcium (see Results and Discussion). See **Appendix D** for a detailed description of the final protocol including all homogenization buffers/solutions and gradients tested.

Briefly, 50 mg liver tissue stored frozen at -80 ^{o}C were thawed on ice, in 2.5 ml of the homogenization buffer/solution (4^{o}C) to be tested, in a Dounce Homogenizer. Tissue was mechanically dissociated using 2-3 strokes with the large clearance pestle for initial sample reduction, and 2-4 strokes with the small 20.32 μm clearance pestle (Kimble Chase Life Science & Research Products, n.d.) to form the final homogenate. The homogenate was transferred and centrifuged in a 5 ml centrifugation tube to collect a nuclei pellet which was, after removing and discarding the supernatant, mixed to 1.2 ml with a given solution (4^{o}C) based on the density and gradient to be tested. The entire resuspension was loaded onto discontinuous gradients (4^{o}C) formed by 2 ml with a density at 1.30 g/ml or above and 1 ml with density in the range 1.24-1.30 g/ml, as exemplified in **Figure 7** for a given Iodixanol gradient tested (gradient 6 in **Appendix D**). The resuspension was centrifuged at 3220 RCF for 75 minutes at 4^{o}C. After centrifugation, the top layer was carefully aspirated and discarded, and between 700-900 μl of the middle-layer containing purified nuclei (Fig. 7 B)

were collected using a p1000 tip and transferred to a pre-chilled 2 ml LoBind Eppendorf tube and stored on ice until downstream processing.

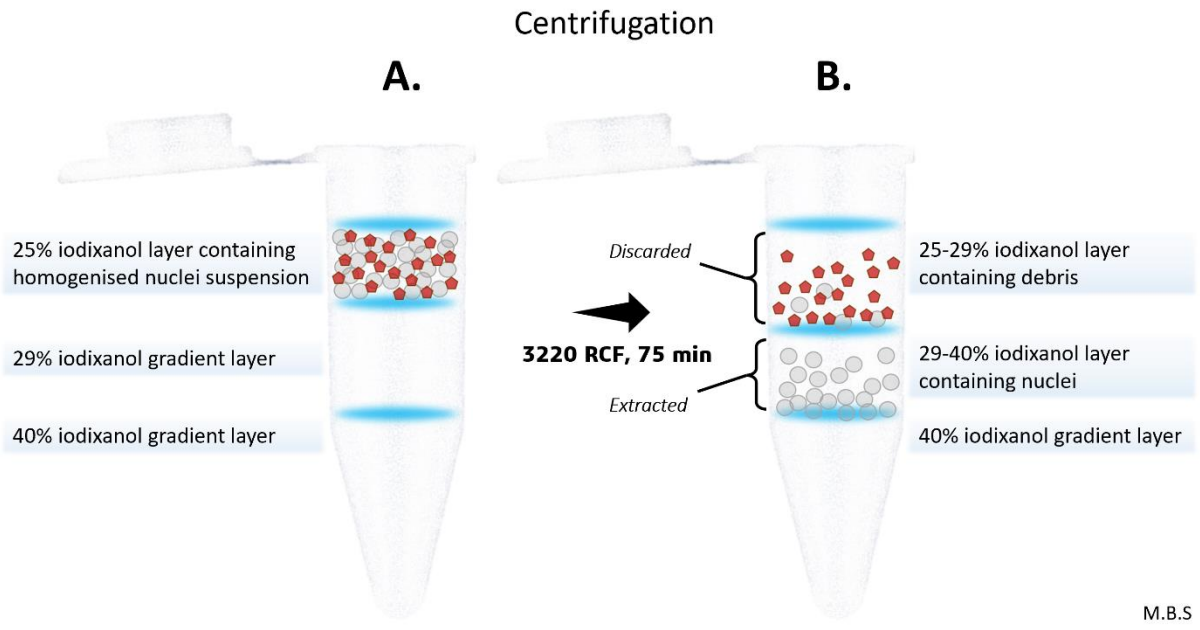

Figure 7 | Concept of gradient centrifugation to separate nuclei from remaining cell and tissue debris exemplified for gradient 6. **A.** *The tissue homogenate (nuclei and debris) can be seen in the 25% iodixanol layer in a 5 ml centrifugation tube before centrifugation.* **B.** *Nuclei can be seen separated from debris in the 29-40% layer after centrifugation. These purified nuclei are extracted to obtain a suspension of isolated nuclei.*

2.3.2 Quality, yield and precision assessment

Examining the integrity of the isolated nuclei and chromatin in addition to critical morphological features, was necessary to uncover underlying effects on quality from using different nuclei isolation conditions and effects from downstream treatments. In addition, determining the yield from nuclei isolations was necessary to evaluate the precision of the isolation protocol.

The quality and yield of the isolated nuclei was assessed subjectively by established microscopy techniques using a Thoma cell. A detailed description of the protocol and calculations of yield and precision are included in **Appendix E**.

Briefly, 10 µl of the nuclei suspension was collected per replicate assessment and transferred to a 0.2 ml PCR tube. The sample was diluted 1:1 volume ratio with Trypan blue staining dye, staining proteins, alternatively with either 1x Hoechst 33342 or 1x SYBR green, staining DNA, shielding the sample from light. Slightly less than 10 µl of the stained nuclei suspension was loaded onto each side of a Thoma cell. The slide was then placed under a

bright-field microscope (in a dark room if the fluorescent dyes were used). The etched grid of the Thoma cell was quickly located and the nuclei were inspected within 3-5 minutes after staining using 10×&20×/0.3 air objectives. When fluorescent dyes were used, the sample was only briefly subjected to full spectrum light, to locate the grid, before setting the correct position for the UV filter sets for SYBR green or Hoechst (**Appendix E**). Images were captured using an Axiocam 105 color, 60N-C 2/3¨ 0.5×, and analyzed later using the ZEN Imaging Software "ZEN 3.0 (blue edition)". To compensate for the subjectivity in manual nuclei counting (relying on individual assessments of whether a nucleus is inside or outside the counting grid), nuclei were counted as illustrated in **Figure 8**.

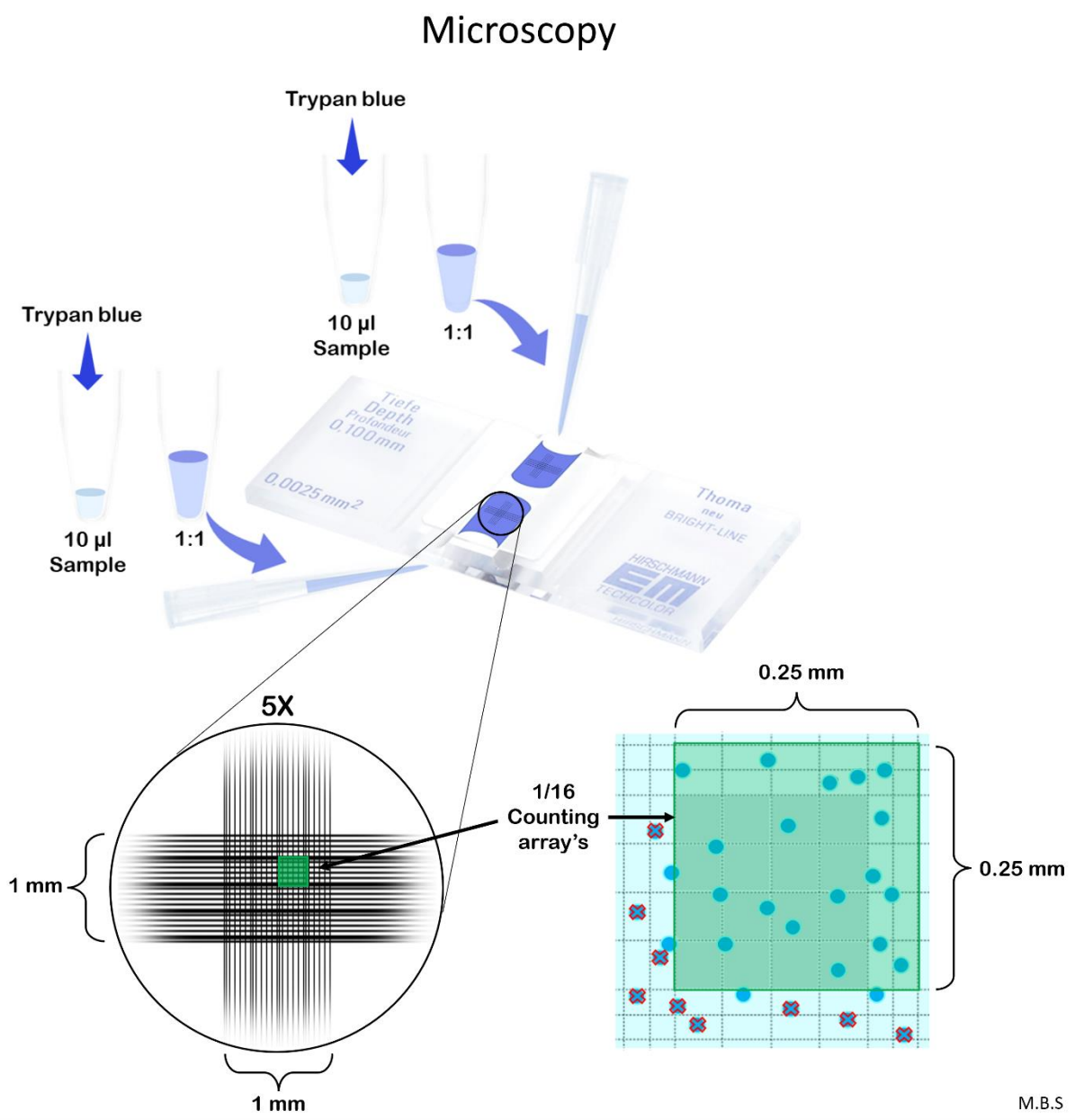

Figure 8 | The bright-field microscopy technique for counting Trypan blue stained nuclei. *The full grid etched in the Thoma cell contains a large central square of 1 mm^2, i.e., the counting area, which can most easily be located and seen in its entirety with the 10× objective (~5X shown). By switching the microscope to the 20× objective, each of the 16 medium squares that the large central square is divided into, can be seen in detail. All the nuclei within each of the 16 medium squares and those that are over the top and right sides (but not the bottom or left sides) of the square, even when they are partially out, were counted.*

Following the customer support article by 10x Genomics, n.d., and Busch, 1967, it was considered that nuclei with high quality would appear round and intact (preserved integrity) with well-defined edges under the bright-field microscope, in addition to containing a visible nucleolus, whereas nuclei of poor quality lose their intactness and begin to show evidence of membrane blebbing (indicating nuclear leakage). For most tests two independent nuclei isolations were performed with the same condition. Two separated subsamples of isolated nuclei were inspected before a conclusion about a specific sample's quality or yield was drawn to reduce the impact of subjectivity.

2.3.3 Supercooling

Supercooled conditions were necessary to test the effect of supercooling on preserving nuclei and nucleoli integrity.

Supercooled conditions were achieved during preliminary experimentation with the procedure in the paper by Huang et al., 2018 (see Results and Discussion).

Briefly, 200-250µl chilled Light Mineral Oil (LMO) were carefully layered on the surface of 550-1300µl nuclei suspensions in 2 ml LoBind Eppendorf tubes, avoiding trapping any air bubbles. The tubes were pre-cooled to 4-7ºC in a fridge for 30 minutes, before a quick 2 second spin down with a table centrifuge and placed on ice. The tubes were cooled slowly at 0.5 degree per minute to sub-zero temperatures (min: -15ºC, max -12ºC) in a self-built cooling chamber (see **Figure 9**) (see **Appendix L** for an alternative). The temperature was measured with a thermometer for laboratory freezers (measuring down to −50ºC with ± 0.1 ºC error) with the waterproof wired probe immersed in a tube with only LMO placed similarly as the samples (**Fig. 9 B**). After storage, the tubes with nuclei suspension were gently collected from supercooling and put on ice to stabilize. The light mineral oil layer was gently aspirated and discarded.

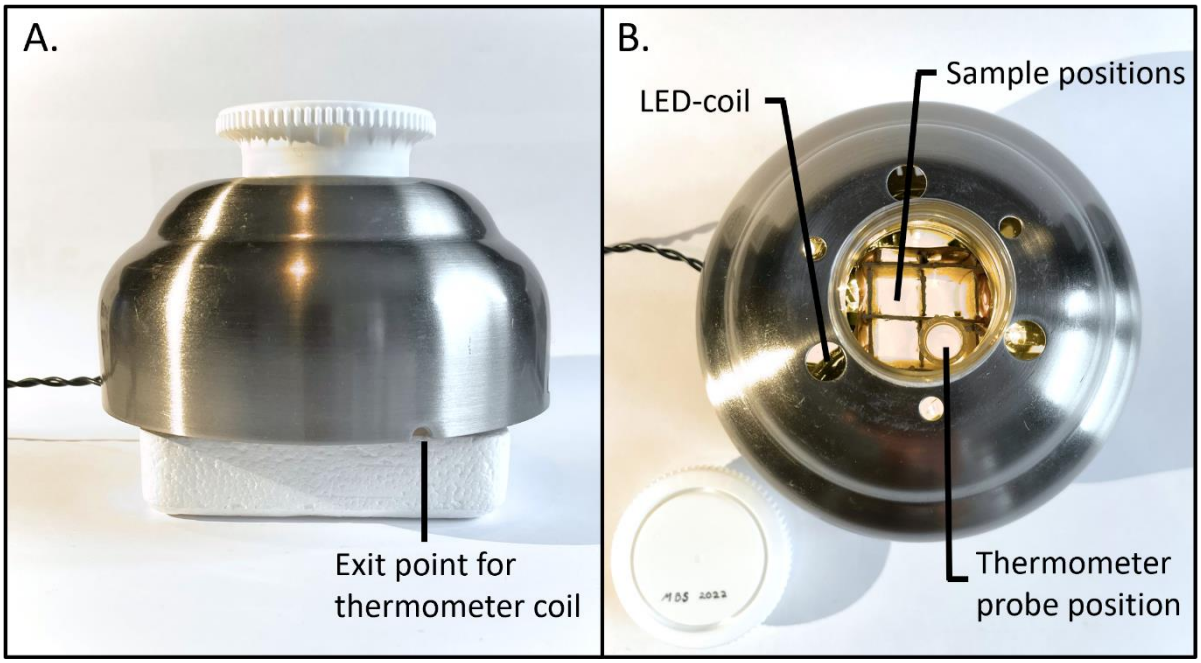

Figure 9 | Self-made cooling chamber. *The chamber is made from a polystyrene Filtropur V50 Vacuum filtration unit (500 ml) cut in half. The bottom holds a coil of Christmas lights. The generated heat from the electric consumption of the LEDs provide a slight temperature increase, which is stable at a slightly higher temperature than the freezer. The top of the Filtropour unit was cut to fit a stainless steel form to provide a see through window. The steel form enables a quick temperature exchange with the surrounding air in the freezer, while the plastic inner wall reduce the temperature loss. In combination this decreases the rate of temperature drop within the chamber when put in the freezer.*

2.3.4 Glutaraldehyde treatment

Treating nuclei with visible nucleoli with glutaraldehyde was necessary to examine if the fixation pattern differed between freshly isolated (control) and supercooled nuclei.

Glutaraldehyde fixation was achieved following the procedure in the paper by Pawełczyk et al., 1994, regarding concentration and quenching of the reaction, with modified time of fixation.

Briefly, nuclei suspensions were treated with 0.37% glutaraldehyde by adding 50% Glutaraldehyde (GA) to the tube, mixing by gently inversion. *Exemplified with a starting volume of 700 µl: C2 = (7µl (V1)*0.5 (C1))/ (700µl + V1) (V2) = 0.37%. → 7 µl added.* The tubes were allowed to stay on ice for 60-90 minutes before quenching the reaction by adding 1M Tris, pH 7.2 to a final concentration of 70mM. *Exemplified with a starting volume of 700 µl: C2 = (70µl (V1)*1 (C1))/ (707µl + V1) (V2) = 0.07M. → 70 µl added.*

2.3.5 High-salt treatment

Treating freshly isolated nuclei with high salt concentrations were necessary to compare salt-induced precipitation of proteins to the effect from supercooling.

The high-salt treatment protocol followed the procedure in the paper by Weber et al., 2003, without filtering the permeabilized nuclei suspension prior to high-salt concentrations. A detailed description of the protocol and calculations are included in **Appendix F**.

Briefly, nuclei in suspension were permeabilized with 0.5% of a nonionic detergent (Triton X-100) before incubating the sample for 15 minutes on ice. The permeabilized nuclei were then mixed 1:1 volume ratio with the Quencher-free high-salt solution containing 4M NaCl to induce precipitation of proteins. The sample was incubated for 5 minutes in room temperature before being directly processed with Hydroxyl Radical Footprinting.

2.3.6 Hydroxyl Radical Footprinting (HRF)

Hydroxyl radical "footprinting" (HRF) was used to induce structural changes to nuclei to discover if nucleoli were sensitive or insensitive to such changes following supercooling.

HRF was achieved during preliminary experimentation with the procedure in the paper by Schwanbeck et al., 2004, with modifications to the concentrations of reactants adapted from Matsufuji & Shibamoto, 2004 (see Results and Discussion). A detailed description of the protocol and calculations are included in **Appendix G**.

Briefly, chilled ascorbate, Fe(II)-EDTA, and H2O2 was added to a suspension of nuclei, or nuclear halos (following high-salt), to a final concentration of 0.75 mM ascorbate, 2.25 mM Fe(II)-EDTA and 2.2mM H2O2. The tube was mixed by gentle inversion before a quick spin down, and allowed to stay on ice for 2 minutes for microscopy or alternatively 1h for lysing nuclei. After incubation, the reaction was quenched with 6 w/v% glycerol by adding chilled HRF quenching solution to the tube or alternatively 30% w/v Glycerol Sample loading solution (Tris-Glycine) for SDS-PAGE or (Lithium) for BN-AGE.

2.3.7 Sodium dodecyl-sulfate polyacrylamide gel electrophoresis (SDS-PAGE)

Determining the size of proteins in different sample fractions with SDS-PAGE was necessary to evaluate the effects produced by high salt concentrations, freezing or supercooling on nuclear proteins.

SDS-PAGE was achieved with a pre-cast Bio-RAD TGX Stain-Free™ gel. Because proteins that do not contain tryptophan are not detected by this gel's Stain-free chemistry, samples lysed with HRF were quenched with 30% w/v Glycerol Sample loading solution Tris-Glycine containing Coomassie brilliant blue G250 (CBB) before being separated with SDS-PAGE. See **Appendix H** for a detailed description of the protocol.

Briefly, CBB stained nuclei lysates were filtered through 0.22µm PVDF membranes by centrifugation at 250 RCF for 6 minutes and 10µl of the filtrate (FIL) and the retentate (RET) fraction was loaded in separate wells on a 15-well 4–15% Mini-PROTEAN® TGX Stain-Free™ Protein Gel. The loaded polyacrylamide gel was placed in a Mini-PROTEAN Electrophoresis Cell and the SDS-PAGE was run using Tris/Glycine/SDS electrophoresis buffer (25 mM Tris, 192 mM glycine, 0.1% SDS, pH 8.3) at 300V for 37min at room temperature. After electrophoresis the gel was removed from the cast and examined with a ChemiDoc™ imaging system and analyzed with the built-in settings for the Stain-free system in the Image Lab™ software.

2.3.8 Blue native agarose gel electrophoresis (BN-AGE)

Determining migration patterns of proteins in different sample fractions with BN-AGE was necessary to evaluate the effects from supercooling on nuclear proteins.

BN-AGE was achieved during preliminary experimentation with the procedure in the paper by Henderson et al., 2000, with modifications. The modifications (see Results and Discussion) included a low-molarity Lithium acetate solution for running the electrophoresis adapted from Brody et al., 2004, and higher voltage and electrophoretic run time. See **Appendix I** for a detailed description of the protocol.

Briefly, a 0.3% agarose gel was prepared with low-molarity Lithium acetate by dissolving 0.3g Low EEO agarose in 100ml 5mM Lithium Acetate electrophoresis running solution by heating in a microwave. The water loss during heating was compensated and the solution was poured into a pre-assembled gel casting tray with a comb, allowed to set for 30 minutes. CBB stained nuclei lysates were filtered through 0.22µm PVDF membranes by centrifugation as

previously and 5µl of the FIL and RET fraction were loaded in separate wells on the 0.3% agarose gel after removing the comb and submerging the gel in 5 mM Lithium Acetate electrophoresis running solution. The electrophoresis was run at 300V for 45 minutes at room temperature. After electrophoresis the gel was removed from the cast and examined with a ChemiDoc^{TM} imaging system and analyzed with the built-in settings for CBB staining in the Image Lab^{TM} software.

3 RESULTS AND DISCUSSION

3.1 RESEARCH QUESTION 1: Does supercooling preserve structural integrity of nuclei?

3.1.1 Nuclei isolation

3.1.1.1 Evaluation of in-lab protocol

The first part of this thesis was to evaluate an already implemented lab protocol (AquaFaang, n.d.) adapted from Corces et al., 2017, for hepatocyte nuclei isolation from Atlantic salmon. The purpose was to see whether it yields sufficiently high nuclei quality, according to three objectives (see section 1.2.8; Busch 1967), to evaluate the effects from supercooling to answer the first research question.

Images in **Figure 10** were provided to me for evaluation and shows a nuclei isolation performed using the in-lab protocol. Subjectively, there are only two observable nucleoli (**Fig. 10 C & D**), indicating an unsatisfactory nuclear product according to objective 1. While many nuclei appear round and intact, some nuclei are not (**Fig. 10 A & B**) according to 10x Genomics, n.d., indicating a possible unsatisfactory nuclear product according to objective 2. Some debris is easily visible (**Fig. 10 B, C & D**), indicating an unsatisfactory nuclear product according to objective 3.

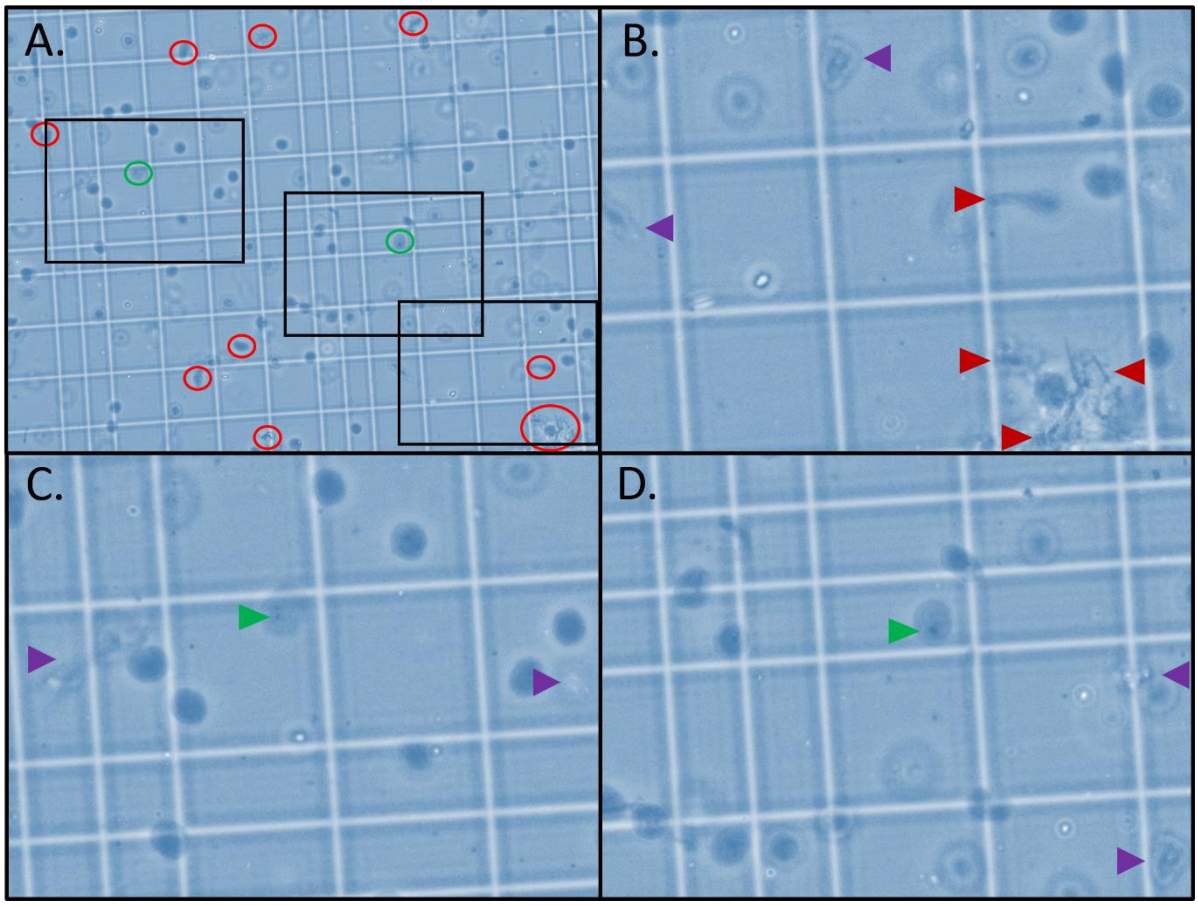

Figure 10 | Provided micrograph of nuclei isolated with the in-lab protocol. *One small square is 50µm x 50µm.* ***Black boxes*** *in A indicate zoomed area in B, C & D.* ***Red ring/arrowhead*** *in A/B indicate compromised nuclei.* ***Green arrowhead*** *in C & D indicate nucleoli.* ***Purple arrowhead*** *in B, C & D indicate debris.*

Based on these observations, and a desire to obtain high quality nuclei, it was decided to address the sources for possible unwanted biochemical and biophysical effects on nucleoli in the experimental conditions, such as pH, crowding, ions, molarity and/or metabolites (section 1.2).

3.1.1.2 Evaluating conditional effects during nuclei isolation

As there are many chemical compounds involved in the lab protocol, it was decided to elucidate on some of the potentially underlying synergistic- or crossover effects that might occur between them.

One problem with synergistic- or crossover effects is that some effects could be shielded, and by adjusting just one compound at a time it would not guarantee that the underlying effects become apparent, and in turn prevent an optimized solution. As many compounds in the lab protocol are added for their stabilizing effects (section 1.2.8), it was decided to change the experimental conditions to a degree where we can expect a certain result, i.e., induce

additional effects with expected results to serve as a baseline for observing differences between tests. Different monovalent, divalent and multivalent cation and anion concentrations were tested under hyperosmotic conditions (from sucrose and NaCl), high pH (via HEPES and Tris-HCl), or both, to see if they provided excessive "stabilization" actually perturbing the nuclear structures, and could be omitted, changed or adjusted.

Stabilizing effect under hyperosmotic conditions and high pH

It was necessary to evaluate the effect of the hyperosmotic conditions alone to get a baseline, and the tested combinations between homogenization solutions/buffers and density gradients to do this, listed in **Appendix D**, are given in **Table 1**.

Table 1 | Combinations of homogenization solutions/buffers and density gradients for Tests A-F.

Test:	Homogenization solution/buffer:	Density gradient:	Testing:
A	1	1	Hyper-osmosis
B	1	6	Iso-osmosis
C	1	2	Hyper-osmosis
D	1	3	Hyper-osmosis
E	2	2	EDTA + K + Mg
F	2	3	EDTA + K + Mg

The results from Test A-F are given in **Figure 11**.

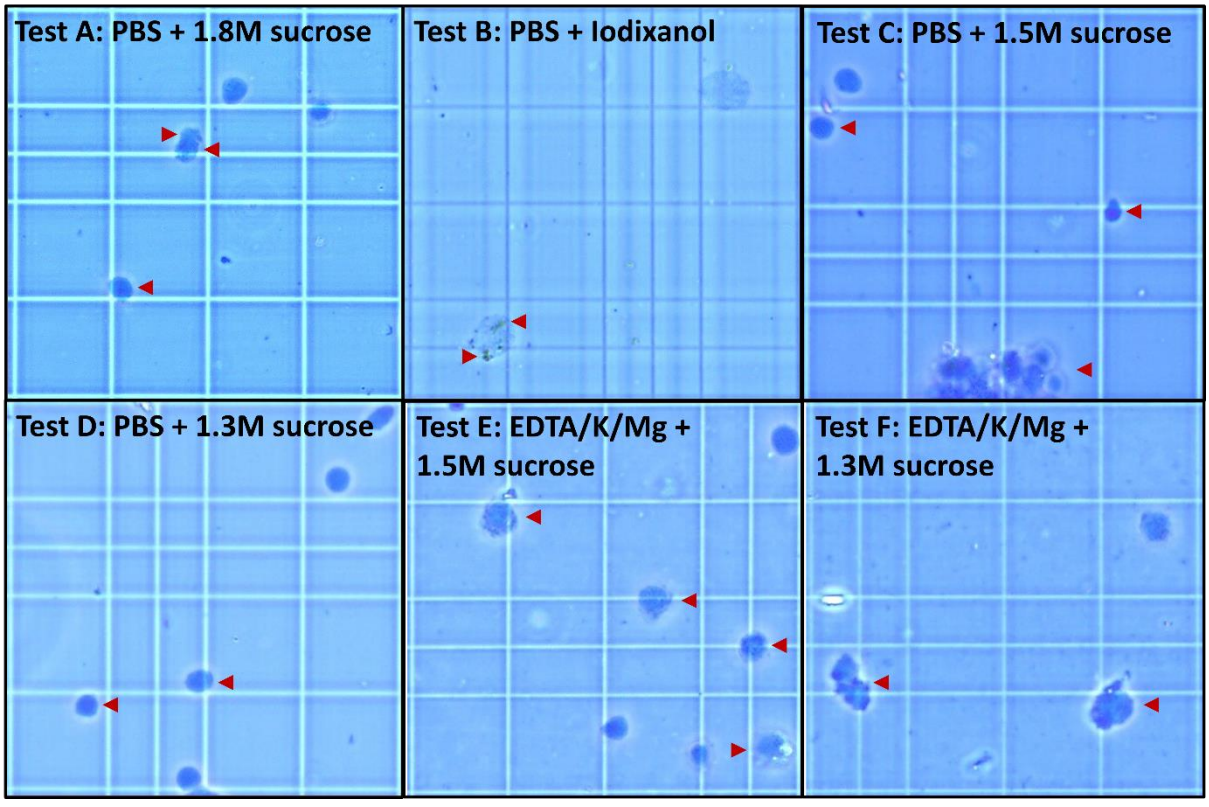

Figure 11 | Micrograph of Trypan blue stained nuclei isolated with combinations given in Table 1. *One small square is 50µm x 50µm.* ***Red arrowhead****= hyperosmotic nuclei (A,C,D)/ impurities (B)/ cluster (C)/ irregular shape (A&D)/ ruffled (E&F)/ blebbing (E&F).*

Tests A, B, C and D (**Fig. 11**) represent homogenization buffers with, relative to normal physiological levels, slightly high osmolarities. In addition, while Test B includes an iso-osmotic Iodixanol gradient, Tests A, C and D includes a high sucrose concentration gradient at 1.8M, 1.5M and 1.3M, respectively, generating hyperosmotic conditions during centrifugation. Test B functions as a contrast to compare the effect of the different sucrose gradients. **Fig. 11 A, C & D** shows that the nuclei were hyperosmotic in Test A, C, and D, however still smaller than in Test B (**Fig. 11. B**), indicating that the sucrose gradient have a quite large effect and can be used as a baseline.

While 5 mM calcium was added in the lab protocol, because calcium is an effective charge shielder (Phengchat et al., 2016), and only trace amounts are found *in vivo* (Nolin et al., 2013), it was tested if EGTA, which has a higher affinity for chelating calcium ions, could replace EDTA. The purpose was to see if the effect of complete calcium depletion in the sample could be countered by the addition of potassium and magnesium at concentrations reported *in vivo* (Nolin et al., 2013). In other words, explore if 0.1mM EGTA, 60mM potassium and 5mM magnesium (Test E) would result in a different effect on nuclei when the gradient centrifugation was hyperosmotic. The 1.5M gradient used in Test C was used in the subsequent Test E. Interestingly, the nuclei in Test E were larger (less hyperosmotic) than in Tests A, C and D, but smaller than in the contrast (Test B).

Note that spermine and spermidine were omitted from the homogenization buffer 2, but spermidine was included in the gradients 1, 2 & 3. All the gradients except 6 in Test B had the same composition and concentrations as in Test E except for the molarity. Spermidine has three N atoms and can chelate divalent cations, however in the gradient it is included to partially compensate for the removal of Mg^{2+}, stabilizing the envelope. The latter detail is mentioned because when comparing the appearance of the nuclei, the nuclei in Test E is more "ruffled" than in the other tests. The same result was observed in Test F using 1.3M gradient, with more blebbing. The poor quality could be a result of lack of available magnesium.

Stabilizing effect under hyperosmotic/isoosmotic conditions and moderate to low pH

In parallel with the above Tests A-F where the pH was 7.5 ± 0.1, it was decided to test the assumption that the pH is the dominating factor as found by Lovtrup-rein & McEwen, 1966.

The tested combinations between homogenization solutions/buffers and density gradients listed in **Appendix D** are given in **Table 2**.

Table 2 | Combinations of homogenization solutions/buffers and density gradients for Tests G-L.

Test:	Homogenization solution/buffer:	Density gradients:	Testing:
G	3	2	pH + hyper-osmosis
H	3	4	pH + volume exclusion
I	3	5	pH + volume exclusion
J	4	2	pH + hyper-osmosis
K	4	5	pH + volume exclusion
L	4	6	pH + iso-osmosis

The five Tests H, I, J, K and L, were all performed in the time period between the above Tests A and C, testing the possible synergistic/crossover effect between a lower pH and Magnesium, Spermine and Spermidine (no EDTA added). Sodium was also added to maintain the ionic concentration, and the pH was reduced to either 7.0 or 6.6 with HEPES instead of Tris, as HEPES, in addition to being a buffering agent, has negligible metal ion binding. The results from Test G-L are given in **Figure 12**.

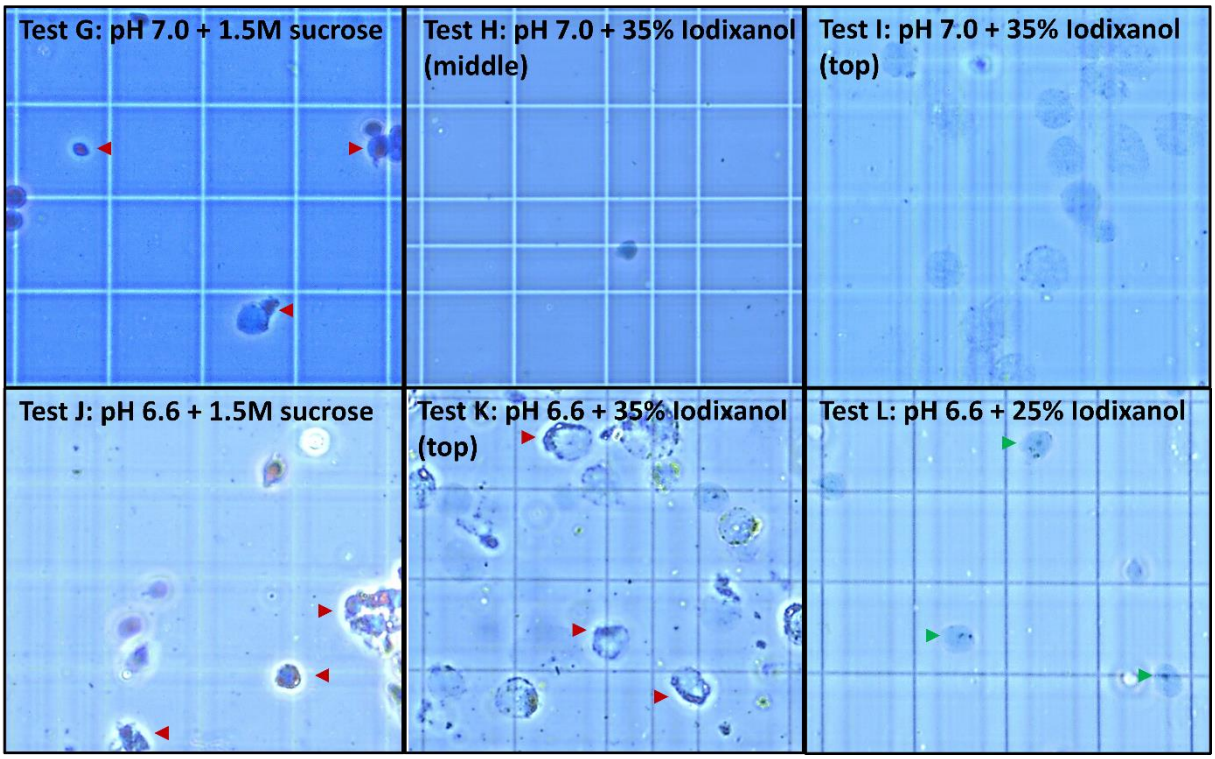

Figure 12 | Micrograph of Trypan blue stained nuclei isolated with combinations given in Table 2. *One small square is 50µm x 50µm.* ***Red arrowhead****= hyperosmotic nuclei (G)/ cluster (J)/ blebbing (J&K).* ***Green arrowhead****= nucleolus.*

First, a pH of 6.5 ± 0.1 (similar to Lovtrup-rein & McEwen, 1966) was tested. As can be seen in Test J (**Fig. 12**), with a 1.5M gradient, the nuclei were hyperosmotic, showing blebbing and formation of clusters. Compared to the previous tests using a 1.5M gradient (Tests C & E), the nuclei appear more dense, even though the homogenization solution was iso-osmotic in Test J compared to the slightly hyperosmotic ones.

Before testing with the same iso-osmotic gradient conditions as in Test B, it was decided to test if the possible volume exclusion effects introduced by the Iodixanol gradient itself, used to separate the nuclei, could influence the stability of nuclei and the possible interpretation of the pH effect. To test this, both Test I and K were performed by mixing the sample to 35% Iodixanol instead of 25%. The density of the sample layer was calculated by computing the solutions mass revealing that the density of 25% and 35% Iodixanol mixed with homogenization solution 3 or 4 was 1.22 g/ml and 1.25 g/ml, respectively (see **Appendix D**), with a percent difference in density of 2.4%. Test K was pH 6.6, while Test I was pH 7.0, and in the former of the tests the nuclei show extensive membrane blebbing in addition to being hypoosmotic, compared to hypoosmotic with less blebbing at pH 7. As can be seen from Test H (also pH 7.0) where the sample was mixed to 35% and layered directly in the middle, almost no nuclei could be retrieved, suggesting that most nuclei could have lower densities than 1.25 g/ml preventing them from retaining in the 35% layer.

To also have the comparison with a test at pH 7.0 and 1.5M sucrose gradient, Test G was performed, showing much more collapsed (hyperosmotic) nuclei than the comparable Test J. Again, it is worth noting that the ionic concentration and osmotic contributions in the homogenization buffer is lower than in the previous Tests C & E. The increased hyperosmosis could therefore be attributed to a cumulative effect from the composition of the homogenization buffer and the sucrose gradient, or a synergistic/crossover effect involving pH.

When Test L was performed with pH 6.6 and the gradient centrifugation conditions were as in Test B (25% Iodixanol), a few nuclei were compromised or showed signs of blebbing, however most were of high quality with a clearly visible, centrally located nucleoli.

Three contradicting observations can be drawn from the above tests:

1. When the samples are mixed to a high density (35%) with Iodixanol, the sample with the lowest pH (6.6) is more negatively affected, indicating a higher sensitivity to crowding conditions.

2. When the samples are run through a high molarity (1.5M) sucrose gradient, the sample with the highest pH (7.0) is more negatively affected, indicating a higher sensitivity to osmotic compression.
3. When the sample with the lowest pH is mixed to a lower density (25%), the nuclei collected between 29%-40% Iodixanol is of mostly high quality with visible nucleoli, indicating a good stability of the nuclei at this pH and crowding conditions.

The reconciling explanation could be that at pH 6.6, proteins are less prone to precipitate, i.e., more soluble than at pH 7.0 (consistent with Tedeschi et al., 2017, and Kurotani et al., 2019). When the nuclei collapses following hyperosmotic conditions, they are therefore less prone to stick together/precipitate following reduced hydration. In addition, the solubility makes them even more sensitive to increased excluded volume effects from Iodixanol, resulting in leakage of proteins at a density threshold at around 35%. Regardless, it is evident from above that a quite large synergistic effect exists between pH and crowding, and that pH 6.6 and 25% Iodixanol strikes a balance between the two, that marginally stabilize nuclei. This combination was used for all subsequent tests as it provides a new basis for testing minor adjustments of single components as any detrimental effects is likely to overcome the balance.

To explore whether or not the ionic contributions can overcome the balance, i.e., testing the possible synergistic/crossover effect between different ionic contributions, additional tests were performed. The tested combinations between homogenization solutions/buffers and density gradients listed in **Appendix D** are given in **Table 3**.

Table 3 | Combinations of homogenization solutions/buffers and density gradients for Tests M-Q & S.

Test:	Homogenization solution/buffer:	Density gradients:	Testing:
M	5	6	pH + K + Mg
N	6	6	Spermine + spermidine
O	6	6	Spermine + spermidine
P	7	6	Spermine + spermidine + Ca
Q	8	6	Spermine + spermidine + Ca
S	9	6	PIC

To the six Tests M-Q and S, 1 mM phosphate was added (less than 1.5 mM to not cause precipitation of the nucleoplasm; Lovtrup-rein & McEwen, 1966), together with equal amounts of potassium and sulphate to slightly increase the ionic conditions. In addition, it was tested whether spermine and spermidine could be adjusted or omitted, by reducing calcium

levels with or without reduction to spermine/spermidine. The results from Test M-Q & S is given in **Figure 13** (Test R discussed later in section 3.1.2.2).

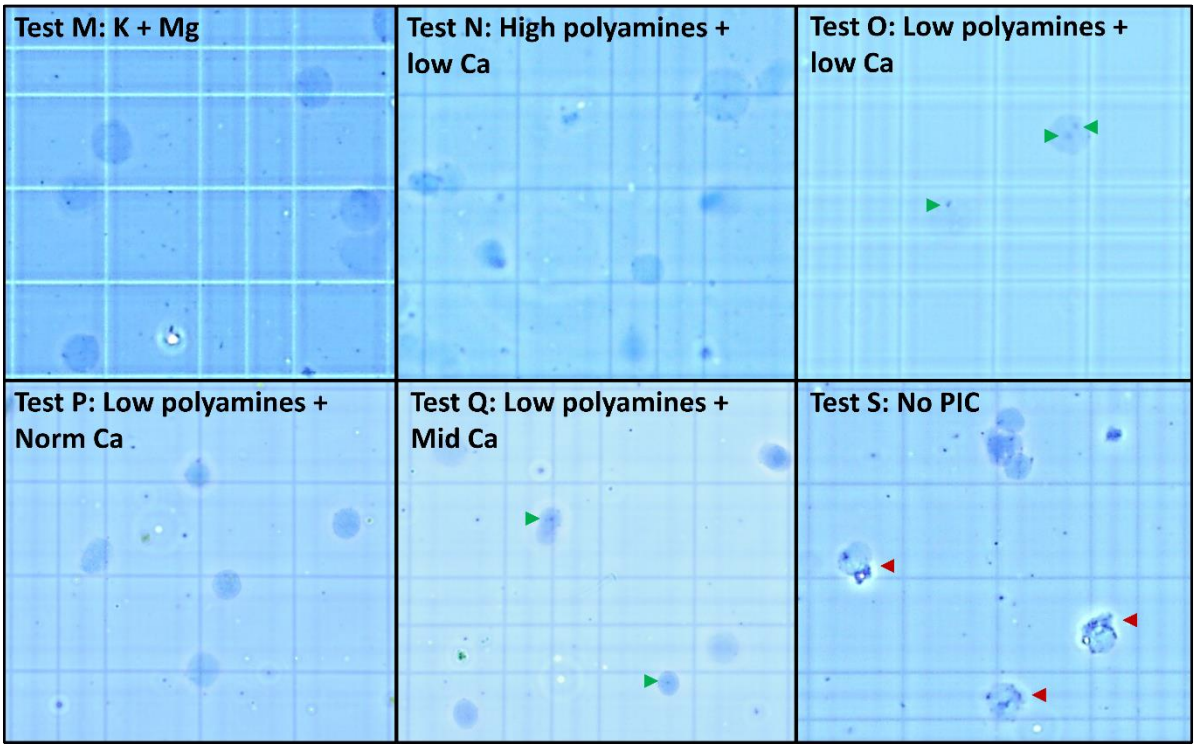

Figure 13 | Micrograph of Trypan blue stained nuclei isolated with combinations given in Table 3. *One small square is 50µm x 50µm.* ***Red arrowhead****= blebbing/compromised nuclei.* ***Green arrowhead=*** *nucleolus.*

As can be seen in Test M (**Fig. 13**), just a slight increase in the ionic conditions cause dissolving of nucleoli. In addition, when spermine/spermidine is kept high (1mM), but calcium is reduced from 500nM to 100nM in Test N, there is little difference. Because it is possible that spermidine is chelating all the calcium at these concentrations, it was tested whether the reduction of spermine/spermidine could make a difference. As shown in Test O this reduction results in the appearance of a few nucleoli, similar to Test L where spermine/spermidine was kept high. Interestingly, when the calcium levels were increased to 500nM in Test P, nucleoli dissolves. When the calcium levels were reduced to 333 nM in Test Q, some faint nucleoli appear. These results might indicate that when the calcium levels are higher than the chelating capacity of the reduced spermine/spermidine levels, it has a negative effect on nucleoli. Alternatively, it could be that there is a crossover effect between calcium and these polyamines, being mitigated when the calcium is not fully chelated. It was decided to omit both spermine and spermidine in the subsequent tests to test if there was a cross-over effect. This resulted in a much stronger and clearer appearance of nucleoli (as can be seen for downstream tests), underlining the negative cross-over effect from including polyamines.

As no chelators are included in this final homogenization solution it was tested whether the available cations like Ca^{2+} and Mg^{2+}, could activate metalloproteases in the absence of PIC. In other words, how effective is PIC in inhibiting proteases without chelators such as EDTA. Test S shows that nuclei become compromised or have extensive membrane blebbing when PIC is omitted compared to Tests R & V discussed below (section 3.1.2.2), serving as controls with the same conditions but with PIC. This could indicate that PIC is efficient at inhibiting proteases at the cation concentrations used, which is consistent with the recommendations of using EDTA-free PIC for inhibition when divalent cations are required (Roche Diagnostics, 2004)

Stabilizing effect from other compounds

The effect of a reducing agent on nucleoli was explored due to β-mercaptoethanol (βMe) being used in the lab protocol. However, βMe can irreversibly denature some proteins by reducing disulfide bonds, destroying the native conformations of proteins and influence DNA binding to histone-depleted chromatin (Lebkowski & Laemmli, 1982B).

To test the effect from a reducing agent, Glutathione (reduced) (GSH) was added to the homogenization solution 9. The rationale to use glutathione is that it has a long half-life at pH 6.5 (Stevens et al., 1983), and that GSH up to 25mM does not negatively influence protein binding to DNA compared to the induced loss of proteins from as little as 0.1 mM βMe (Lebkowski & Laemmli, 1982B), indicating that it has little influence on native protein conformations.

The result from Test T, a combination between homogenization solution 9 + density gradient 6, with 1mM GSH added (adapted from Hancock, 2004) is given in **Figure 14**.

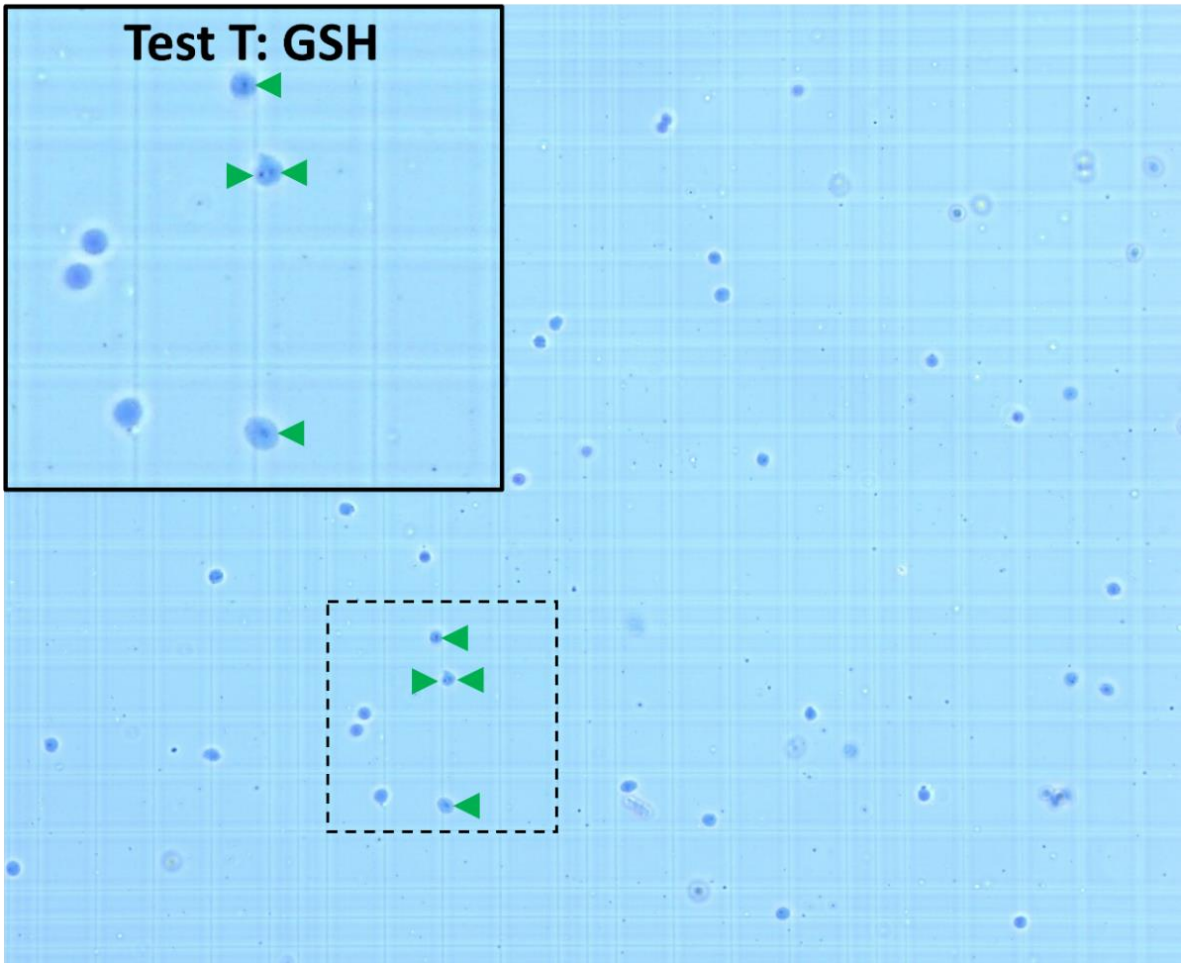

Figure 14 | Micrograph of Trypan blue stained nuclei isolated with the final protocol with added GSH. *One small square is 50µm x 50µm.* ***Green arrowhead****= nucleoli.*

In Test T (**Fig 14**), the addition of 1mM GSH did not result in particularly large effects, with clearly visible nucleoli. However the nuclei yield was surprisingly low, and GSH was not included in the subsequent tests. While all the Tests A-T included a replicate (n=2, i.e., a control performed with the same conditions on the same day), for the previous Test H and Test T, the control samples were not assessed. At the time it was prematurely concluded that the generality of the observations would be reduced by the low yield, i.e., not comparable to the other tests. In retrospective, the reduced yield for Tests H and T should be an even better reason to check the replicate, as the low yield could be a one-time event for that particular isolation. Because an average value for the yield was not obtained, it is not possible to draw any convincing conclusions from it and further investigations of the possible role of a reducing agent should be opted.

Effect from abundant cellular metabolites

The effect of ATP (section 1.2.8) on nucleoli was explored due to its potential influence on LLPS (Zhou et al., 2021; section 1.2.6). The *in vivo* concentration of ATP in Atlantic salmon cells is not available to date (only a percentage for different treatments; Søderstrøm et al., 2022). For this reason, an intermediate value between the high and low values reported by Kang et al., 2018, was chosen in Test U.

The results from Test U, a combination between homogenization solution 9 + density gradient 6, with 5mM ATP added is given in **Figure 15**.

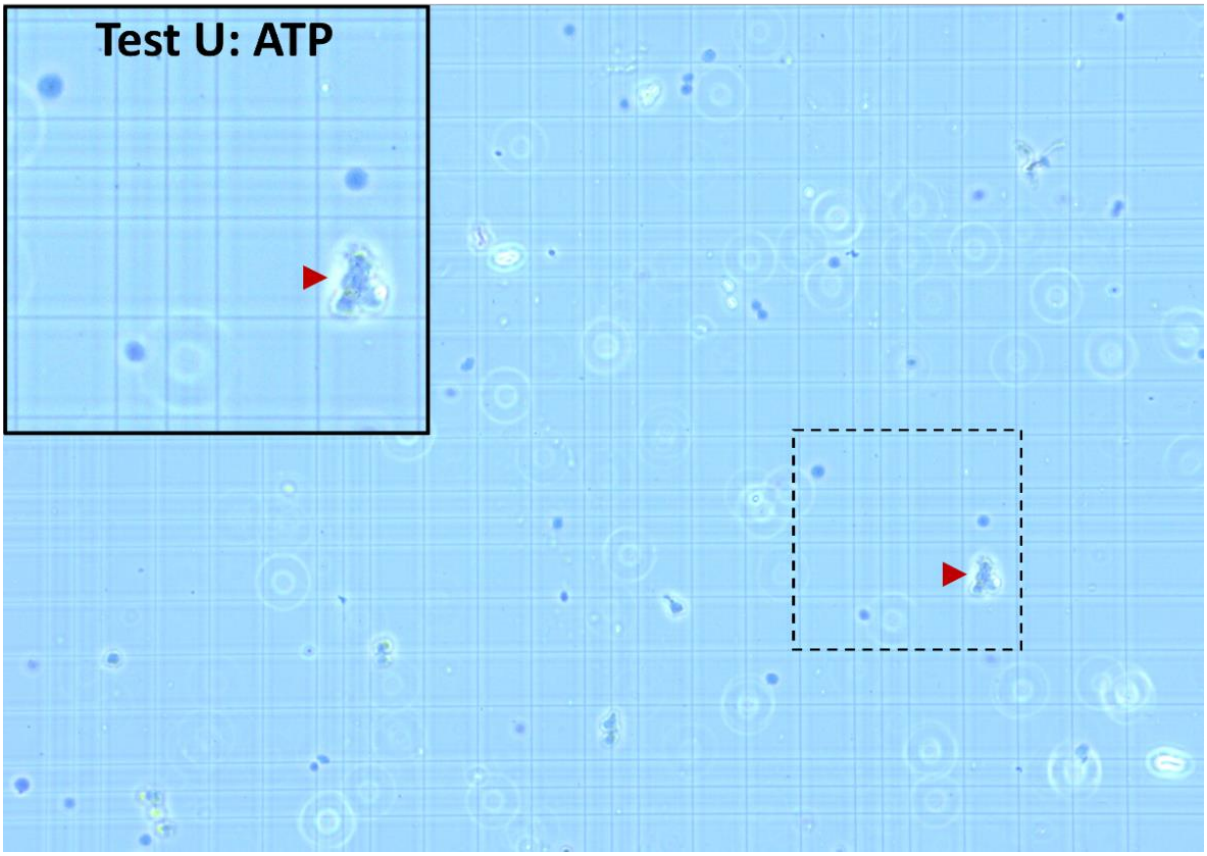

Figure 15 | Micrograph of Trypan blue stained nuclei isolated with the final protocol with added ATP. *One small square is 50µm x 50µm.* ***Red arrowhead****= compromised nuclei/blebbing.*

During isolation, although seemingly normal before centrifugation, the gradient layers collapsed together when 5mM ATP was present in all solutions. This prevented the extraction of the nuclei-layer as illustrated in **Fig. 7** (Methods and Materials). The reason for why the gradients collapsed is not known, but could be due to ATP acting as a biological hydrotrope (Kang et al., 2018), diminishing the interface tension between the different density layers. Regardless, only a few isolated nuclei was obtained from the Test U (**Fig. 15**) replicates. Nucleoli was not visible in any of the nuclei, and many were compromised with signs of blebbing (**Fig. 15**). Because any addition of ATP during the isolation step, not matching intra-

nuclear concentrations exactly, could disturb nucleoli directly or indirectly via chromatin organization (discussed in section 1.2.8), it could be that this has occurred in Test U. Due to time limitations, it was not attempted any modifications to the protocol to enable the capture of also ATP-treated nuclei, and ATP was omitted for this reason.

3.1.1.3 Evaluating the precision of the final isolation protocol

The homogenization buffer used in the lab protocol consisted of 0.32M sucrose, 3mM Mg(Ac)2 , 5mM CaCl2 , 0.1mM EDTA, 0.5mM spermidine, 0.15mM spermine, 10mM Tris-HCl (pH 7.8), 0.1% NP40, 0.0167mM PMSF, 0.167mM βMe, 1xPIC, pH 7.4. From the Tests A-U (Test R discussed below in section 3.1.2.2) several modifications were done including a lower pH, the addition of Sodium and Potassium, the omitting of Spermine, Spermidine, EDTA, NP40, PMSF and βMe, the changing of acetate to chloride and sulphate and Tris-HCl to HEPES, and the adjustment of sucrose, magnesium and calcium. The final homogenization solution consisted of 0.25 M Sucrose, 10mM NaCl, 1mM KH_2PO_4, 1mM $MgSO_4$, 500nM $CaCl_2$, 3mM HEPES (pH 7.2), 1xPIC, pH 6.7, and was used without further modifications from hereon.

The precision of the final isolation protocol was evaluated from 8 independent nuclei isolations using the same sample (J7) and amount of material. Each replicate was sampled and measured two times (duplicate). In total 16 nuclei counts were performed and the estimated yields calculated. The counts are summarized in **Figure 16**.

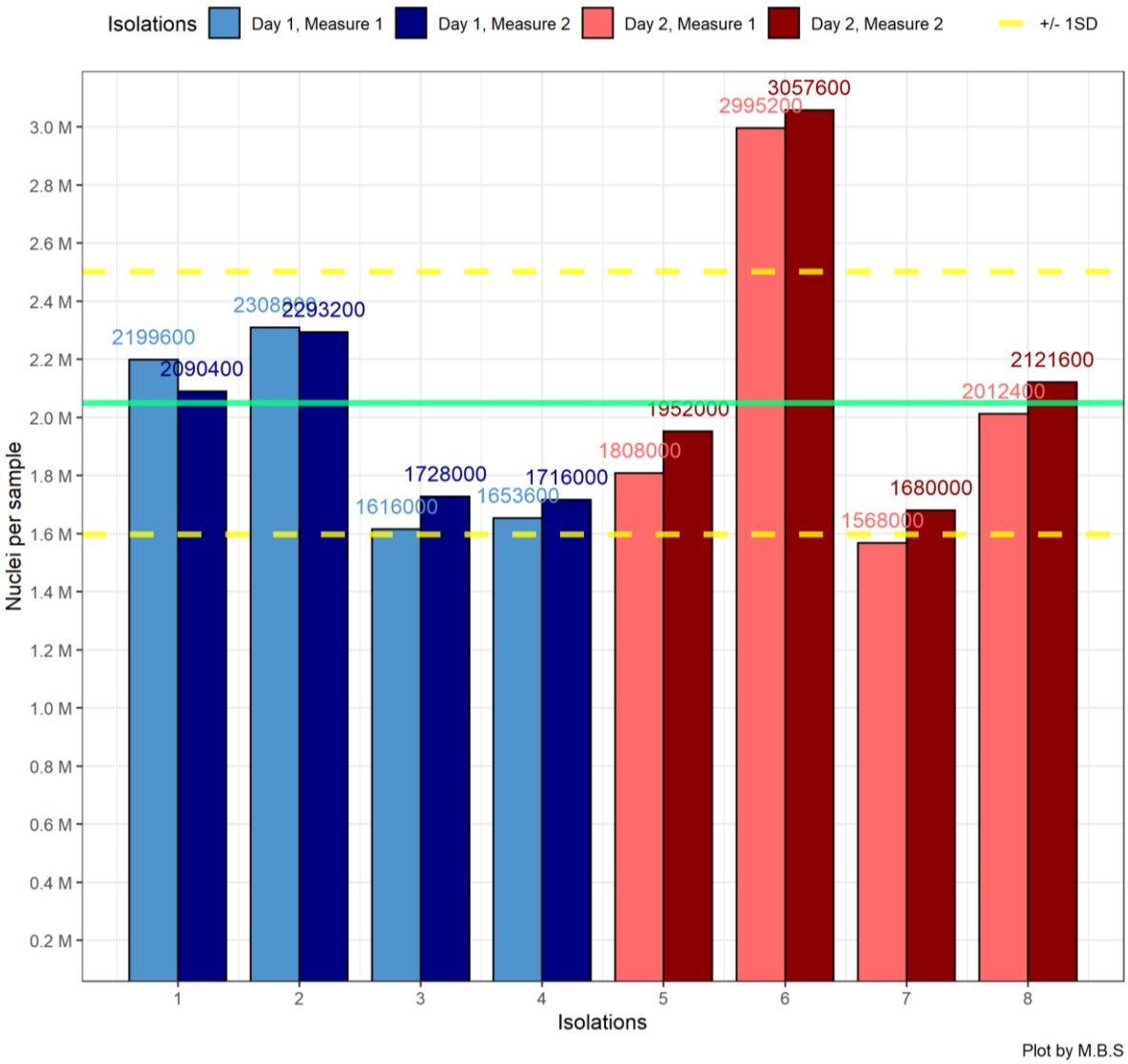

Figure 16 | Nuclei counts with mean and standard deviation (SD). *Green line=the mean of all counts. Yellow dotted line= ± 1SD. Blue colored bars=Isolations performed the first day. Red colored bars=Isolations performed the second day. Light/dark shaded bars=Repeated measurements. Figure created with the statistical programming language R.*

As shown in **Figure 16**, most isolations fall within ± 1 standard deviation, except isolation 6. This isolation was run in parallel with isolation 8, however the yield was much higher for isolation number 6. The percent difference between measure 1 for isolation 6 and 8 was 39%, between measure 1 and measure 2 it was 34%, and between measure 2 it was 36%. The mean percent difference between them was therefore 36%. Due to the frozen liver tissue sample being distributed into each of the two parallel isolations separately, and because each sample was roughly ~20-25 mg, it is likely that additional sample may have accidentally been added to the tube for isolation 6. This could occur as the sample stored at -80°C was much colder than the chilled tweezers used to extract them, so that it may have been frozen to the tweezer

when distributing, resulting in ~70 mg tissue instead of 50 mg (percent difference = 33%). Comparing total yields divided on weight of the reference amounts of tissue used, cannot correct for this, it can only correct if isolation 6 used a frozen tissue sample that was relatively, but not visibly, larger than the other 7 isolations. The small deviations from the average between the other replicates could be due to individual variabilities in the biological samples, manual douncing or nuclei collection from the 29-40% Iodixanol layer.

Nevertheless, the low standard deviation indicates that the nuclei yields do not vary much from the mean. In other words, the isolation protocol have repeatedly consistent yields, indicating high precision.

3.1.2 Supercooling

3.1.2.1 Establish supercooling

The second major goal of this thesis was to establish an efficient supercooling procedure in the lab, to evaluate the effects from supercooling on high quality nuclei.

The first attempts to achieve supercooling according to the paper by Huang et al., 2018, was performed directly in a freezer holding −20ºC → −26ºC (± 0.1ºC error) by covering small volumes (<500µl) and larger volumes (>1500µl) of water with various volumes of light mineral oil (LMO) or heavy mineral oil (HMO). In all cases the water froze solid along with HMO, while the LMO remained liquid. The LMO was therefore used in all subsequent tests, and by measuring the rate of temperature decrease in a tube with only LMO, it was found that the temperature decreased steadily at ~2 degrees per minute. Because this steep decline in temperature resulted in ice formation for all volumes of water, it was tested if a more moderate decline could be better suited. A cooling chamber (**Fig. 9**, Methods and Materials) was designed to slow the cooling rate. When testing, six main parameters were found to be influential:

Cooling rate: The time it took for the samples to reach −12ºC, was measured to calculate the cooling rate. Several modifications to the chamber design were made, decreasing the cooling rate to ~1 degree per minute or 0.5 degree per minute. A cooling rate of 0.5 degree per minute was found to be the most optimal and prevented ice formation in the larger volumes.

Starting temperature: The sample should not be raised above 4-7ºC ± 1 prior to being placed in the chamber. A higher starting temperature closer to 22ºC always resulted in freezing, likely due to large temperature fluctuations. A lower starting temperature closer to 0ºC usually

resulted in freezing, correlating with the decreased time it took to reach −12°C. A starting temperature of 4°C was found to be the most consistent in preventing ice formation.

Sample volume: The minimum sample volume that did not freeze was found to be 550µl. In some tests, freezing was prevented in volumes down to ~450µl but this was not consistent.

Minimum temperature: While the first chamber design only allowed cooling of the samples to a minimum of −7.3°C (± 0.1°C), other chamber designs allowed lower minimums of −12.8°C, −15.4°C and −17.0°C (± 0.1°C), respectively. The lowest temperature at which freezing did not occur in the tests was −15.4°C, close to the limit found by Huang et al., 2018.

Thickness of the mineral oil (MO) layer: A minimum volume of 200 µl LMO layered on top of the sample in a round-bottom 2ml Eppendorf tube was found to be the minimum that still prevented ice formation, i.e., it successfully removed the air-liquid interface which acts as nucleation sites for ice-formation. In some tests freezing was prevented with ~150 µl LMO but this was not consistent. At 100 µl the layer barely covered the solution, and it did not prevent freezing.

Centrifugation prior to freezing: The purpose of centrifugation was to get any air bubbles trapped between the LMO layer and the solution away from the interface before cooling, to limit ice nucleation sites. A short spin down of around 2 seconds was usually sufficient (too long centrifugations could potentially pellet nuclei). If many bubbles were seen rising in the LMO layer, the tube was left for 2 minutes before repeating the centrifugation once. It was found that longer spin downs resulted in the LMO layer forming a biconcave surface on top of the solution and usually resulted in freezing. This is likely the result of the LMO layer being thinner in the middle with a similar effect as discussed above.

In summary, the preliminary experimentation was sufficient to establish the feasibility of the supercooling concept and define some of the experimental parameters.

3.1.2.2 Effect of freezing versus supercooling on nuclei appearance

Cryopreservation at the cell or tissue stage is a widely used approach for maintaining nuclei over time, as freezing or cryopreservation of nuclei easily damage nuclear membranes resulting in leakage. However, even the treatment with cryoprotectants at the cell stage, with or without subsequent freezing, is linked to several detrimental effects such as nuclear envelope shrinkage, strong chromatin condensation, reorganization and structural changes, correlating with each other and with reduced cell viability (Kratochvílová et al., 2018). On the

other hand, for untreated cells, freezing strongly damages the nuclear envelope and disrupts the chromatin structure, becoming hypocondensed or structureless, due to osmotic shock from freeze-dehydration, resulting in 90% cell death (Kratochvílová et al., 2018).

Two tests were performed to see if supercooling can reduce the detrimental effects from freezing. Nuclei were isolated from 50mg, and 70mg tissue to reveal if potential clustering of nuclei (indication of leakage) is yield dependent. Each suspension was split into two aliquots of ~800µl stored under two different conditions; frozen or in supercooled conditions at −13ºC → −15ºC for 3 or 15 days, representing the long-term storage tests R & V, respectively.

The results from Test R & V, a combination between homogenization solution 9 + density gradient 6, stored under supercooling is given in **Figure 17**.

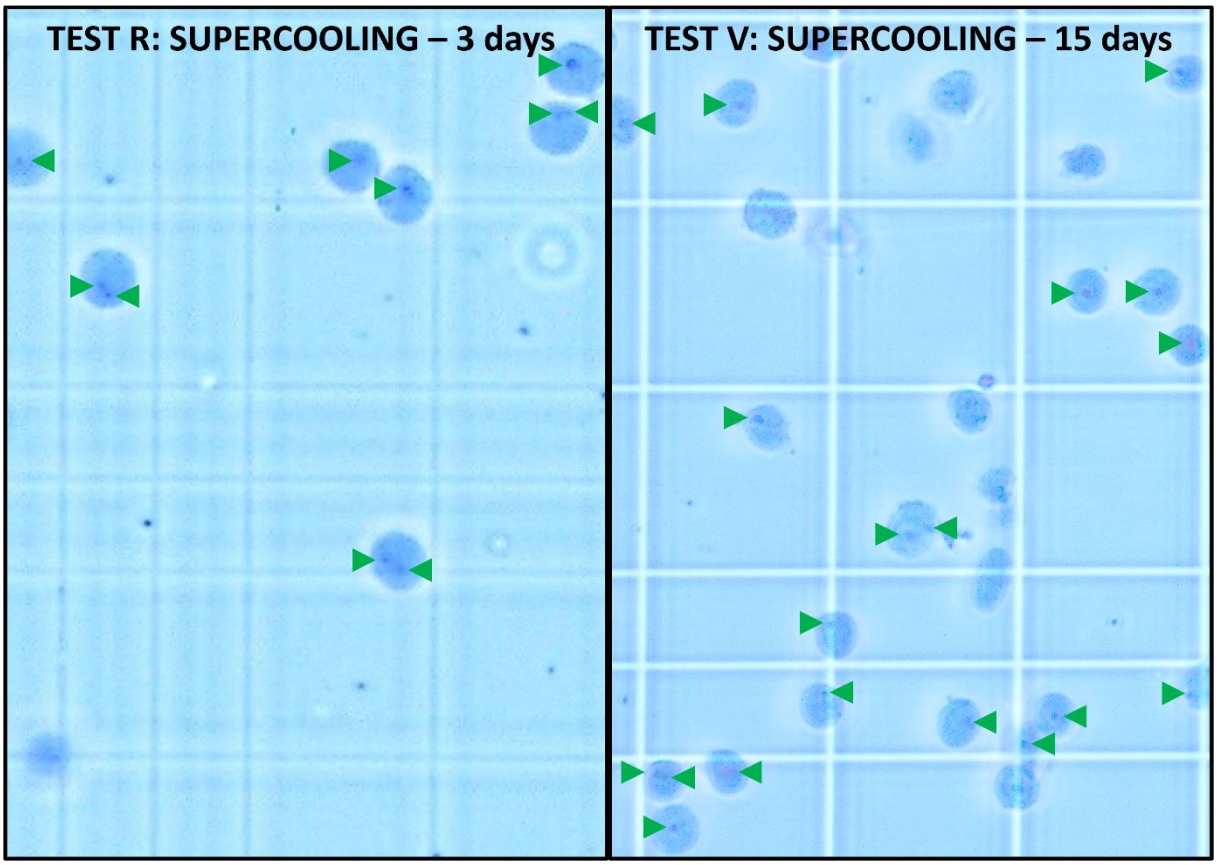

Figure 17 | Micrograph of Trypan blue stained nuclei isolated with the final protocol and stored under supercooled conditions. *One small square is 50µm x 50µm.* ***Green arrowhead****= nucleoli.*

A subjective interpretation of the Tests R and V (**Fig. 17**) is that there is no difference in terms of appearance of nuclei after different periods of storage at 3 or 15 days in supercooling. This contrasted with the nuclei stored frozen that were fully destroyed and indistinct after 3 and 15 days (no images captured for this reason). As seen for both Tests R & V, nucleoli are clearly

visible and there are no signs of clustering, even when the yield was high for Test V. The main difference between these tests is that the nuclei in Test R appears slightly larger than the nuclei in Test V. Estimating the diameter based on the size of one half of a tiny square in the Thoma cell being 0.025 mm, the diameter of nuclei in test R were roughly between 15-17.5 µm (between 0.6 and 0.7 times 0.025 mm). In comparison, the diameter of nuclei in test V were roughly between 10-12.5 µm (between 0.4 and 0.5 times 0.025 mm). These estimates are not very different and could be ascribed to biological variability such as sex differences. For Test R, the sample material used originated from a female (J11), while for Test V it originated from a male (J7). Standardized testing with the exact same input should have been performed for the above tests. However, for yield estimates a comparison of Test V with a control with the exact same input (J7) was made, as given in **Figure 18**.

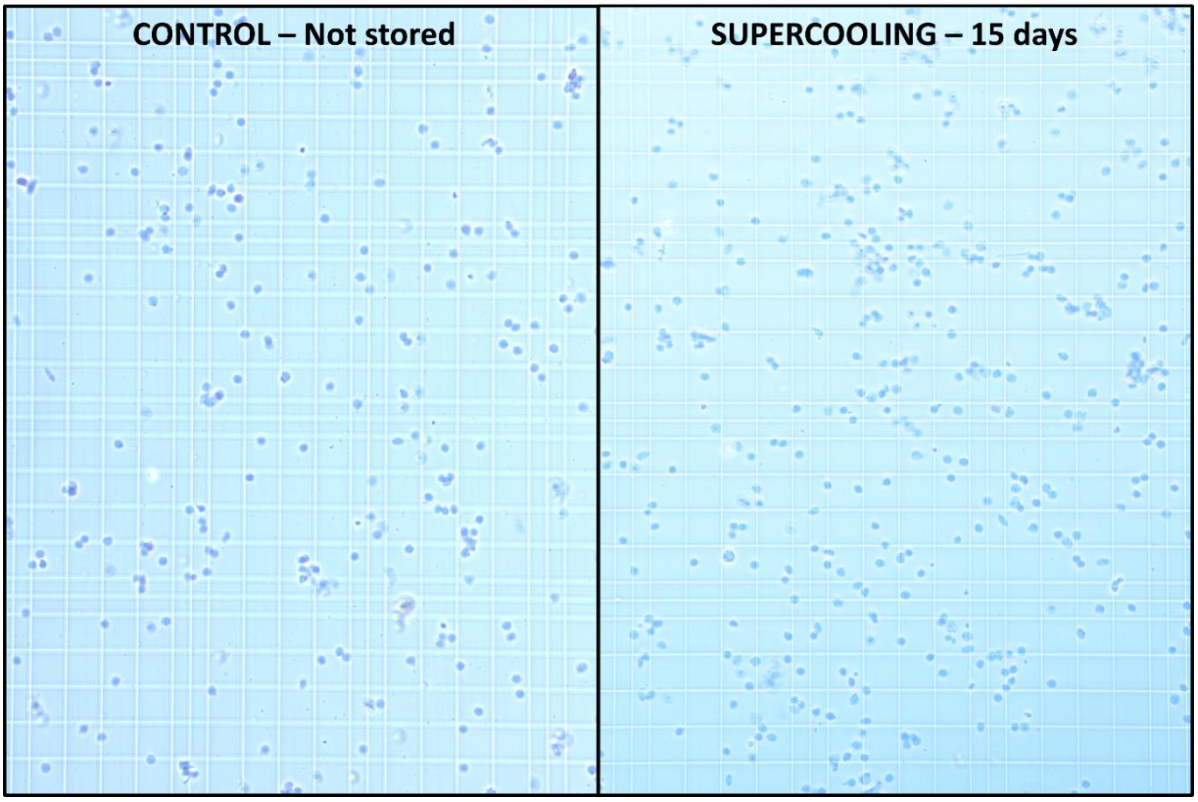

Figure 18 | Micrograph of Trypan blue stained nuclei isolated with the final protocol. *One small square is 50µm x 50µm.* ***Green arrowhead****= nucleoli.*

Compared to the control in **Fig. 18**, nuclei remain well separated with no clear clustering even after 15 days in supercooling. This indicates that nuclei remain intact. Together, there is no signs of any detrimental effect from supercooling from Tests R and V.

3.1.3 ANSWER TO RESEARCH QUESTION 1

The first goal of this master project was to *establish supercooling in the lab and identify if the overall structure of the nucleus is influenced by supercooling,* to answer if supercooling preserves the structural integrity of nuclei. While the impact of supercooling on red blood cells (which lack nuclei) has been evaluated (Huang et al., 2018), there are currently no publications describing the effects of supercooling on nuclei. The observations made in this thesis cannot therefore be discussed considering comparable results. However a broad change in structure was <u>not</u> observed in isolated nuclei with clearly visible nucleoli following supercooling. Although more research is necessary to confirm or reject the above observations, supercooling could represent an alternative to chemical cryopreservation. The main advantage over cryopreservation is that no additional cryoprotectants are required, and nuclei can be stored directly in the solution they are suspended in after isolation. One solution (0.25 M Sucrose, 10mM NaCl, 1mM KH_2PO_4, 1mM $MgSO_4$, ~500nM $CaCl_2$, ~3mM HEPES (pH 7.2), 1xPIC, pH 6.7, together with Iodixanol at 25%) was found to have negligible impact on nuclei, which were kept well-separated and intact with no evidence of nuclear leakage or membrane degradation even after 15 days at $-13\,^{o}C \rightarrow -15^{o}C$.

3.2 RESEARCH QUESTION 2: Does supercooling influence nuclear bodies?

3.2.1 Structural change

3.2.1.1 Effect from hypo-osmosis on nucleoli

Because there is no current knowledge on the influence of supercooling on nuclei morphology, and the supercooled nuclei are identical to freshly isolated nuclei (untreated control), it was decided to include a hypo-osmotic test to test if some changes have occurred to one nuclear body, the nucleolus. Under hypo-osmotic conditions the nucleolus is expected to dissolve rapidly as the nuclei swell (Hancock, 2004). Because the dilution from the Trypan staining (see **Appendix D**) is enough to induce hypo-osmotic effects visible in nuclei after only 15 minutes, it is possible to achieve good contrasts by taking pictures within the first 2 minutes after staining and again after 15 minutes. The difference between the hypo-osmotic tests on freshly isolated and supercooled nuclei are given in **Figure 19**.

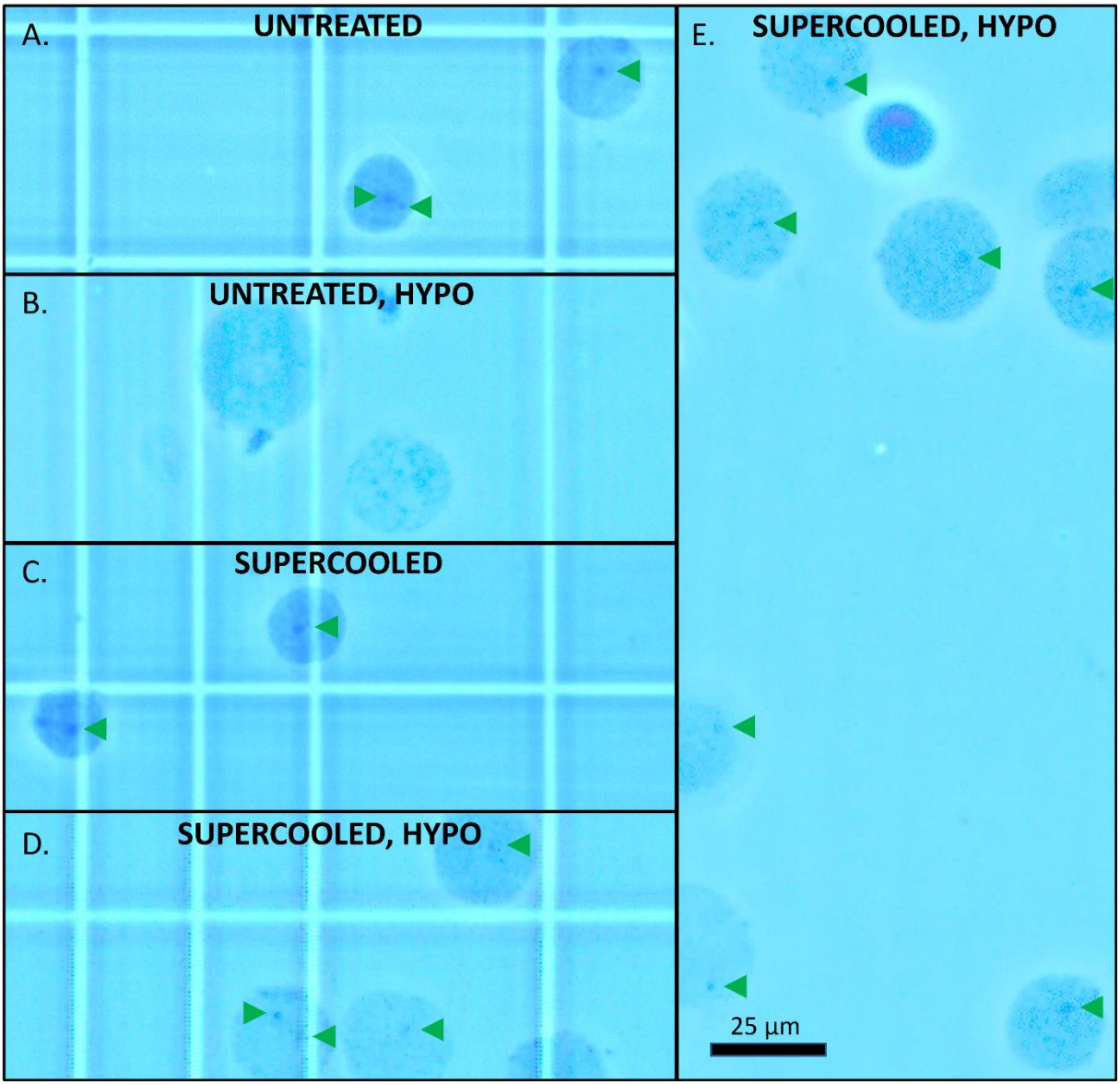

Figure 19 | Micrograph of Trypan blue stained nuclei isolated with the final protocol. ***HYPO****= Hypoosmotic (>15min in dilute conditions),* ***Green arrowhead****= Nucleoli.* ***A & C*** *represent Trypan stained nuclei (1:1 vol. dilution with the staining dye), where pictures were taken <2 minutes after adding the dye, while* ***B & D*** *represent pictures taken again after 15 minutes.*

A subjective interpretation of the above images is that both supercooled and untreated nuclei appears to contain nucleoli (**Fig. 19 A & C**). Similarly, most of the hypo-osmotic supercooled nuclei, expanded to roughly twice the size, still have a central and visible darker spot in the same focus (**Fig. 19 D & E**). A more detailed evaluation of this observation is given in **Figure J1**, **Appendix J**. In contrast, this is not seen in the hypo-osmotic untreated nuclei in **Fig. 19 B.** Because the observations were reproducible (**Fig. 19 D** and **E**, and **Fig. J1**, **Appendix J** were from three individual tests) it could be interpreted as a potential effect of supercooling on nucleolus-like structures, as they can be observed in hypo-osmotic supercooled nuclei

while dissolved in untreated nuclei. However, due to the subjectivity in the interpretations, it is not possible to conclude that supercooling has an effect on nucleoli from the above images. It was therefore decided to search for methods to evaluate the potential change induced by supercooling with two assumptions:

Assumption 1. ***The change (to nuclei) is irreversible***.

based on the observation that nucleolus-like structures were retained during hypo-osmotic conditions.

Assumption 2. ***The change is specific for phase separated entities (nucleoli)***

based on the lack of observations of more widespread changes to be expected if additional (structured) proteins in the nucleoplasm is affected.

Exploring these assumptions is important for the overriding research question as it can help confirm or reject if supercooling influences structural integrity on a global scale, with implications for its use as a cryopreservation technique, or at the scale of only nuclear bodies with implications mostly for studying them.

3.2.1.2 Effect from Hydroxyl Radical Footprinting on nucleoli

Based on the chromatin-tension sensitivity of nuclear bodies (sections 1.1 & 1.2), it was decided to test if oxidative damage and cleavage of DNA could reveal if the nucleolus-like structures subjectively observed in **Fig. 19**, dissolves (sensitive) or behave differently (insensitive) between supercooled and freshly isolated nuclei serving as the untreated control.

For studies relying on DNA cleavage, permeabilization of nuclei is often necessary to enable enzymatic reactions to occur within the genomic regions. Due to the disadvantages of permeabilizing nuclei (section 1.2 & 1.3) it was decided to use a non-enzymatic approach previously used to cleave DNA around bound proteins named Hydroxyl radical "footprinting" (HRF) by Tullius & Dombroski, 1986. HRF is based on a modified Fenton reaction to produce hydroxyl radicals that induce oxidative damage and cleavage of DNA via several proposed mechanisms (Evans et al., 2004). Due to the small size of the reactants, they are believed to diffuse into unpermeabilized nuclei, and this reaction can thus be used directly on isolated nuclei (Rivière et al., 2006). The modification to the general Fenton reaction is the controlled addition of EDTA, which prevents iron ions from binding to DNA (as hypothesized by Matsufuji & Shibamoto, 2004) or other substrates like ATP (Floyd, 1983). This accelerates hydroxyl radical formation, making even low reactant concentrations

effective in whole nuclei (Kuban-Jankowska et al., 2015). The general Fenton reaction (without EDTA) alone would target lipids, proteins and DNA. However, the HRF approach used by Tullius & Dombroski, 1986, take advantage of the higher sensitivity DNA have towards the short-range radicals produced, so that the reaction can be stopped before it influences proteins and lipids too much, enabling the reaction to target DNA more specifically. This has been successfully used to map nucleosome positioning on DNA with higher accuracy than enzymatic approaches (Schwanbeck et al., 2004).

Previous tests of the optimal ratios between Fenton reagents have found that maximum DNA oxidation is achieved for ascorbate between 1-3 mM, 3mM Fe(II) and 3mM H2O2. By modifying the reaction with EDTA, even higher oxidation rates were achieved, reaching maximum oxidation after 30 minutes (Matsufuji & Shibamoto, 2004). These results were reported for combinations of reactants with 0.5 mg/mL of DNA. Based on the mean nuclei yield of approx. 2 million nuclei reported in **Fig. 16**, and a minimum collected sample volume of 700µl (**Appendix D**), a conservative DNA concentration estimate for an average nuclei isolation using the final protocol would be 0.017 mg/ml (calculations given in **Appendix E**). Thus, the above reactant concentrations would theoretically be sufficient for my samples.

Because the DNA in my samples were not free in solution but concentrated in nuclei it was decided to start testing with higher concentrations, believed to give higher local concentrations within the nuclei to accommodate a higher DNA concentration. The first attempt to achieve HRF used 10mM Ascorbate, 30mM Fe(II)-EDTA and 30mM H2O2, while the second attempt used 5mM Ascorbate, 15mM Fe(II)-EDTA and 15mM H2O2. Both reactions were run for 30 minutes before quenching and staining, however they were unsuccessful in inducing any effects on nuclei. A third attempt, using 1mM Ascorbate, 3mM Fe(II)-EDTA and 3mM H2O2 (hereafter referred to as 1X) resulted in visible changes after 30 minutes as given in **Figure 20 B**. By reducing the concentration to 0.75 times the reactant concentrations for 1X (referred to as 0.75X), no nuclei could be located. It was therefore tested if the incubation time was too long and if an incubation for 2 minutes (as in the original paper by Tullius & Dombroski) resulted in any differences as given in **Figure 20 C & D**.

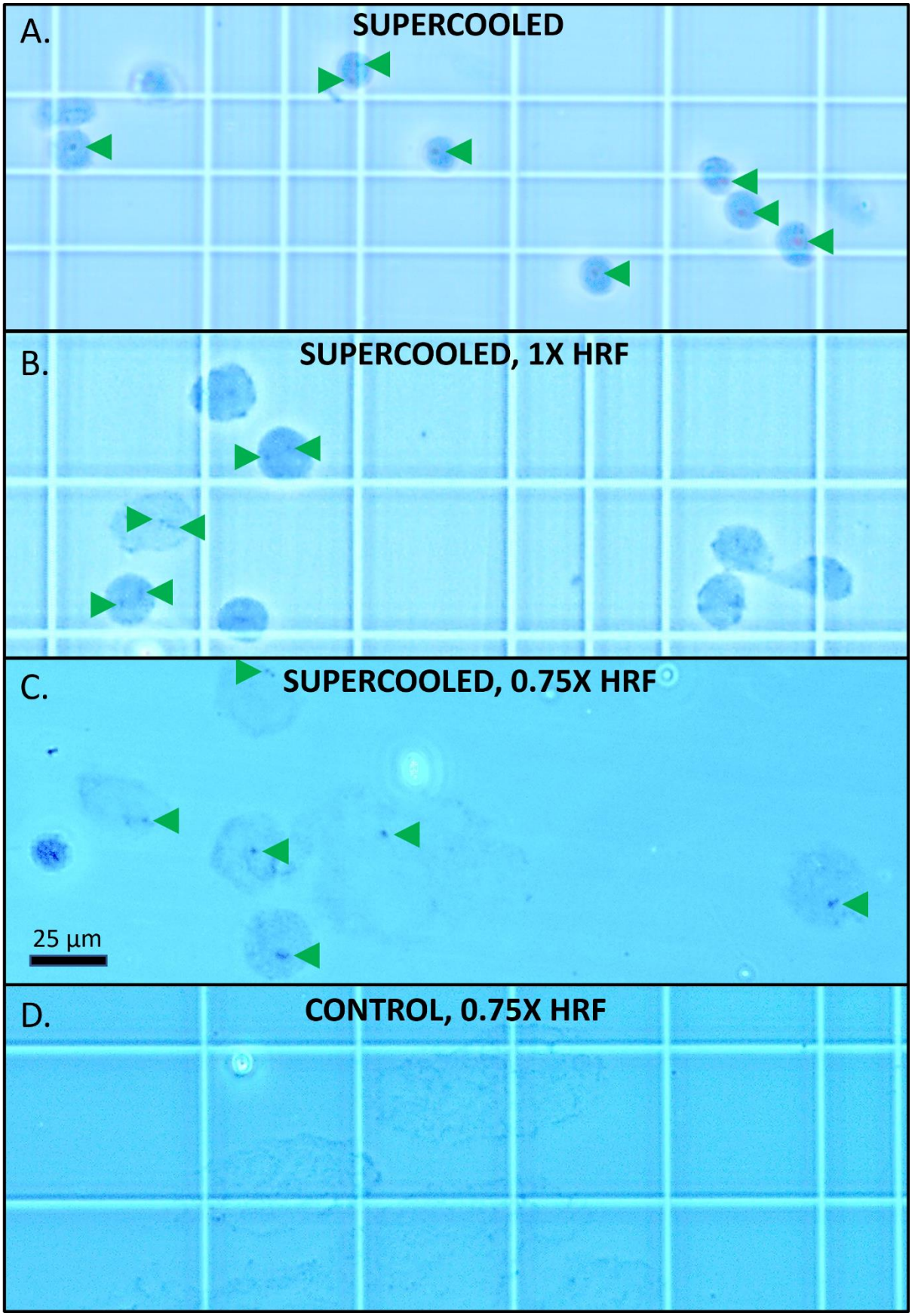

Figure 20 | Micrograph of Trypan blue stained nuclei isolated with the final protocol. HRF*= Hydroxyl Radical Footprinting (1X allowed to work for 30 min, 0.75X for 2 min).*

A subjective interpretation of the above images is that nuclei with initially normal chromatin condensation (**Fig. 20 A**) gradually disappeared when subjected to 1X HRF for 30 minutes, resulting in slightly enlarged and "wobbly" morphology (**Fig. 20 B**). In comparison, when nuclei were subjected to 0.75X HRF for 2 minutes, the majority of nuclei were quite enlarged and had mostly structureless (hypo-condensed) chromatin (**Fig. 20 C & D**), with a few having hyper-condensed chromatin (left-most nuclei in **Fig. 20 C**). In other words, the 0.75X HRF for 2 min, is more effective than 1X HRF for 30 min. It was thus concluded that 0.75X (0.75 mM L-ascorbate, 2.25 mM Fe(II)-EDTA and 2.2mM H2O2) was the optimal reaction strength to induce the desired structural changes.

The 0.75X reaction was used in the subsequent tests to evaluate the effect of supercooling. However, it can already be argued that there is a difference between the control (not supercooled) and supercooled nuclei in **Fig. 20 C & D**, although both were subjected to the same HRF reaction. A subjective interpretation is that the supercooled nuclei have a visible dark spot centrally located, indistinct from nucleoli (**Fig. 20 C**), while the freshly isolated nuclei lacked such spots. However, the images cannot be directly compared as it proved difficult to capture several nuclei in one view-plane within the grid for the supercooled sample subjected to 0.75X HRF (**Fig. 20 C**). It is likely that the very fragile condition the nuclei were in after the treatment resulted in most of the nuclei being destroyed from loading the sample on the Thoma cell (even with a p100 tip), which is also the reason why the image in **Fig. 20 D** were taken at the edge of the grid.

<u>Addressing Assumption 1.</u>

When testing HRF on the supercooled nuclei, it was observed that nuclei loose structure, being highly swelled. At the same time, nucleolus-like structures were observable in many nuclei (**Fig. 20 B & C**), in contrast to directly tested (not supercooled nuclei) where they rapidly dissolved (**Fig. 20 D).** The differences observed between supercooled and directly tested nuclei, was interpreted as support for the assumption that supercooling induces an irreversible change of some sort ("*change is irreversible")*.

3.2.2 Fixation pattern

3.2.2.1 Effect from glutaraldehyde on nucleoli

Because the structures indistinct from nucleoli in supercooled nuclei in **Fig. 19** appeared to resist dissolving following hypo-osmosis, and similarly in **Fig. 20**, appeared to resist dissolving following HRF treatment, it was speculated if this insensitivity to the environment

was due to an effect on the components of nucleoli. One possibility is protein aggregation, explaining the insensitivity of the otherwise sensitive nature of protein condensates.

Glutaraldehyde is a fixative that only cross-links proteins and not DNA, in contrast to other aldehyde-based fixatives such as PFA (Hopwood, 2005). Glutaraldehyde targets some of the solvent exposed residues frequently occurring in disordered regions of proteins (section 1.4.5), in addition to other residues prominent in ordered proteins, making it able to crosslink most proteins in the nucleus. If supercooling is specifically influencing disordered proteins in protein condensates, the variability from different momentary sizes of nuclear bodies, such as nucleoli with size ranging from 0.5-5µm (Lyon & Lamond, 2000), might result in differently sized aggregates following fixation if pre-aggregated by supercooling. Comparable to rolling a snowball, even a small size difference in pre-formed aggregates could potentially lead to large differences in the growth of these during the same fixation period. A larger surface would enable multiple opportunities for not yet crosslinked proteins in close proximity to be crosslinked and contribute to a rapid expansion. Interactions between diffusing single proteins would not form equally large aggregates in the same time period. This is in line with the rapid expansion in glutaraldehyde-crosslinked albumin microspheres when albumin form a supercooled-induced nucleation site (Öner & Groves, 1993).

It was decided to test the effect of glutaraldehyde on both supercooled and freshly isolated nuclei (control), to see if the possible insensitive nucleolus-like structures in supercooled nuclei (**Fig. 19 & 20**), form different nucleation sites for further fixation. The differences between supercooled and freshly isolated nuclei treated with glutaraldehyde and/or 0.75X HRF are given in **Figure 21**.

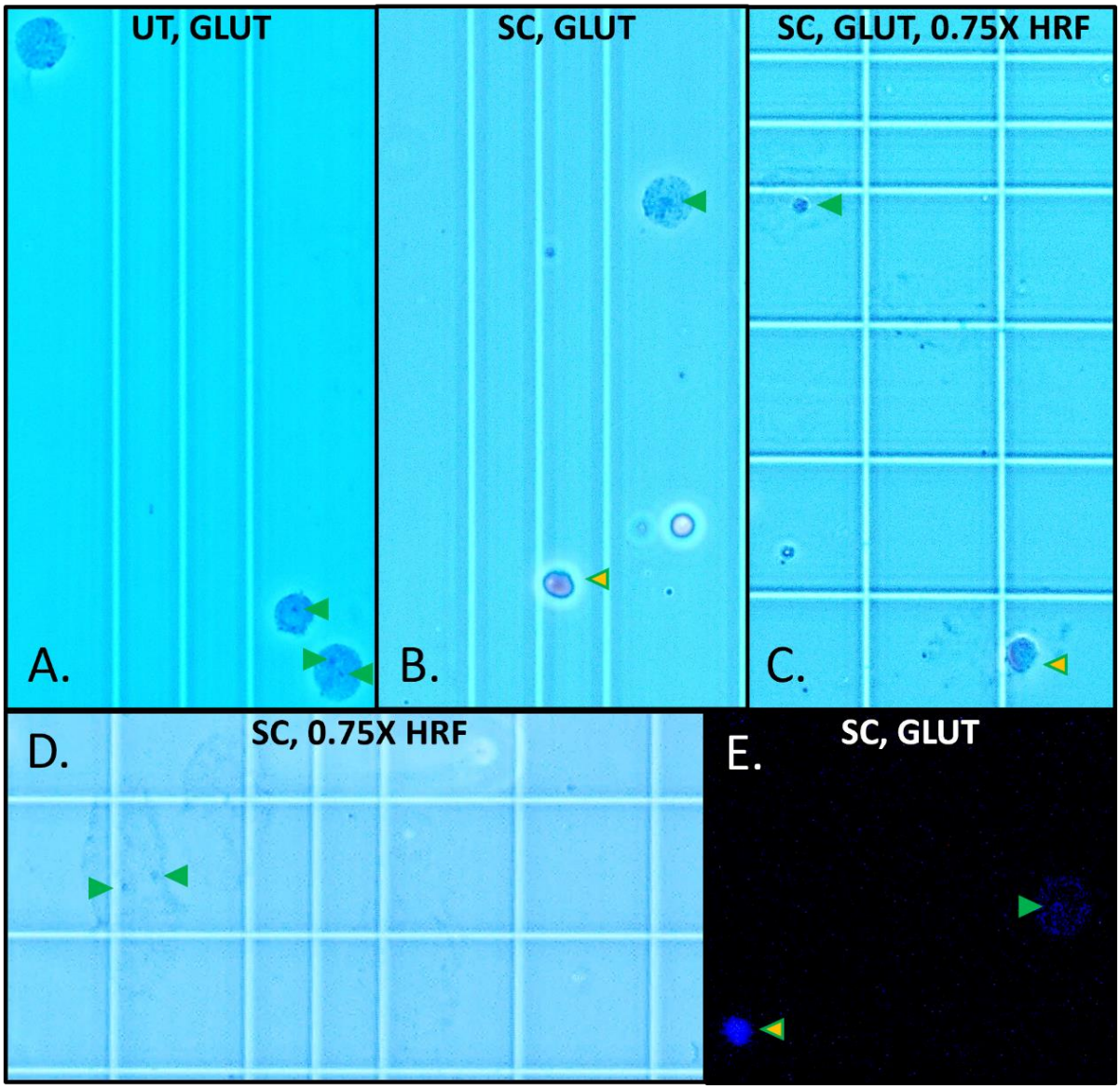

Figure 21 | Micrograph of Trypan blue- or Hoechst-stained nuclei isolated with the final protocol. ***UT****= Untreated.* ***GLUT****= Glutaraldehyde.* ***SC****= Supercooled (> 12h).* ***HRF****= Hydroxyl Radical Footprinting (allowed to work for 2 min).* ***B & E****: same conditions, but overlapping fluorescence and trypan blue comparison was not tested, thus images are from individual samples.*

A subjective interpretation of the above images in **Fig. 21** is that the nuclear morphology is slightly distorted for nuclei treated with glutaraldehyde. A more detailed evaluation of this observation is given in **Fig. K1**, **Appendix K**. However, nucleolus-like structures are maintained in most of the freshly isolated nuclei subjected to glutaraldehyde (**Fig. 21 A**), with visually similar sizes as the nucleolus-like structures maintained in supercooled nuclei treated with 0.75X HRF (**Fig. 21 D**). In contrast, supercooled nuclei treated with glutaraldehyde appears to experience differences in the fixation process visible with both Trypan blue (**Fig. 21 B**) and Hoechst (**Fig. 21 E**). Some nuclei appear to collapse like the bottom-most nucleus

in **Fig. 21 B & E**, while others like in the top-most nuclei do not. The uncollapsed nuclei in **Fig. 21 B & E** maintain instead a core-structure larger than the nucleolus-sized structures in **Fig. 21 A & D**. For supercooled nuclei treated with both glutaraldehyde and 0.75X HRF, the rather digital collapse-event (complete or not) following fixation, seems to be restricted to a core in the middle of the nucleus (**Fig. 21 C**) similar in size as in **Fig. 21 B**, with the nucleus losing structure (hypo-condensed) in the periphery, similar to supercooled nuclei only treated with 0.75X HRF (**Fig. 21 D**).

It is assumed that the concentrations of proteins remain quite similar between nuclei of different sizes, although different types of proteins can change (section 1.1.2). If the visual extent of crosslinking increases in space with duration of fixation and at a constant rate, we would assume that because protein concentrations remain equal, they will exhibit equal extents of crosslinking. A possible reconciling explanation for the different fixation patterns where some nuclei appear to contain a larger core than others, is that there were differently sized nucleation sites for aggregation. Although it cannot be concluded from the subjective interpretations from the above images, it is plausible that **Fig. 21 B & C** visualizes such an impact from a size related head-start, suggesting an effect from supercooling.

Addressing Assumption 2.

When testing fixation by glutaraldehyde it was observed that differently sized, densely stained cores form in the supercooled nuclei (**Fig. 21 B, C & E**), in contrast to directly tested (not supercooled) nuclei where nucleolus-like structures were smaller (**Fig. 21 A**). The differences observed between supercooled and directly tested nuclei, were interpreted as support for the assumption that supercooling induces a change in nucleoli without other large scale nuclear changes ("*change is specific for phase separated entities"),* in the form of a transition from an environmental sensitive structure (section 1.1 & 1.2) to an insensitive structure.

3.2.3 Electrophoretic migration

3.2.3.1 Effect from centrifugation investigated with SDS-PAGE

Considering the above observations that supercooling might induce a change to nucleoli, making it less sensitive to its environment, it was decided to test how strong these supercooling-induced structures were.

Although swelling of nuclei following hypoosmotic conditions, or HRF, does not seem to dissolve these potential supercooled-induced structures, i.e., insensitive, these forces are very weak. It is not known if greater forces from centrifugation, could dismantle these structures. It

was decided to test this by filter different untreated, high-salt treated, frozen and supercooled samples, lysed with 0.75X HRF, through a 0.22 μm pore-sized membrane. This pore size is smaller than many nucleoli in untreated nuclei being between 0.5-5 μm, with similarly sized HRF-insensitive nucleolus-like structures observed in the supercooled nuclei in **Fig. 20**. If centrifugation is not strong enough to disassemble any potential structures, then the resulting FIL- and RET-fractions could potentially contain different proteins. If they fall apart, it is likely that both the filtrate and retentate would show similar composition as an untreated control.

By looking at the size distributions of proteins using Bio-RAD's TGX Stain-Free™ gels for SDS-PAGE, it could be possible to differentiate between samples with or without centrifugation-resistant structures larger than 0.22 μm, if certain types of proteins are involved in the structures. Bio-Rad's Stain free chemistry allows direct fluorescent detection of proteins without staining or destaining steps, as the precast gels include trihalo compounds that react with tryptophan residues in a UV-induced reaction to produce fluorescence within the gels (Bio-Rad, n.d.(A) & (B)). This approach is very sensitive and low numbers of tryptophan residues can generate signal detectable by the ChemiDoc™ imaging system. However, 10% of proteins from all organisms lack tryptophan (Bio-Rad, n.d.(A)), used to detect proteins in the Stain free gels. Because tryptophan is among the most order-promoting residues (Zhao & Kurgan, 2022), and some relatively disordered proteins are low in tryptophan (exemplified by albumin in section 1.4.5; Litus et al., 2018), there is a possibility that highly disordered proteins are not detected with this method.

Because nucleoli are enriched in disordered proteins, it was decided to include pre-staining with CBB, able to bind the surface of all proteins through Van der Waals forces, hydrophobic interactions and by charge (although to a lesser extent; Compton & Jones, 1985). Because most of the proteins that lack tryptophan are less than 10 kD in size (Bio-Rad, n.d.(A)), it could theoretically be possible to observe whether different sample fractions contain more or less proteins lacking tryptophan, by observing the relative interference with the UV-induced reaction from the Stain-free chemistry in the lowest size range.

In addition, to account for possible day-to-day variation, the untreated, high-salt treated and supercooled samples were in replicates from two independent isolations on consecutive days. However the nuclei from the first day were stored inadequately at 4°C until use the following day, which in retrospective might instead *induce* day-to-day variation. The size distributions from the SDS-PAGE run with CBB are given in **Figure 22**.

SDS-PAGE

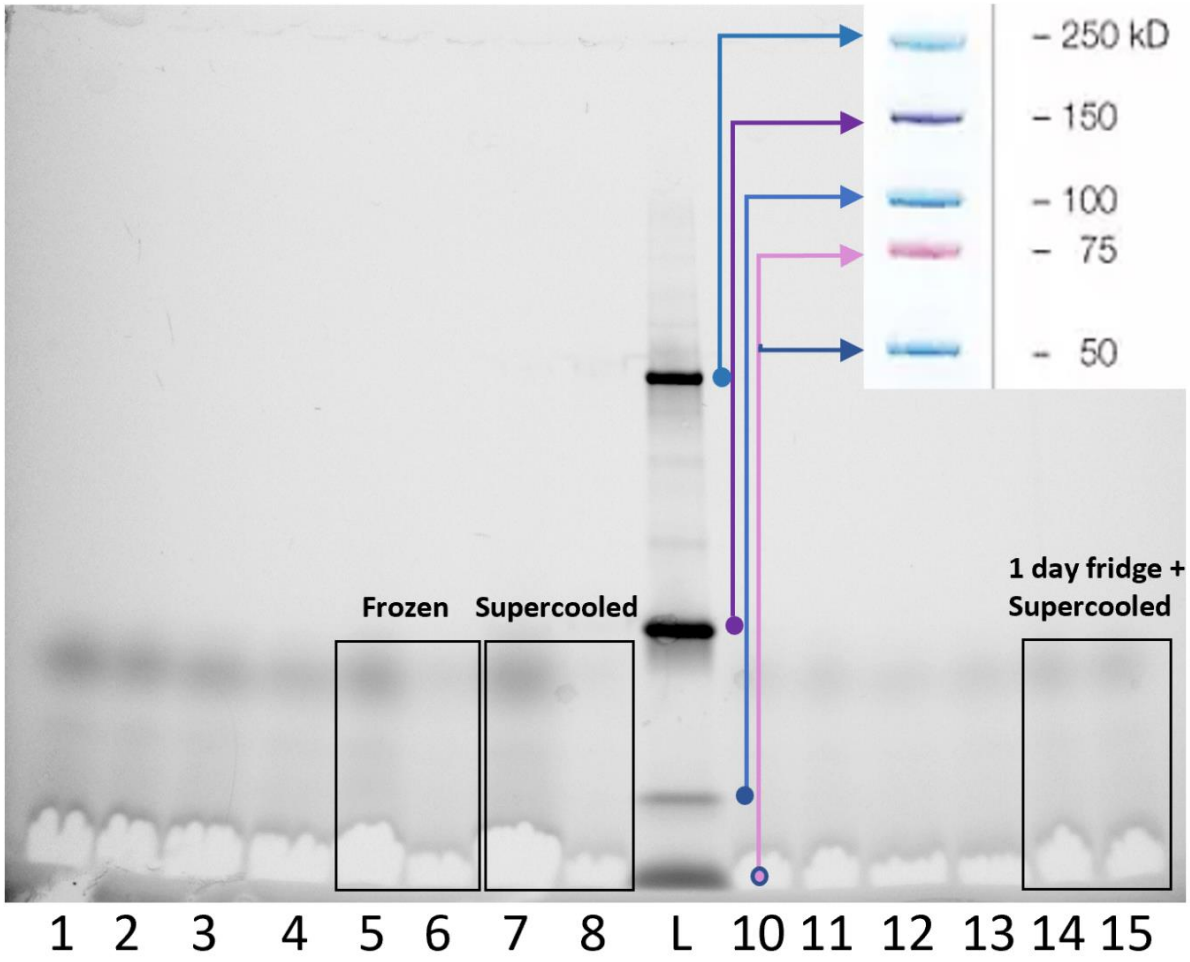

Figure 22 | Size distribution of nuclear proteins from a SDS-PAGE run. UT= *Untreated,* ***HS****= High-salt treated,* ***ICE****= Frozen,* ***SC****= Supercooled (>3h).* ***1****=UT RET,* ***2****=UT FIL,* ***3****=HS RET,* ***4****= HS FIL,* ***5****=ICE RET,* ***6****=ICE FIL, 7=SC RET,* ***8****=SC FIL,* ***L****=Ladder,* ***10****=UT RET*,* ***11****=UT FIL*,* ***12****=HS RET*,* ***13****= HS FIL*,* ***14****=SC RET*,* ***15****=SC FIL*. *nuclei from isolations at day 1 stored overnight. The weaker band densities in the samples from isolations at day 1 is due to a lower nuclei yield from that isolation and thus lower protein concentration. Image captured with the ChemiDoc™ imaging system using standard settings for Stain-free gels.*

A subjective interpretation of the above image in **Fig. 22** is that there was no difference amongst the samples from the independent isolations, except between the samples 5 → 6, and 7 → 8 from isolations at day 2 (processed the same day). They represent Frozen RET and FIL fractions, and Supercooled RET and FIL fractions, respectively. The signal difference could indicate a few more large proteins in the RET fractions compared to the FIL fractions. It also appears to be more small proteins in the RET fractions, possibly with less tryptophan as shown with the relative difference in the white bands at the bottom, interpreted as interference from CBB. This could mean that aggregates larger than 0.22µm have been stopped by the filter without disassembly by centrifugation. The fridge-stored nuclei from isolations at day 1

showed similar and very slight bands for both the RET and FIL fractions for all samples. If supercooling influences nucleoli, the lack of difference could be explained by a possible disassemble of potential nucleoli due to the inadequate storing, before supercooling. In other words, no structures remained to be influenced.

Regardless, a standardization of the sample loading scheme, based on empirical measures of protein concentrations, was not achieved in this thesis, although CBB is the basis for the Bradford assay used to determine protein concentrations. Since the interpretations of the image above is based on signal intensity, this limits the conclusions that can be drawn from it. The only samples that can be compared are those coming from the same starting material (same isolation) not treated with additional reagents, e.g., untreated, frozen and supercooled. No conclusions can be drawn from the high-salt treated samples or between the samples from the different dates. Due to the subjectivity in the interpretations of **Fig. 22**, it is not possible to conclude anything from the above image other than that the size of most proteins in the samples are below 150kDa. This is within the size limit of about 300kDa for most native proteins in the nucleus of animals (Wühr et al., 2015), indicating that the harsh conditions of the SDS-PAGE have dismantled any potential complexes.

3.2.3.2 Size test with BN-AGE

The size, in addition to shape and charge, are the physiochemical properties that electrophoresis relies on to separate particles in a solution by differences in migration through a gel, when an electrical field is applied. As both agarose and polyacrylamide gels are readily available and inexpensive due to their popularity, they serve as a highly attractive choices to separate large protein complexes by electrophoresis.

It was decided to test whether BN-AGE could be used to separate potential protein complexes in the supercooled sample and how it compares to an untreated sample. BN-AGE was originally developed as an optimization of a method called BN-PAGE, in order to separate large multi-protein complexes up to 10 **M**Da under native conditions (Henderson et al., 2000). The BN-PAGE method itself was introduced as a method to separate proteins under native pH conditions when the isoelectric points were not known in advance by utilizing a negative charge shift on the proteins (Schägger & Jagow, 1991). One of the compounds found to be most useful for inducing this charge shift was CBB, enabling the electrophoretic mobility of proteins towards the cathode at neutral pH (Schägger & Jagow, 1991). CBB undergoes a red shift in λ_{max} from 465 to 595 nm (Wenrich et al., 2012) when bound to protein, or nucleic

acids (Wenrich et al., 2012), and the absorbance can be used to distinguish bands in a gel from unbound dye or the gel itself, using a gel imager with built-in settings for detecting CBB.

For BN-AGE, preliminary testing with Tris-Glycine electrophoresis running solution resulted in the 0.3% agarose gel to melt at the high voltage used. The electrophoresis running solution were therefore replaced by low-molarity Lithium acetate to avoid melting the agarose gel, as it produces less heat during electrophoresis than Tris-containing buffers (Brody et al., 2004). The migration pattern of nuclear proteins from the final BN-AGE run is given in **Figure 23 B**.

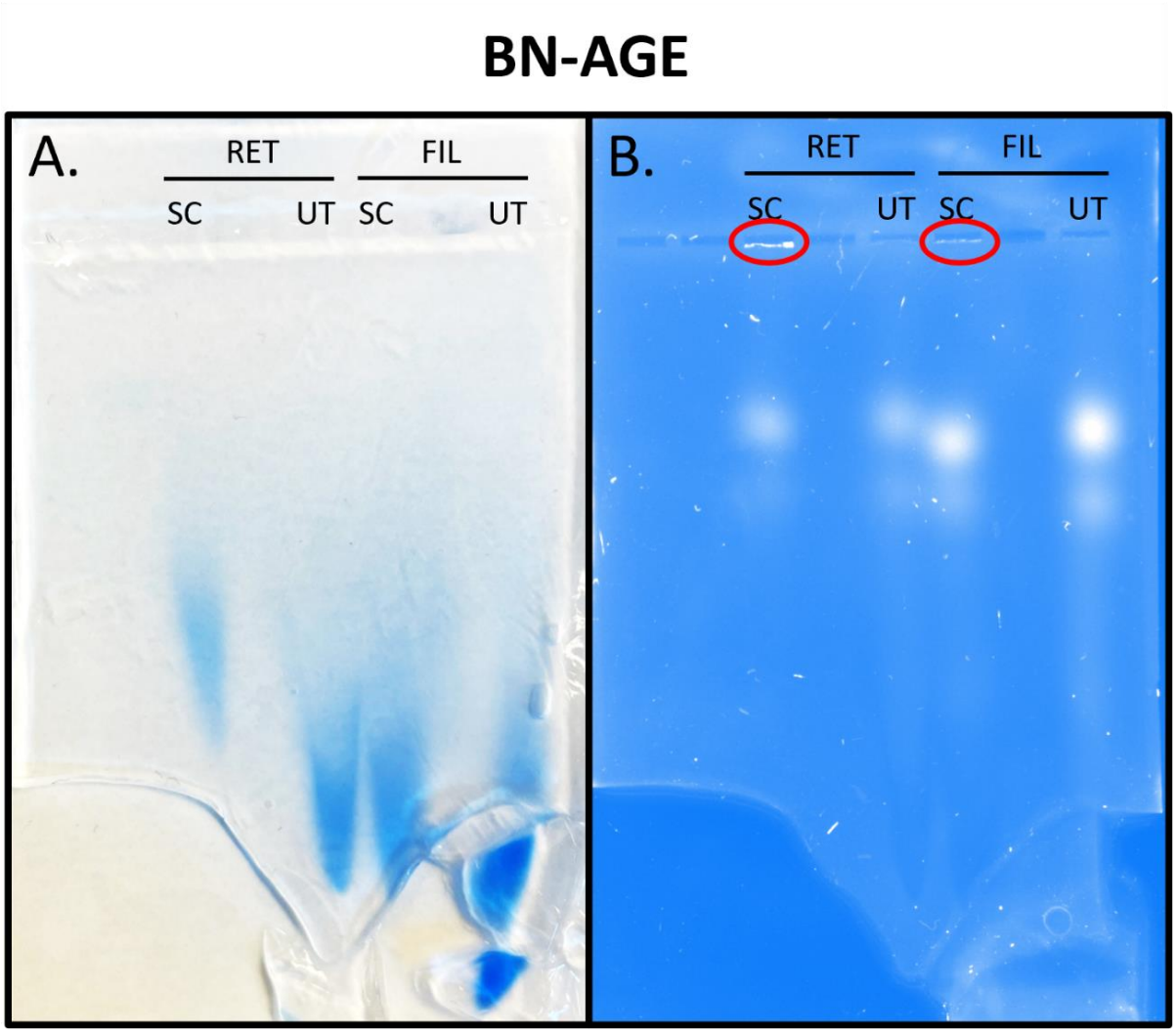

***Figure 23 | Migration pattern of nuclear proteins from a BN-AGE run. RET**= Retentate, **FIL**= Filtrate. **SC**= Supercooled, **UT**= Untreated. **A:** Image taken before placing the gel on the imaging plate. The dilute agarose gel was very fragile and broke when moving the gel onto the imaging plate. **B:** Image captured with the ChemiDoc™ imaging system using standard CBB-settings. **A&B:** Samples were nuclei suspensions from two independent isolations performed over two separate days, where the sample from the first isolation was supercooled overnight, while the second isolation was directly processed. Both samples were lysed with HRF and stained with the CBB containing quencher before separated by BN-AGE.*

A subjective interpretation of **Fig. 23 B** is that the nuclear proteins largely splits into a slower moving fraction, and a faster moving fraction trailing behind a slight smear in the front. It also appears to be a very slight difference in the travelled length between the RET (left) and the FIL (right) samples. However, the migration pattern is almost identical between the supercooled and untreated samples following BN-AGE (**Fig. 23 B**), in contrast to the possible difference in size distribution of proteins for untreated and supercooled nuclei following SDS-PAGE (**Fig. 22**). The only obvious difference between the samples following BN-AGE is that there is signal coming from both of the wells from the supercooled sample, indicating that some of the sample have not entered into the gel. As the signal is coming from the side of the well facing the direction of the anode, it is likely that this is a result of size limitations of the sample to enter the gel.

Interestingly, the smear in front of the faster moving fraction for the untreated sample and the SC FIL, is not easily visible in the SC RET. A subjective interpretation of this is that the smaller proteins expected in the smears are part of the supercooled sample withheld in the wells. Considering the interpretation of the SDS-PAGE (**Fig. 22**), where the RET-fraction of the supercooled sample appear to have more proteins lacking tryptophan in the lower size range, this could suggest that they are involved in supercooling-induced structures resisting disassemble by centrifugation.

Of note, Precision Plus Protein™ Kaleidoscope™ Prestained Protein Standards are usually able to enter such dilute agarose gels as used above, however it was not included in the BN-AGE. Regardless, considering that most proteins from the denaturing SDS-PAGE conditions were between 50-150kDa (**Fig. 22**), it can be argued that the proteins in the supercooled sample form centrifugation-resistant complexes greater in size than the largest proteins of 250kDa in the ladder known to enter such gels.

3.2.4 ANSWER TO RESEARCH QUESTION 2

The second goal of this master project was to *establish conditions to evaluate the effect of supercooling on nuclear bodies,* to answer if supercooling influence nuclear bodies such as the nucleolus, without other large scale nuclear changes. Both under hypo-osmotic conditions generated by dilution with Trypan blue, and conditions generated from HRF, freshly isolated nuclei expanded and the nucleoli rapidly dissolved. However, nuclei from supercooled samples retained their nucleolus-like structures, indicating that supercooling could have an effect. To see if the effect of supercooling was restricted to these nucleolus-like structures, it

was tested whether treatment with glutaraldehyde induces variations in the fixation pattern of supercooled nuclei compared to freshly isolated nuclei. After treatment with glutaraldehyde, or a combination of glutaraldehyde and HRF, core-like structures with varying but larger sizes than the initial nucleolus-like structures appeared similar to nucleoli in the centers of the nuclei. Such large cores did not appear in freshly isolated nuclei treated with glutaraldehyde, indicating that supercooling have induced a change likely involving proteins in the nucleolus-like structure.

It was further tested if the nucleolus-like structures in supercooled nuclei resisted centrifugation. Untreated and supercooled samples lysed by HRF, were filtered through a membrane with pore-size smaller than the nucleolus-like structures. By running the filtrate or retentate with SDS-PAGE and BN-AGE, it was interpreted that the retentate from the supercooled sample contained large centrifugation-resistant complexes containing mostly small proteins, potentially lacking tryptophan. Because low levels of tryptophan are common for disordered proteins, which nuclear bodies like the nucleolus is enriched for, this could indicate that supercooling maintain the structure of nuclear bodies to a certain degree, without other large scale nuclear changes.

3.3 CONCLUDING REMARKS AND FURTHER PERSPECTIVES

Preserving the native structure of nuclear bodies remain largely unachieved by assays commonly used in studies exploring genome topology today. In this thesis an alternative approach to achieve this was explored; supercooling. Both an optimized protocol for the isolation of high-quality Atlantic salmon hepatocyte nuclei, and a method for supercooling of nuclei to −15.3ºC without ice formation is described. The structural integrity and over-time stability of nuclei stored in supercooled conditions was investigated revealing unnoticeable deterioration after 15 days storage (the longest period tested). This indicates that supercooling could be used as an alternative to chemical cryopreservation for storing isolated nuclei. To date, the use of frozen, chemically cryopreserved gametes for species preservation and selective breeding purposes represents a gold standard, although research on cryopreserved cell genetic and epigenetic defects remain limited (Kratochvílová et al., 2018). The use of chemical cryopreservation in *in vitro* fertilization in humans has been suggested as a factor contributing to epigenetic modifications and changes in gene expression (Kratochvílová et al., 2018). If it can be confirmed that supercooling has a more limited effect, there are likely

unexploited opportunities not only for storing isolated nuclei, but gametes and other biological materials as well.

While supercooling at the temperatures used in this thesis is unable to irreversibly aggregate structured proteins, it may be that intrinsically disordered proteins enriched in nuclear bodies, such as nucleoli, can form irreversible aggregates at such temperatures, thereby preserving information about DNA-protein interactions within. Several conditions were tested in this thesis including hypo-osmosis, hydroxyl radical footprinting, glutaraldehyde and centrifugation, pointing to supercooling influencing the disorder enriched nucleoli without other large scale nuclear changes. Further investigations are required to confirm this. If found to be the case, then supercooling could not only be used for storing isolated nuclei, but possibly circumvent disadvantages, such as with chemical fixation, for the investigation of nuclear bodies. This could pave the way for the development of methods to separate dynamic nuclear body-associated genomic regions, without perturbing the overall chromatin structure.

4 REFERENCES

10x genomics, Inc. ("10x"). (n.d.). *How can I assess the quality of my nuclei for Single Cell ATAC or Single Cell Multiome ATAC+GEX Sequencing*. https://kb.10xgenomics.com/hc/en-us/articles/360020348651-How-can-I-assess-the-quality-of-my-nuclei-for-Single-Cell-ATAC-or-Single-Cell-Multiome-ATAC-GEX-Sequencing-. ●WEBPAGE

Amin, Anil B. (1991). *Histologisk atlas: normalstruktur hos laksefisk.* Akvapatologisk laboratorium, ISBN: 8299240603, s. 96, 112-113, 114-115. ●BOOK

An, H., de Meritens, C.R., & Shelkovnikova, T.A. (2021). Connecting the "dots": RNP granule network in health and disease. *Biochimica et biophysica acta. Molecular cell research, 1868*(8). https://doi.org/10.1016/j.bbamcr.2021.119058 ●REVIEW

Anchel, D., Ching, R.W., Cotton, R., Li, R., & Bazett-Jones, D.P. (2016). A novel single cell method to identify the genetic composition at a single nuclear body. *Scientific Reports, 6*(1). https://doi.org/10.1038/srep29191

AquaFaang (n.d.). *OmniATAC protocol using Frozen Tissue.* https://data.faang.org/api/fire_api/experiments/NMBU_SOP_OmniATAC_protocol_20200429.pdf. ●WEBPAGE

Avrameas, S., & Ternynck, T. (1969). The cross-linking of proteins with glutaraldehyde and its use for the preparation of immunoadsorbents. *Immunochemistry, 6(1)*, 53-66. https://doi.org/10.1016/0019-2791(69)90178-5

Baudement, M., Cournac, A., Court, F., Seveno, M., Parrinello, H., Reynès, C., Sabatier, R., Bouschet, T., Yi, Z., Sallis, S., Tancelin, M., Rebouissou, C., Cathala, G., Lesne, A., Mozziconacci, J., Journot, L., & Forné, T. (2018). High-salt–recovered

sequences are associated with the active chromosomal compartment and with large ribonucleoprotein complexes including nuclear bodies. *Genome Research*, *28*(11), 1733-1746. DOI: 10.1101/gr.237073.118

Begovich, K., & Wilhelm, J.E. (2020). An In Vitro Assembly System Identifies Roles for RNA Nucleation and ATP in Yeast Stress Granule Formation. *Molecular cell*, *79*(6), 991-1007. https://doi.org/10.1016/j.molcel.2020.07.017

Biochrom Ltd. (2020). *BIOCHROM Lithium Regeneration Buffer 6 SDS* (Ver 1.13). http://www.biochrom.co.uk/msds/English/(en-GB)80-2038-20_1.13.pdf ●WEBPAGE

Bio-Rad Laboratories, Inc. (n.d.(A)). *What is Stain-Free Imaging?*. https://www.bio-rad.com/en-no/applications-technologies/stain-free-imaging-technology?ID=NZ0G1815. ●WEBPAGE

Bio-Rad Laboratories, Inc. (n.d.(B)). *A Guide to Polyacrylamide Gel Electrophoresis and Detection* (Bulletin 6040 Ver C). https://www.bio-rad.com/webroot/web/pdf/lsr/literature/Bulletin_6040.pdf. ●WEBPAGE

Braem, C., Recolin, B., Rancourt, R.C., Angiolini, C., Barthès, P., Branchu, P., Court, F., Cathala, G., Ferguson-Smith, A.C., & Forné, T. (2008). Genomic Matrix Attachment Region and Chromosome Conformation Capture Quantitative Real Time PCR Assays Identify Novel Putative Regulatory Elements at the Imprinted Dlk1/Gtl2 Locus*. *Journal of Biological Chemistry*, *283*(27), 18612-18620. https://doi.org/10.1074/jbc.M801883200

Brody, J.R., Calhoun, E.S., Gallmeier, E., Creavalle, T.D., & Kern, S.E. (2004). Ultra-fast high-resolution agarose electrophoresis of DNA and RNA using low-molarity conductive media. *BioTechniques*, *37*(4), 598-602. https://doi.org/10.2144/04374ST04

Busch, H. (1967). [51] Isolation and purification of nuclei. *Methods in Enzymology*, *12*, 421-448. https://doi.org/10.1016/S0076-6879(67)12061-2

Byrne, J.M., Beamish, F.W., & Saunders, R.L. (1972). Influence of Salinity, Temperature, and Exercise on Plasma Osmolality and Ionic Concentration in Atlantic Salmon (Salmo salar). *Wsq: Women's Studies Quarterly*, *29*, 1217-1220.

Chen, T., Song, J., & Chan, H.S. (2015). Theoretical perspectives on nonnative interactions and intrinsic disorder in protein folding and binding. *Current opinion in structural biology*, *30*, 32-42. https://doi.org/10.1016/j.sbi.2014.12.002

Collins, J.S., & Goldsmith, T.H. (1981). Spectral properties of fluorescence induced by glutaraldehyde fixation. *The journal of histochemistry and cytochemistry: official journal of the Histochemistry Society*, *29*(3), 411-414. https://doi.org/10.1177/29.3.6787116

Compton, S.J., & Jones, C.G. (1985). Mechanism of dye response and interference in the Bradford protein assay. *Analytical biochemistry*, *151*(2), 369-374. https://doi.org/10.1016/0003-2697(85)90190-3

Corces, M.R., Trevino, A.E., Hamilton, E.G., Greenside, P., Sinnott-Armstrong, N.A., Vesuna, S., Satpathy, A.T., Rubin, A.J., Montine, K.S., Wu, B., Kathiria, A.S.,

Cho, S.W., Mumbach, M.R., Carter, A.C., Kasowski, M., Orloff, L.A., Risca, V.I., Kundaje, A., Khavari, P.A., Montine, T.J., Greenleaf, W.J., & Chang, H.Y. (2017). An improved ATAC-seq protocol reduces background and enables interrogation of frozen tissues. *Nature Methods, 14*(10), 959-962. https://doi.org/10.1038/nmeth.4396

Davidovic, M., Mattea, C., Qvist, J., & Halle, B. (2009). Protein cold denaturation as seen from the solvent. *Journal of the American Chemical Society, 131*(3), 1025-36. https://doi.org/10.1021/ja8056419

Deviri, D., & Safran, S.A. (2021). Physical theory of biological noise buffering by multicomponent phase separation. *Proceedings of the National Academy of Sciences, 118*(25). https://doi.org/10.1101/2021.01.05.425486

Eckmann, D.M., Ranganathan, A., Owiredu, S., & Jang, D.H. (2019). Compartmentalization of Bioenergetic Substrate Delivery in Intact Cells. *ASME Journal of Heat and Mass Transfer, 141*(5). https://doi.org/10.1115/1.4042186

Engler, A.J., Sen, S., Sweeney, H.L., & Discher, D.E. (2006). Matrix Elasticity Directs Stem Cell Lineage Specification. *Cell, 126*(4), 677-689. https://doi.org/10.1016/j.cell.2006.06.044

Evans, M.D., Dizdaroglu, M., & Cooke, M.S. (2004). Oxidative DNA damage and disease: induction, repair and significance. *Mutation research, 567*(1), 1-61. https://doi.org/10.1016/j.mrrev.2003.11.001

Feric, M., Vaidya, N., Harmon, T.S., Mitrea, D.M., Zhu, L., Richardson, T.M., Kriwacki, R.W., Pappu, R.V., & Brangwynne, C.P. (2016). Coexisting Liquid Phases Underlie Nucleolar Subcompartments. *Cell, 165*(7), 1686-1697. https://doi.org/10.1016/j.cell.2016.04.047

Floyd, R.A. (1983). Direct demonstration that ferrous ion complexes of di- and triphosphate nucleotides catalyze hydroxyl free radical formation from hydrogen peroxide. *Archives of biochemistry and biophysics, 225*(1), 263-270. https://doi.org/10.1016/0003-9861(83)90029-2

Ford, T.C., Graham, J., & Rickwood, D. (1994). Iodixanol: a nonionic iso-osmotic centrifugation medium for the formation of self-generated gradients. *Analytical biochemistry, 220*(2), 360-366. https://doi.org/10.1006/abio.1994.1350

Frege, T., & Uversky, V.N. (2015). Intrinsically disordered proteins in the nucleus of human cells. *Biochemistry and Biophysics Reports, 1*, 33-51. https://doi.org/10.1016/j.bbrep.2015.03.003

Garaizar, A., Sanchez-Burgos, I., Collepardo-Guevara, R., & Espinosa, J.R. (2020). Expansion of Intrinsically Disordered Proteins Increases the Range of Stability of Liquid–Liquid Phase Separation. *Molecules, 25*(20), 1-18. https://doi.org/10.3390/molecules25204705

Gialitakis, M., Arampatzi, P., Makatounakis, T., & Papamatheakis, J. (2010). Gamma Interferon-Dependent Transcriptional Memory via Relocalization of a Gene Locus to PML Nuclear Bodies. *Molecular and Cellular Biology, 30*(8), 2046-2056. https://doi.org/10.1128/MCB.00906-09

Graham, J.M. (1993). The isolation of nuclei and nuclear membranes from rat liver. *Methods in molecular biology, 19*, 19-28. https://doi.org/10.1385/0-89603-236-1:19

Görisch, S.M., Wachsmuth, M., Ittrich, C., Bacher, C.P., Rippe, K., & Lichter, P. (2004). Nuclear body movement is determined by chromatin accessibility and dynamics. *Proceedings of the National Academy of Sciences of the United States of America, 101*(36), 13221-13226. https://doi.org/10.1073/pnas.0402958101

Hancock, R. (2004). A role for macromolecular crowding effects in the assembly and function of compartments in the nucleus. *Journal of structural biology, 146*(3), 281-290. https://doi.org/10.1016/j.jsb.2003.12.008

Henderson, N.S., Nijtmans, L.G., Lindsay, J.G., Lamantea, E., Zeviani, M., & Holt, I.J. (2000). Separation of intact pyruvate dehydrogenase complex using blue native agarose gel electrophoresis. *ELECTROPHORESIS, 21*(14), 2925-2931. https://doi.org/10.1002/1522-2683(20000801)21:14%3C2925::AID-ELPS2925%3E3.0.CO;2-2

Henninger, J.E., Oksuz, O., Shrinivas, K., Sagi, I., Leroy, G., Zheng, M.M., Andrews, J.O., Zamudio, A.V., Lazaris, C., Hannett, N.M., Lee, T., Sharp, P.A., Cissé, I.I., Chakraborty, A.K., & Young, R.A. (2020). RNA-Mediated Feedback Control of Transcriptional Condensates. *Cell, 184*(1), 207-225. https://doi.org/10.1016/j.cell.2020.11.030

Herrmann, C., Avgousti, D.C., & Weitzman, M.D. (2017). Differential Salt Fractionation of Nuclei to Analyze Chromatin-associated Proteins from Cultured Mammalian Cells. *Bio-protocol, 7*(6). DOI: 10.21769/BioProtoc.2175

Hoffman, L.M., Smith, M.A., Jensen, C.C., Yoshigi, M., Blankman, E., Ullman, K.S., & Beckerle, M.C. (2020). Mechanical stress triggers nuclear remodeling and the formation of transmembrane actin nuclear lines with associated nuclear pore complexes. *Molecular Biology of the Cell, 31*(16), 1774-1787. DOI: 10.1091/mbc.E19-01-0027

Hopwood, D. (2005). The reactions of glutaraldehyde with nucleic acids. *The Histochemical Journal, 7*(3), 267-276. https://doi.org/10.1007/BF01003595

Huang, H., Yarmush, M.L., & Usta, O.B. (2018). Long-term deep-supercooling of large-volume water and red cell suspensions via surface sealing with immiscible liquids. *Nature Communications, 9*(1). https://doi.org/10.1038/s41467-018-05636-0

Irgen-Gioro, S., Yoshida, S., Walling, V., & Chong, S. (2022). Fixation can change the appearance of phase separation in living cells. *eLife, 11*. https://doi.org/10.7554/eLife.79903

Irianto, J., Swift, J., Martins, R.P., McPhail, G.D., Knight, M.M., Discher, D.E., & Lee, D.A. (2013). Osmotic challenge drives rapid and reversible chromatin condensation in chondrocytes. *Biophysical journal, 104*(4), 759-769. https://doi.org/10.1016/j.bpj.2013.01.006

Kang, J., Lim, L., & Song, J. (2018). ATP enhances at low concentrations but dissolves at high concentrations liquid-liquid phase separation (LLPS) of ALS/FTD-causing

FUS. *Biochemical and biophysical research communications, 504*(2), 545-551. https://doi.org/10.1016/j.bbrc.2018.09.014

Kiani, K., Sanford, E.M., Goyal, Y., & Raj, A. (2022). Changes in chromatin accessibility are not concordant with transcriptional changes for single-factor perturbations. *Molecular Systems Biology, 18*(9). https://doi.org/10.15252/msb.202210979

Kimble Chase Life Science & Research Products, LLC (n.d.). *TISSUE GRINDERS (20140701KC-1278).* http://www.kimble-chase.com/literature/TissueGrinders.pdf. ●WEBPAGE

Krainer, G., Welsh, T.J., Joseph, J.A., Espinosa, J.R., Wittmann, S., Csilléry, E.D., Sridhar, A.M., Toprakcioglu, Z., Gudiškytė, G., Czekalska, M.A., Arter, W.E., George-Hyslop, P.S., Hyman, A.A., Collepardo-Guevara, R., Alberti, S., & Knowles, T.P. (2020). Reentrant liquid condensate phase of proteins is stabilized by hydrophobic and non-ionic interactions. *Nature Communications, 12*(1). https://doi.org/10.1038/s41467-021-21181-9

Kratochvílová, I., Kopecna, O., Bačíková, A., Pagáčová, E., Falková, I., Follett, S.E., Elliott, K.W., Varga, K., Golan, M., & Falk, M. (2018). Changes in Cryopreserved Cell Nuclei Serve as Indicators of Processes during Freezing and Thawing. *Langmuir : the ACS journal of surfaces and colloids, 35*(23), 7496-7508. https://doi.org/10.1021/acs.langmuir.8b02742

Kuban-Jankowska, A., Gorska, M.M., Jaremko, L., Jaremko, M., Tuszynski, J.A., & Wozniak, M. (2015). The physiological concentration of ferrous iron (II) alters the inhibitory effect of hydrogen peroxide on CD45, LAR and PTP1B phosphatases. *Biometals, 28*(6), 975-986. https://doi.org/10.1007/s10534-015-9882-4

Kumaran, R. I., & Spector, D. L. (2008). A genetic locus targeted to the nuclear periphery in living cells maintains its transcriptional competence. *The Journal of Cell Biology, 180*(1), 51-65. https://doi.org/10.1083/jcb.200706060

Kurotani, A., Tokmakov, A.A., Sato, K., Stefanov, V.E., Yamada, Y., & Sakurai, T. (2019). Localization-specific distributions of protein pI in human proteome are governed by local pH and membrane charge. *BMC Molecular and Cell Biology, 20*(36). https://doi.org/10.1186/s12860-019-0221-4

Kurzbach, D., Platzer, G., Schwarz, T.C., Henen, M.A., Konrat, R., & Hinderberger, D. (2013). Cooperative Unfolding of Compact Conformations of the Intrinsically Disordered Protein Osteopontin. *Biochemistry, 52*(31), 5167-5175. https://doi.org/10.1021/bi400502c

Küffner, A.M., Linsenmeier, M., Grigolato, F., Prodan, M., Zuccarini, R., Capasso Palmiero, U., Faltova, L., & Arosio, P. (2021). Sequestration within biomolecular condensates inhibits Aβ-42 amyloid formation†. *Chemical Science, 12*(12), 4373-4382. https://doi.org/10.1039/D0SC04395H

Leamy, K.A., Yennawar, N.H., & Bevilacqua, P.C. (2017). Cooperative RNA Folding under Cellular Conditions Arises From Both Tertiary Structure Stabilization and

Secondary Structure Destabilization. *Biochemistry, 56*(27), 3422-3433. https://doi.org/10.1021/acs.biochem.7b00325

Lebkowski, J.S., & Laemmli, U.K. (1982A). Non-histone Proteins and Long-range Organization of HeLa Interphase DNA. *Journal of molecular biology, 156*(2). 325-344. https://doi.org/10.1016/0022-2836(82)90332-1

Lebkowski, J.S., & Laemmli, U.K. (1982B). Evidence for two levels of DNA folding in histone-depleted HeLa interphase nuclei. *Journal of molecular biology, 156*(2), 309-324. https://doi.org/10.1016/0022-2836(82)90331-X

Li, J., Rajagopalan, R., & Jiang, J. (2008). Role of solvent in protein phase behavior: Influence of temperature dependent potential. *The Journal of chemical physics, 128*(23), 235104, 235104-1 - 235104-6. https://doi.org/10.1063/1.2943204

Lien, S., Koop, B.F., Sandve, S.R., Miller, J.R., Kent, M.P., Nome, T., Hvidsten, T.R., Leong, J.S., Minkley, D.R., Zimin, A.V., Grammes, F., Grove, H., Gjuvsland, A.B., Walenz, B.P., Hermansen, R.A., Schalburg, K.V., Rondeau, E.B., Génova, A.D., Samy, J.K., Vik, J.O., Vigeland, M.D., Caler, L., Grimholt, U., Jentoft, S., Våge, D.I., Jong, P.J., Moen, T., Baranski, M., Palti, Y., Smith, D.R., Yorke, J.A., Nederbragt, A.J., Tooming-Klunderud, A., Jakobsen, K.S., Jiang, X., Fan, D., Hu, Y., Liberles, D.A., Vidal, R., Iturra, P., Jones, S.J., Jonassen, I., Maass, A., Omholt, S.W., & Davidson, W.S. (2016). The Atlantic salmon genome provides insights into rediploidization. *Nature, 533*(7602), 200-205. https://doi.org/10.1038/nature17164

Litus, E.A., Permyakov, S.E., Uversky, V.N., & Permyakov, E.A. (2018). Intrinsically Disordered Regions in Serum Albumin: What Are They For? *Cell Biochemistry and Biophysics, 76*, 39-57. https://doi.org/10.1007/s12013-017-0785-6

Lovtrup-rein, H., & McEwen, B.S. (1966). ISOLATION AND FRACTIONATION OF RAT BRAIN NUCLEI. *The Journal of Cell Biology, 30*(2), 405-415. https://doi.org/10.1083/jcb.30.2.405

Lyon, C.E., & Lamond, A.I. (2000). The nucleolus. *Current Biology, 10*. https://doi.org/10.1016/S0960-9822(00)00455-3

Mansisidor, A.R., & Risca, V.I. (2022). Chromatin accessibility: methods, mechanisms, and biological insights. *Nucleus, 13*(1), 238-278. https://doi.org/10.1080/19491034.2022.2143106

Mathias, A., & Wynter, C.V. (1973). The uses of metrizamide in the fractionation of nuclei from brain and liver tissue by zonal centrifugation. *FEBS Letters, 33*(1), 18-22. https://doi.org/10.1016/0014-5793(73)80149-8

Matsufuji, H., & Shibamoto, T. (2004). The role of EDTA in malonaldehyde formation from DNA oxidized by Fenton reagent systems. *Journal of Agricultural and Food Chemistry, 52*(10), 3136-3140. https://doi.org/10.1021/jf035337+

Meng, F., Na, I., Kurgan, L., & Uversky, V.N. (2015). Compartmentalization and Functionality of Nuclear Disorder: Intrinsic Disorder and Protein-Protein Interactions in Intra-Nuclear Compartments. *International Journal of Molecular Sciences, 17*(1). https://doi.org/10.3390/ijms17010024

Mitrea, D.M., Cika, J., Stanley, C.B., Nourse, A., Onuchic, P.L., Banerjee, P.R., Phillips, A.H., Park, C., Deniz, A.A., & Kriwacki, R.W. (2018). Self-interaction of NPM1 modulates multiple mechanisms of liquid–liquid phase separation. *Nature Communications, 9(1)*. https://doi.org/10.1038/s41467-018-03255-3

Miyagi, T., Yamazaki, R., Ueda, K., Narumi, S., Hayamizu, Y., Uji-i, H., Kuroda, M., & Kanekura, K. (2022). The Patterning and Proportion of Charged Residues in the Arginine-Rich Mixed-Charge Domain Determine the Membrane-Less Organelle Targeted by the Protein. *International Journal of Molecular Sciences, 23*(14). https://doi.org/10.3390/ijms23147658

Moses, D., Yu, F., Ginell, G.M., Shamoon, N.M., Koenig, P., Holehouse, A.S., & Sukenik, S. (2020). Revealing the Hidden Sensitivity of Intrinsically Disordered Proteins to their Chemical Environment. *The journal of physical chemistry letters*, *11*(23), 10131-10136. https://doi.org/10.1021/acs.jpclett.0c02822

Mota, V.C., Nilsen, T.O., Gerwins, J., Gallo, M., Kolarevic, J., Krasnov, A., & Terjesen, B.F. (2020). Molecular and physiological responses to long-term carbon dioxide exposure in Atlantic salmon (Salmo salar). *Aquaculture, 519*. https://doi.org/10.1016/j.aquaculture.2019.734715

Naughton, C., Avlonitis, N., Corless, S., Prendergast, J.G., Mati, I.K., Eijk, P.P., Cockroft, S.L., Bradley, M., Ylstra, B., & Gilbert, N. (2013). Transcription forms and remodels supercoiling domains unfolding large-scale chromatin structures. *Nature structural & molecular biology, 20*(3), 387-395. https://doi.org/10.1038/nsmb.2509

Nava, M.M., Miroshnikova, Y.A., Biggs, L.C., Whitefield, D.B., Metge, F., Bouças, J., Vihinen, H., Jokitalo, E., Li, X., García Arcos, J.M., Hoffmann, B., Merkel, R., Niessen, C.M., Dahl, K.N., & Wickström, S.A. (2020). Heterochromatin-Driven Nuclear Softening Protects the Genome against Mechanical Stress-Induced Damage. *Cell, 181*(4), 800 - 817. https://doi.org/10.1016/j.cell.2020.03.052

Nolin, F., Michel, J., Wortham, L., Tchélidzé, P., Balossier, G., Banchet, V., Bobichon, H., Lalun, N., Terryn, C., & Ploton, D. (2013). Changes to cellular water and element content induced by nucleolar stress: investigation by a cryo-correlative nano-imaging approach. *Cellular and Molecular Life Sciences, 70*(13), 2383-2394. DOI: 10.1007/s00018-013-1267-7

Nomoto, A., Nishinami, S., & Shiraki, K. (2021). Solubility Parameters of Amino Acids on Liquid–Liquid Phase Separation and Aggregation of Proteins. *Frontiers in Cell and Developmental Biology, 9*. https://doi.org/10.3389/fcell.2021.691052

Paloni, M, Bussi, G, Barducci, A. (2021). Arginine multivalency stabilizes protein/RNA condensates. *Protein Science*, *30*(7), 1418-1426. https://doi.org/10.1002/pro.4109

Pandya-Jones, A., Markaki, Y., Serizay, J., Chitiashvili, T., Mancia Leon, W.R., Damianov, A., Chronis, C., Papp, B., Chen, C., McKee, R., Wang, X., Chau, A.C., Sabri, S., Leonhardt, H., Zheng, S., Guttman, M., Black, D.L., & Plath, K. (2020). A protein assembly mediates Xist localization and gene silencing. *Nature, 587*(7832), 145-151. https://doi.org/10.1038/s41586-020-2703-0

Pawełczyk, T., Easom, R.A., & Olson, M.S. (1994). The dependence of electrophoretic and spectroscopic properties of the pyruvate dehydrogenase complex on mono-

and divalent ions. *Acta biochimica Polonica*, *41*(1), 63-72. https://doi.org/10.18388/abp.1994_4775

Phengchat, R., Takata, H., Morii, K., Inada, N., Murakoshi, H., Uchiyama, S., & Fukui, K. (2016). Calcium ions function as a booster of chromosome condensation. *Scientific Reports*, *6*(1). https://doi.org/10.1038/srep38281

Quail, T., Golfier, S., Elsner, M., Ishihara, K., Murugesan, V., Renger, R., Jülicher, F., & Brugués, J. (2021). Force generation by protein–DNA co-condensation. *Nature Physics*, *17*(9), 1007-1012. https://doi.org/10.1038/s41567-021-01285-1

Riback, J.A., Bowman, M.A., Zmyslowski, A.M., Knoverek, C.R., Jumper, J.M., Hinshaw, J.R., Kaye, E.B., Freed, K.F., Clark, P.L., & Sosnick, T.R. (2017). Innovative scattering analysis shows that hydrophobic disordered proteins are expanded in water. *Science, 358*(6360), 238-241. DOI: 10.1126/science.aan5774

Riback, J.A., Zhu, L., Ferrolino, M.C., Tolbert, M., Mitrea, D.M., Sanders, D.W., Wei, M.T., Kriwacki, R.W., & Brangwynne, C.P. (2020). Composition-dependent thermodynamics of intracellular phase separation. *Nature, 581*(7807), 209-214. https://doi.org/10.1038/s41586-020-2256-2

Rivière, J., Ravanat, J., & Wagner, J.R. (2006). Ascorbate and H2O2 induced oxidative DNA damage in Jurkat cells. *Free radical biology & medicine, 40*(12*)*, 2071-2079. https://doi.org/10.1016/j.freeradbiomed.2006.02.003

Roche Diagnostics (2004). *The Complete Guide for Protease Inhibition (12/04)*.https://iti.stanford.edu/content/dam/sm/iti/documents/himc/immunoassays/ProteaseInhibitionGuide.pdf. ●WEBPAGE

Roy, B., Venkatachalapathy, S., Ratna, P., Wang, Y., Jokhun, D.S., Nagarajan, M., & Shivashankar, G.V. (2018). Laterally confined growth of cells induces nuclear reprogramming in the absence of exogenous biochemical factors. *Proceedings of the National Academy of Sciences of the United States of America, 115*(21), E4741-E4750. https://doi.org/10.1073/pnas.1714770115

Sabari, B.R., Dall'Agnese, A., Boija, A., Klein, I.A., Coffey, E.L., Shrinivas, K., Abraham, B.J., Hannett, N.M., Zamudio, A.V., Manteiga, J.C., Li, C.H., Guo, Y.E., Day, D.S., Schuijers, J., Vasile, E., Malik, S., Hnisz, D., Lee, T., Cissé, I.I., Roeder, R.G., Sharp, P.A., Chakraborty, A.K., & Young, R.A. (2018). Coactivator condensation at super-enhancers links phase separation and gene control. *Science, 361*(6400). DOI: 10.1126/science.aar3958

Sasmal, D.K., Ghosh, S., Das, A.K., & Bhattacharyya, K. (2013). Solvation dynamics of biological water in a single live cell under a confocal microscope. *Langmuir: the ACS journal of surfaces and colloids, 29*(7), 2289-2298. https://doi.org/10.1021/la3043473

Schwanbeck, R., Xiao, H., & Wu, C. (2004). Spatial Contacts and Nucleosome Step Movements Induced by the NURF Chromatin Remodeling Complex*. *Journal of Biological Chemistry*, *279*(38), 39933-39941. https://doi.org/10.1074/jbc.M406060200

Schägger, H., & von Jagow, G. (1991). Blue native electrophoresis for isolation of membrane protein complexes in enzymatically active form. *Analytical biochemistry, 199*(2), 223-231. https://doi.org/10.1016/0003-2697(91)90094-A

Shin, Y., Chang, Y., Lee, D.S., Berry, J.D., Sanders, D.W., Ronceray, P., Wingreen, N.S., Haataja, M.P., & Brangwynne, C.P. (2018). Liquid Nuclear Condensates Mechanically Sense and Restructure the Genome. *Cell, 175*(6), 1481-1491. https://doi.org/10.1016/j.cell.2018.10.057

Song, J. (2021). Adenosine triphosphate energy-independently controls protein homeostasis with unique structure and diverse mechanisms. *Protein Science, 30*(7), 1277-1293. https://doi.org/10.1002/pro.4079 ●REVIEW

Stephens, A.D., Liu, P.Z., Kandula, V., Chen, H., Almassalha, L.M., Herman, C., Backman, V., O'Halloran, T.V., Adam, S.A., Goldman, R.D., Banigan, E.J., & Marko, J.F. (2019). Physicochemical mechanotransduction alters nuclear shape and mechanics via heterochromatin formation. *Molecular Biology of the Cell, 30*(17), 2320-2330. https://doi.org/10.1091/mbc.E19-05-0286

Stevens, R., Stevens, L., & Price, N.C. (1983). The stabilities of various thiol compounds used in protein purifications. *Biochemical Education, 11*(2), 70-70. https://doi.org/10.1016/0307-4412(83)90048-1

Szyperski, T., Mills, J.L., Perl, D., & Balbach, J. (2006). Combined NMR-observation of cold denaturation in supercooled water and heat denaturation enables accurate measurement of ΔCp of protein unfolding. *European Biophysics Journal, 35*(4), 363-366. https://doi.org/10.1007/s00249-005-0028-4

Søderstrøm, S., Lie, K.K., Lundebye, A.K., & Søfteland, L. (2022). Beauvericin (BEA) and enniatin B (ENNB)-induced impairment of mitochondria and lysosomes - Potential sources of intracellular reactive iron triggering ferroptosis in Atlantic salmon primary hepatocytes. *Food and Chemical Toxicology, 161*. https://doi.org/10.1016/j.fct.2022.112819

Tedeschi, G., Mangiagalli, M., Chmielewska, S., Lotti, M., Natalello, A., & Brocca, S. (2017). Aggregation properties of a disordered protein are tunable by pH and depend on its net charge per residue. *Biochimica et biophysica acta. General subjects, 1861*(11), 2543-2550. https://doi.org/10.1016/j.bbagen.2017.09.002

Tullius, T.D., & Dombroski, B. (1986). Hydroxyl radical "footprinting": high-resolution information about DNA-protein contacts and application to lambda repressor and Cro protein. *Proceedings of the National Academy of Sciences of the United States of America, 83*(15), 5469-5473. DOI: 10.1073/pnas.83.15.5469

Vicioso-Mantis, M., Fueyo, R., Navarro, C., Cruz-Molina, S., van IJcken, W.F., Rebollo, E., Rada-Iglesias, Á., & Martínez-Balbás, M.A. (2022). JMJD3 intrinsically disordered region links the 3D-genome structure to TGFβ-dependent transcription activation. *Nature Communications, 13*(1). https://doi.org/10.1038/s41467-022-30614-y

Vogelstein, B., Pardoll, D.M., & Coffey, D.S. (1980). Supercoiled loops and eucaryotic DNA replication. *Cell, 22*(1), 79-85. https://doi.org/10.1016/0092-8674(80)90156-7

von Storp, B., Engel, A., Boeker, A., Ploeger, M.J., & Langer, K. (2012). Albumin nanoparticles with predictable size by desolvation procedure. *Journal of Microencapsulation, 29*(2), 138-146. https://doi.org/10.3109/02652048.2011.635218

Weber, M., Hagège, H., Murrell, A., Brunel, C., Reik, W., Cathala, G., & Forné, T. (2003). Genomic Imprinting Controls Matrix Attachment Regionsin the Igf2Gene. *Molecular and Cellular Biology, 23*(24), 8953-8959. https://doi.org/10.1128/MCB.23.24.8953-8959.2003

Wuttke, R., Hofmann, H., Nettels, D., Borgia, M.B., Mittal, J., Best, R.B., & Schuler, B. (2014). Temperature-dependent solvation modulates the dimensions of disordered proteins. *Proceedings of the National Academy of Sciences, 111*(14), 5213-5218. https://doi.org/10.1073/pnas.1313006111

Wühr, M., Güttler, T., Peshkin, L., McAlister, G.C., Sonnett, M., Ishihara, K., Groen, A.C., Presler, M., Erickson, B.K., Mitchison, T.J., Kirschner, M.W., & Gygi, S.P. (2015). The Nuclear Proteome of a Vertebrate. *Current Biology, 25*(20), 2663-2671. https://doi.org/10.1016/j.cub.2015.08.047

Zhao, B., & Kurgan, L. (2022). Compositional Bias of Intrinsically Disordered Proteins and Regions and Their Predictions. *Biomolecules, 12*(7). https://doi.org/10.3390/biom12070888

Zhao, B., Katuwawala, A., Uversky, V.N., & Kurgan, L. (2020). IDPology of the living cell: intrinsic disorder in the subcellular compartments of the human cell. *Cellular and Molecular Life Sciences, 78*(5), 2371-2385. https://doi.org/10.1007/s00018-020-03654-0

Zhou, Q., Usluer, S., Zhang, F., Lenard, A.J., Bourgeois, B.M., & Madl, T. (2021). ATP regulates RNA-driven cold inducible RNA binding protein phase separation. *Protein Science: A Publication of the Protein Society, 30*(7), 1438-1453. https://doi.org/10.1002/pro.4123

Öner, L., & Groves, M.J. (1993). Properties of Human Albumin Microparticles Prepared by a Chilled Cross-linking Technique. *Journal of Pharmacy and Pharmacology, 45*(10), 866-870. https://doi.org/10.1111/j.2042-7158.1993.tb05610.x

Appendix

APPENDIX A: BIOLOGICAL SAMPLES

Samples: The samples J11 (9 months old sexually immature female) and J7 (7 months old sexually immature male) were reported obtained from healthy domesticated diploid gonochoric Atlantic salmon supplied by AquaGen, fed with Nutra XP 0,7/Sprint 1,0/Olympic 1,5/ Nutra RC2, and kept in a closed water system (recirculatory) with controlled parameters (density in tank: 0,011 kg/l, water temperature: 7.5^{o}C, Oxygen: 8.07 mg/l, Salinity: 0, Photoperiod 24L:0D). The fishes were starved for 24 hours before being killed using a Schedule 1 method following the Animals (Scientific Procedures) Act of 1986, in accordance with the Norwegian Animal Welfare Act of 2010, of which the fishes were euthanized with a lethal dose of Tricaine methanesulfonate (MS-222). The livers were subsequently removed from the fishes after cutting the hepatic vein and washed in a PBS filled petri dish. The livers were transferred to a second petri dish containing fresh PBS and minced into small 20-30 mg chunks using a sterilized scalpel, and snap-freezed on dry ice. The pieces were distributed into two tubes for each liver as technical replicates marked L1/L2. The tubes were stored directly in −80^{o}C until use.

APPENDIX B: READY-TO-USE REAGENTS AND KITS

Disclaimers: Some reagents/kits are composed of several chemical substances and therefore lack a CAS number, in those cases the manufacturer of the reagent used in-lab is given. For all substances with a CAS number, the molecular formula is written as Hill notation, except chemicals where the linear formula is the most commonly used.

4–15% Mini-PROTEAN™ TGX Stain-Free™ Protein Gels, 15 well, 15 µl (Bio-RAD, Cat. No.: #4568086)

cOmplete^{TM}, EDTA-free Protease inhibitor cocktail tablets (Roche. Ref: 05056489001). Stored according to package label in the fridge (⚠**CRITICAL**).

Glacial acetic acid [CH_3COOH. Synonym: Acetic acid (pure*). CAS No.: 64-19-7. Molecular Weight: 60.05g/mol]. *Acetic acid can contain a significant amount of water, whereas glacial acetic acid contains less than 1% water and thus regarded as pure.

Glutardialdehyde [$OHC(CH_2)_3CHO$. Synonyms: Glutaraldehyde solution, Glutaric dialdehyde solution, Pentane-1,5-dial. CAS No.: 111-30-8. Molecular Weight: 100.12 g/mol] , 50% solution in water.

Glycerol, 100% [$C_3H_8O_3$. CAS No.: 56-81-5. Molecular Weight: 92.09 g/mol].

HEPES Zwitterionic Organic Chemical buffer solution [$C_8H_{18}N_2O_4S$. Synonym(s): N-2-Hydroxyethylpiperazine-N-2-Ethane Sulfonic Acid. CAS No.: 7365-45-9. Molecular Weight: 238.30 g/mol], 1 M in dH_2O, pH range 7.2 to 7.5. Stored according to bottle label in the fridge.

Hydrochloric acid [HCl. Synonym: Hydrogen chloride solution. CAS No.: 7647-01-0. Molecular weight: 36.46 g/mol] solution, 12 N.

Hydrogen peroxide solution [H_2O_2. CAS No.: 7722-84-1. Molecular weight: 34.01 g/mol], 30% (w/w) in dH_2O. Stored according to bottle label in the fridge shielded from light (⚠ **CRITICAL**).

Lithium Regeneration Buffer 6 (Biochrom Ltd. Ref: 80-2038-20), 1.3 w/w% Lithium hydroxide (monohydrate) [$LiOH \cdot H_2O$. Synonym: Lithine hydrate. CAS No.: 1310-66-3. Molecular Weight: 41.96g/mol]. Stored according to the bottle label shielded from light (⚠ **CRITICAL**).

Magnesium Chloride [MgCl2. CAS No.: 7786-30-3. Molecular Weight: 95.211 g/mol], 1M in dH20.

OptiPrep Density Gradient Medium [$C_{35}H_{44}I_6N_6O_{15}$. CAS No.: 92339-11-2. Molecular Weight: 1550.18 g/mol], 60% (w/v) solution of iodixanol in water (sterile). Stored according to the bottle label shielded from light (⚠**CRITICAL**).

Phosphate buffered saline (PBS), 0.01M in dH_2O, pH 7.4. Similar to 137 mM NaCl, 2.7 mM KCl, 8 (or 10) mM Na_2HPO_4, 2 (or 1.76) mM KH_2PO_4. Example: 10X PBS Buffer (Thermo scientific. AM9625) diluted to 1X.

Precision Plus Protein™ Kaleidoscope™ Prestained Protein Standards (Bio-RAD, Cat. No.: #1610375).

SDS-PAGE Running buffer, 30.0 g Tris base, 144.0 g glycine, and 10.0 g SDS in 1000 ml of dH2O, pH 8.3. Example: 10x Tris/Glycine/SDS premixed electrophoresis buffer (Bio-RAD, Cat. No.: #1610732).

Triton™ X-100 [$C_{14}H_{22}O(C_2H_4O)n(n=9-10)$. CAS No.: 9002-93-1. Specific gravity: 1.065 at 25°C. Approximate molecular weight = 625 g/mol, giving effective molarity = 1.7 M for the liquid].

Trizma® hydrochloride [$C_4H_{11}NO_3 \cdot HCl$. Synonym: Tris-HCl. CAS No.: 1185-53-1. Molecular Weight: 157.60 g/mol] solution, 1.0 M, pH 7.4/7.8/8.0.

Trypan blue staining dye, 0.4% [$C_{34}H_{24}N_6Na_4O_{14}S_4$. CAS No.: 72-57-1. Molecular weight: 960.82 g/mol]. Stored at room temperature according to bottle label.

White mineral oil* [CAS No.: 8042-47-5]. *Commercially available as both a light and heavy fraction depending on the ratio of saturated and aromatic hydrocarbons. They have different uses and both types were used in this thesis.

APPENDIX C: PREPARED STOCK SOLUTIONS

Disclaimers: Some very viscous solutions were prepared to w/v (weight of solute per final solution volume) instead of v/v (volume of reagent per final solution volume) for accuracy and ease. When a volumetric flask was used for preparing specific solutions, any plastic stopper or similar used during twirling was removed some minutes before making the final volume adjustment, to include solution trapped by the stopper moving slowly down the neck of the flask. Sterile filtration using a 0.22-µm polyvinylidene difluoride (PVDF) filter system is recommended for all stock solutions, especially for sucrose and glycerol containing buffers. Alternatively, sterilization can be achieved by autoclaving (20 minutes at 15 lb/sq.in. (psi) from 121-124°C on liquid cycle).

WARNING: If redoing the experiments in this thesis make sure to familiarize yourself with the appropriate Material Safety Data Sheets and consult your institution's Environmental Health and Safety Office if needed to ensure proper handling of equipment and hazardous reagents used in the protocols.

0.5M Adenosine 5′-triphosphate (disodium salt hydrate) [$C_{10}H_{14}N_5Na_2O_{13}P_3 \cdot xH_2O$. Synonym: 5′-ATP-$Na_2$. CAS No.: 34369-07-8. Molecular Weight: 551.14 g/mol] stock solution – *2ml*: 551.1 **mg** of ATP was weighed out directly (see note) into a small 5 ml graduated beaker. *The amount to weigh was given by (0.002 L)(0.5 mol/L)(551.14 g/mol)=0.55114g =551.1mg*. 200-300µl 5M KOH was added to the beaker to dissolve the ATP together with a small stir bar and put on stirring at low speed. When all the ATP powder

was dissolved, 1.2 ml deionized/Milli-Q water was added. The pH was measured at 4ºC and carefully adjusted to pH 7 with 5 M KOH (see note). The stir bar was removed and the volume was raised to the 2ml mark with deionized/Milli-Q water (~120µl). The solution was NOT sterile-filtered, but stored in small aliquots (250 µl) at –20°C (–80°C for long-time storage). *Note: The ATP is stored at -20 in the freezer. The weighing should therefore be performed very rapidly to avoid the remaining powder in the bottle to reach room temperature. It is usually not necessary to add much more than 300µl KOH in total (400µl gives pH 8).*

0.001 M Calcium Chloride (dihydrate) [$CaCl_2 \cdot 2H_2O$. CAS No.: 10035-04-8. Molecular Weight: 147.01 g/mol] stock solution – *100 ml:* A 100 ml volumetric flask was filled about a quarter full with deionized/Milli-Q water. 14.7 **mg** $CaCl_2 \cdot 2H_2O$ was carefully weighed out in a tared weighing boat and the solid transferred to the volumetric flask through a laboratory funnel. *The amount to weigh was given by (0.001 mol/L)(0.1 L)(147.01 g/mol) = 0.014701 g = 14.7 mg.* The tared weighing boat was rinsed into the funnel with water to make certain all of the solute was transferred. The solution was twirled until completely dissolved (~1 min). The volume was adjusted to the 100 ml mark with deionized / Milli-Q water. The solution was sterile-filtered before transferring it to an appropriately labeled container stored at room temperature (15–25ºC) for months.

10% (w/v) Coomassie® Brilliant blue G 250 (C.I. 42655) [$C_{47}H_{48}N_3O_7S_2Na$. Abbreviation: CBB. CAS No.: 6104-58-1. Molecular Weight: 854.02] stock solution – *10mL:* 1000 **mg** Coomassie® Brilliant blue G 250 powder was weighed out in a tared weighing boat and the solid transferred to a 10 ml graduated beaker. The tared weighing boat was rinsed with 9 ml deionized/Milli-Q water into the beaker to make certain all of the solute was transferred. A stir bar was added to the beaker and the solution put on low stirring with gentle heating (see note) until completely dissolved and the solution turned bright blue. The volume was raised to the 10 mL mark (see comment) and the solution was sterile-filtered before transferring it to an appropriately labeled container stored at 2-8 ºC for months. *Note: If using cold water, stir the solution for 3-4 hours until dissolved (only slightly soluble in cold water). Comment: Preferably at 4ºC, when density of water is ρ=1.000 g/mL to get exactly 10% (w/v)).*

0.5M Disodium Ethylene Diamine Tetra-Acetate (dihydrate) [$C_{10}H_{14}N_2Na_2O_8 \cdot 2H_2O$. Synonym(s): EDTA-$Na_2$, EDTA disodium salt, Ethylenediaminetetraacetic acid disodium salt dihydrate, Disodium ethylenediaminetetraacetate dihydrate. CAS No.: 6381-92-6. Molecular Weight: 372.24 g/mol] stock solution, pH 7.5 – *100ml*: A 100 ml graduated beaker was filled

about one fifth a quarter full with deionized/Milli-Q water. 18.62 g EDTA powder was weighed out in a tared weighing boat and the solid was transferred to the volumetric flask through a laboratory funnel. *The amount to weigh was given by (0.5 mol/L)(0.1 L)(372.3 g/mol) = 18.615 g.* The tared weighing boat was rinsed with water into the funnel to make certain all of the solute was transferred. The volume was raised to the 90 ml mark with deionized/Milli-Q water. A stir bar was added to the beaker and it was put on a slow stir, while pH was being monitored. 3.5-4g NaOH pellets (see note) was added immediately, but the rest was added carefully to not overshoot (see comment) the desired pH of pH 7.5 (the exact amount required is slightly above 4g). When completely dissolved the stir bar was removed and the volume was raised to a final volume of 100 ml with deionized / Milli-Q water and mixed. The solution was sterile-filtered before transferring it to an appropriately labeled container stored at room temperature (15–25ºC) for months. *Note: The disodium salt of EDTA might not go into solution until the pH of the solution is adjusted to approximately 8.0 by the addition of NaOH. If that is the case, aim for pH 8.0 instead. Comment: If overshooting the pH, adjust the pH back to 7.5 with HCl (!CAUTION: wear gloves, eye protection and work under a fume hood with this acid solution).*

0.5M Ethylene Glycol Tetra-Acetic Acid [[-$CH_2OCH_2CH_2N(CH_2CO_2H)_2]_2$. Synonym(s): EGTA, Egtazic acid, Ethylene-bis(oxyethylenenitrilo)tetraacetic acid, Glycol ether diamine tetraacetic acid. CAS No.: 67-42-5. Molecular Weight: 380.35 g/mol] stock solution, pH 7.5 – *100ml*: A 100 ml graduated beaker was filled about one fifth a quarter full with deionized/Milli-Q water. 19.02 g EGTA powder was weighed out in a tared weighing boat and the solid was transferred to the volumetric flask through a laboratory funnel. *The amount to weigh was given by (0.5 mol/L)(0.1 L)(380.4 g/mol) = 19.02 g.* The tared weighing boat was rinsed with water into the funnel to make certain all of the solute was transferred. The volume was raised to the 90 ml mark with deionized/Milli-Q water. A stir bar was added to the beaker and it was put on a slow stir, while pH was being monitored. 3.5-4g NaOH pellets (see note) was added immediately, but the rest was added carefully to not overshoot (see comment) the desired pH of pH 7.5 (the exact amount required is slightly above 4g). When completely dissolved the stir bar was removed and the volume was raised to a final volume of 100 ml with deionized / Milli-Q water and mixed. The solution was sterile-filtered before transferring it to an appropriately labeled container stored at room temperature (15–25ºC) for months. *Note: EGTA will not go into solution without NaOH. Once the pH has been raised sufficiently (alkaline) it dissolves quickly. Comment: if overshooting, adjust the pH*

back to 7.5 with HCl (!CAUTION: wear gloves, eye protection and work under a fume hood with this acid solution).

30mM Fe(II)-EDTA: 30mM Ferrous ammonium sulfate hexahydrate [$H_8FeN_2O_8S_2$*$6H_2O$. Synonym(s): Ammonium iron(II) sulfate hexahydrate, $(NH_4)_2Fe(SO_4)_2 \cdot 6H_2O$. CAS No.: 7783-85-9. Molecular weight: 392.14 g/mol] and 60 mM Ethylenediaminetetraacetic acid disodium salt (dihydrate) [$C_{10}H_{14}N_2Na_2O_8$* 2 H_2O. Synonym(s): EDTA disodium salt, $Na_2EDTA \cdot 2H2O$. CAS No.: 6381-92-6. Molecular weight: 372.24 g/mol] stock solution– *5.1 ml:* 60 **mg** of (NH4)2Fe(SO4)2·6H2O beads were weighed out in a tared weighing boat and the solid transferred to a 15 ml Falcon centrifuge tube through a laboratory funnel. *The amount to weigh was given by (0.03 mol/L)(0.0051 L)(392.14 g/mol) = 0.06000 g.* 114 **mg** of Na2EDTA·2H2O powder was weighed out in another tared weighing boat and the solid was transferred to the tube through a laboratory funnel. *The amount to weigh was given by (0.06 mol/L)(0.00625 L)(372.24 g/mol) = 0.11391 g.* Both of the tared weighing boats were rinsed into the funnel with 2.5 ml deionized/Milli-Q water to each to make certain that all of the solute was transferred. An additional 100 µl dH2O was added and the solution was vortexed for several minutes to dissolve as much solid as possible. Foam is normal. When completely dissolved, the solution was filtered through a 0.45-µm polypropylene filter obtaining a very greenish-yellow solution. 100 µL aliquots were transferred to appropriately labeled microcentrifuge tubes and store at –20°C for several months.

0.5M L-Glutathione (reduced) [$H_2NCH(CO_2H)CH_2CH_2CONHCH(CH_2SH)CONHCH_2CO_2H$**.** Synonym(s): GSH, γ-L-Glutamyl-L-cysteinyl-glycine. CAS Number: 70-18-8. Molecular Weight: 307.32 g/mol] stock solution – *2ml*: 307.3 **mg** of GSH was weighed out directly into a small 5 ml graduated beaker. *The amount to weigh was given by (0.002 L)(0.5 mol/L)(307.32 g/mol)=0.30732g =307.3mg*. 800µl 0.5M EDTA was added to the beaker together with a small stir bar and put on stirring at low speed. *The volume to add was given by ((0.002 L)(0.2 mol/L))/(0.5 mol/L) = 0.0008 L = 800 µl.* When all the GSH powder was dissolved, the stir bar was removed and the volume was raised to the 2ml mark with deionized/Milli-Q water. The solution was NOT sterile-filtered, but stored in small aliquots (250 µl) at –20°C (–80°C for long-time storage).

> ⚠**CRITICAL**: While GSH is stable as a powder for 5 years at 4°C, it is highly unstable when it is solubilized in aqueous solutions. The solution should therefore be prepared on the same day, however it can be stored if the solution is sealed and frozen

immediately after preparation at below –20°C. The sealed tube must be kept at room temperature for at least an hour before opening it after thawing.

50% (v/v) Glycerol [$C_3H_8O_3$. CAS No.: 56-81-5. Molecular Weight: 92.09 g/mol] stock solution – *100ml:* 50 ml of 100% glycerol solution (see comment) was measured out (see note) and added to a 250 ml bottle. 50 ml of deionized/Milli-Q water was added to the bottle. The bottle cap was put on and the bottle shaken vigorously. The solution was rested for 1 h or until all the foam was gone. *Note: When pipetting glycerol, use ethanol sterilized scissors to cut the end of a pipette to make pipetting easier. Comment: Glycerol is available in ultrapure powder or solution form. I have used a 100% solution.*

2M Glycine [$C_2H_5NO_2$. CAS No.: 56-40-6. Molecular weight: 75.07 g/mol] stock solution – *0.2L:* 100ml deionized/Milli-Q water was added to a 200 ml volumetric flask. 30.03 g Glycine was weighed out in a tared weighing boat and the solid transferred to the volumetric flask through a laboratory funnel. *The amount to weigh was given by (2 mol/L)(0.2 L)(75.07 g/mol) = 30.028 g.* The tared weighing boat was rinsed with water into the funnel to make certain all of the solute was transferred. The solution was twirled until completely dissolved (~1 min). The volume was adjusted to the 200 ml mark with deionized / Milli-Q water. The solution was sterile-filtered before transferring it to an appropriately labeled container stored at 2-8ºC for months.

0.5 M Magnesium Chloride [MgCl2. CAS No.: 7786-30-3. Molecular Weight: 95.211 g/mol] – *10 ml*: 3.0 ml of deionized/Milli-Q water was added to a 10 ml volumetric flask. 5 ml of 1M Magnesium Chloride solution was added to the flask. The solution was twirled, and the volume was adjusted to the 10 ml mark with deionized / Milli-Q water. The solution was sterile-filtered before transferring it to an appropriately labeled container stored at room temperature (15–25ºC) for months.

0.5 M Magnesium Sulfate (heptahydrate, see comment) [$MgSO_4 \cdot 7H_2O$. CAS No.: 10034-99-8. Molecular weight: 246.47 g/mol] stock solution – *100 ml:* A 100 ml volumetric flask was filled about a quarter full with deionized/Milli-Q water. 12.32 g $MgSO_4 \cdot 7H_2O$ was weighed out in a tared weighing boat and the solid transferred to the volumetric flask through a laboratory funnel. *The amount to weigh was given by (0.5 mol/L)(0.1 L)(246.47 g/mol) = 12.324 g.* The tared weighing boat was rinsed into the funnel with water to make certain all of the solute was transferred. The solution was twirled until the solid was completely dissolved (~1 min). The volume was adjusted to the 100 ml mark with deionized / Milli-Q water. The

solution was sterile-filtered by passing it through a filter unit containing a membrane with a pore size of 0.22 µm before transferring it to an appropriately labeled container stored at 2-8 ºC for months. *Comment*: *Magnesium sulfate ($MgSO_4$) is available in anhydrous as well as hydrated forms. It is difficult to weigh the anhydrous form accurately as it is highly hygroscopic, i.e. quickly absorbs water from the air adding to the weight, and should therefore not be used for preparing accurate concentrations unless it has been stored in a very effective dessicator, as we don't know how much water has accumulated,. Magnesium sulfate heptahydrate is better for this purpose as it is more stable.*

1M Potassium Chloride [KCl. CAS No.: 7447-40-7. Molecular Weight: 74.55 g/mol] stock solution – *100ml*: A 100 ml volumetric flask was filled about one fifth a quarter full with deionized/Milli-Q water. 7.46 g KCl was weighed out in a tared weighing boat and the solid was transferred to the volumetric flask through a laboratory funnel. *The amount to weigh was given by (1 mol/L)(0.1 L)(74.55 g/mol) = 7.455 g.* The tared weighing boat was rinsed with water into the funnel to make certain all of the solute was transferred. The solution was twirled until completely dissolved (~1 min). The volume was adjusted to the 100 ml mark with deionized / Milli-Q water. The solution was sterile-filtered before transferring it to an appropriately labeled container stored at room temperature (15–25ºC) for months.

5M Potassium hydroxide [KOH. CAS No.: 1310-58-3. Molecular Weight: 56.11 g/mol] stock solution – *200ml*: 5 ml deionized/Milli-Q water was added to a graduated beaker of minimum 250 ml together with a large stir bar. The beaker was put on a robust stir plate (see note of caution) to stir at low speed. 56.11 g of KOH pellets was weighed out in a tared weighing boat. *The amount to weigh was given by (0.2 L)(5 mol/L)(56.11g/mol) = 56.11 g*. A few pellets were transferred at the time to the beaker through a laboratory funnel, waiting for the pellets to dissolve in between. The volume was raised to 180 ml with deionized/Milli-Q water before the stir bar was removed and the volume adjusted to 200 ml with deionized / Milli-Q water. The solution was sterile-filtered before transferring it to an appropriately labeled container stored at 2-8ºC for months. (!CAUTION: This reaction is exothermic and gets quite hot, possibly generating some steam. Avoid any unstable stirring plates etc. that could lead to spilling of this hot and highly corrosive reagent).

0.5 M Potassium phosphate (monobasic) [KH_2PO_4. CAS No.: 7778-77-0. Molecular Weight: 136.09 g/mol] stock solution – *100 ml:* A 100 ml volumetric flask was filled about a quarter full with deionized/Milli-Q water. 6.80 g KH_2PO_4 was weighed out in a tared weighing boat and the solid transferred to the volumetric flask through a laboratory funnel. *The amount to*

weigh was given by (0.5 mol/L)(0.1 L)(136.09 g/mol) = 6.8045 g. The tared weighing boat was rinsed into the funnel with water to make certain all of the solute was transferred. The solution was twirled until completely dissolved (~1 min). The volume was adjusted to the 100 ml mark with deionized / Milli-Q water. The solution was sterile-filtered before transferring it to an appropriately labeled container stored at 2-8 ^{o}C for months.

5 M Sodium Chloride [NaCl. CAS No.: 7647-14-5. Molecular weight: 58.44 g/mol] stock solution – *100ml:* A 100 ml volumetric flask was filled about one fifth a quarter full with deionized/Milli-Q water. 29.22 g NaCl was weighed out in a tared weighing boat and the solid was transfered to the volumetric flask through a laboratory funnel. *The amount to weigh was given by (5 mol/L)(0.1 L)(58.44 g/mol) = 29.22 g.* The tared weighing boat was rinsed with water into the funnel to make certain all of the solute was transferred. The solution was twirled until completely dissolved (~5 min). The volume was adjusted to the 100 ml mark with deionized / Milli-Q water. The solution was sterile-filtered before transferring it to an appropriately labeled container stored at room temperature (15–25^{o}C) for months.

2.5 M Sucrose [$C_{12}H_{22}O_{11}$. CAS No.: 57-50-1. Molecular weight: 342.30 g/mol] stock solution – 2*00ml:* 5 ml deionized/Milli-Q water was added to a graduated beaker of minimum 250 ml together with a large stir bar. 171.15 g sucrose powder was weighed out and transferred to the beaker through a laboratory funnel to avoid clumps. *The amount to weigh was given by (2.5 mol/L)(0.2 L)(342.3 g/mol) = 171.15 g.* A mini vortexer was used to shake the sucrose grains down to compaction. The volume was raised to 180 ml with deionized/Milli-Q water and stirred on a stir plate with heating (see note) until no grains were visible (~15 min). The stir bar was removed and the volume adjusted to 200 ml with deionized / Milli-Q water. The solution was sterile-filtered before transferring it to an appropriately labeled container stored at 2-8^{o}C for months. *Note: The temperature should be well below 186^{o}C to avoid caramelization through decomposing.*

2M Tris base [$NH_2C(CH_2OH)_3$. Synonyms: Trizma® base, Tris base, Tris(hydroxymethyl)aminomethane. CAS No.: 77-86-1. Molecular Weight: 121.14 g/mol] solution – *0.2L:* 100ml deionized/Milli-Q water was added to a 200 ml volumetric flask. 48.46 g Tris base was weighed out in a tared weighing boat and the solid transferred to the volumetric flask through a laboratory funnel. *The amount to weigh was given by (2 mol/L)(0.2 L)(121.14 g/mol) = 48.456 g.* The tared weighing boat was rinsed with water into the funnel to make certain all of the solute was transferred. The solution was twirled until completely dissolved (~1 min). The volume was adjusted to the 200 ml mark with deionized / Milli-Q

water. The solution was sterile-filtered before transferring it to an appropriately labeled container stored at 2-8 ºC for months.

1M Tris(-HCl) [$NH_2C(CH_2OH)_3$. Synonyms: Trizma® base, Tris base, Tris(hydroxymethyl)aminomethane. CAS No.: 77-86-1. Molecular Weight: 121.14 g/mol] stock solutions, pH 7.2 – *100ml*: 12.11 g Tris Base powder was weighed out into a 100 mL beaker. *The amount to weigh was given by (1 mol/L)(0.1 L)(121.14 g/mol) = 12.114 g.* The volume was raised to 70 ml with deionized/Milli-Q water and a stir bar was added and the beaker put on a stir plate at low stirring until the Tris Base was completely dissolved (~1 min). The pH of the solution was monitored (see note) at 4ºC (the temperature at which the buffer was used). 39ml of 12 M HCl was slowly added to the corresponding labelled beaker (!CAUTION: wear gloves, eye protection and work under a fume hood with this acid solution). The solution was then allowed to cool to room temperature before making final adjustments to the target pH of 7.2. Once the pH of the solution was correct (see comment), the stir bar was removed, and the volume was raised to the 100 ml mark with deionized/Milli-Q water. The solution was sterile-filtered before transferring to an appropriately labeled container stored at 2-8 ºC for months. Because the pH of Tris solutions is extremely temperature-dependent (decreasing approximately 0.03 pH units for each 1°C temperature increase), the temperature at which the Tris buffer was prepared was indicated when labelling. *Note: It should be basic (pH >7.4). Comment: Assuming that there is no overshoot while adjusting pH, this method does not change the ionic strength. However, after overshoot and readjusting with NaOH, or using Tris HCl and adjusting the pH with NaOH, there is a change in ionic strength. Depending on the intended use of the Tris buffer, such a change may or may not be important (2M Tris base solution (below) is used for electrophoresis).*

> ⚠**CRITICAL**: Use a Tris-compatible electrode when adjusting the pH. Single-junction Ag/AgCl electrodes can exhibit instability when used with Tris buffers because the silver gradually precipitates and clogs the electrode.
> ⚠**CRITICAL**: If the final 1 M solution has a yellow color, discard it and obtain better quality Tris.

1M Spermidine (free-base form) [$NH_2(CH_2)_3NH(CH_2)_4NH_2$. CAS Number: 124-20-9. Molecular Weight: 145.25 g/mol] stock solution – *10ml*: 1.45 g spermidine was weighed out into a 10 mL graduated beaker. *The amount to weigh is given by (1 mol/L)(0.01 L)(145.25 g/mol) = 1.4525 g.* The volume was raised to 8 ml with deionized / Milli-Q water. A stir bar was added to the beaker and put on a stir plate at low stirring until completely dissolved (~1

min). The stir bar was removed and the volume was raised to the 10 ml mark with deionized / Milli-Q water. The solution was NOT sterile-filtered, but stored in small aliquots (1 ml) at –20°C for maximum 1 month.

1M Spermine [$NH_2(CH_2)_3NH(CH_2)_4NH(CH_2)_3NH_2$. CAS Number: 71-44-3. Molecular Weight: 202.34 g/mol] stock solution – *10ml*: 2.02 g spermine was weighed out into a 10 mL graduated beaker. *The amount to weigh was given by (1 mol/L)(0.01 L)(202.34 g/mol) = 2.0234 g.* The volume was raised to 8 ml with deionized / Milli-Q water. A stir bar was added to the beaker and put on a stir plate at low stirring until completely dissolved (~1 min). The stir bar was removed and the volume was raised to the 10 ml mark with deionized / Milli-Q water. The solution was NOT sterile-filtered, but stored in small aliquots (1 ml) at –20°C for maximum 1 month.

APPENDIX D: NUCLEI ISOLATION PROTOCOL

PREPARATIONS:

Homogenization buffers/solutions tested:

All solutions/buffers except PBS were prepared as 3X concentrations (like in the optimal 3x Homogenization solution Stable Master Mix below). Final 1X concentration of buffers:

1. **PBS (stock):** 150mM NaCl, 10mM K2HPO4*3H2O and KH2PO4, pH 7.4.

2. **HBv1:** 0.32 M Sucrose, 15mM NaCl, 60 mM KCl, 5mM MgCl2, 0.1mM EGTA, 15mM Tris-HCl (pH 7.2), pH 7.6.

3. **HB7.0:** 0.25 M Sucrose, 10mM NaCl, 1mM $MgCl_2$, ~500nM $CaCl_2$, ~10mM HEPES (pH 7.2), pH 7.0.

4. **HB6.6:** 0.25 M Sucrose, 10mM NaCl, 1mM $MgCl_2$, ~500nM $CaCl_2$, ~3mM HEPES (pH 7.2), pH 6.6.

5. **HB6.6v2:** 0.25 M Sucrose, 10mM NaCl, 1mM KH2PO4, 1mM MgSO4, ~500nM CaCl2, ~3mM HEPES (pH 7.2), pH 6.6.

6. **HB6.6v3:** 0.25 M Sucrose, 10mM NaCl, 1mM KH2PO4, 1mM MgSO4, ~100nM CaCl2, ~3mM HEPES (pH 7.2), pH 6.6.

7. **HBv2:** 0.25 M Sucrose, 10mM NaCl, 1mM KH_2PO_4, 1mM $MgSO_4$, ~500nM $CaCl_2$, ~3mM HEPES (pH 7.2), pH 6.6.

8. **HBv2.2:** 0.25 M Sucrose, 10mM NaCl, 1mM KH_2PO_4, 1mM $MgSO_4$, ~333nM $CaCl_2$, ~3mM HEPES (pH 7.2), pH 6.6.

9. **HBv3*:** 0.25 M Sucrose, 10mM NaCl, 1mM KH_2PO_4, 1mM $MgSO_4$, ~500nM $CaCl_2$, ~3mM HEPES (pH 7.2), pH 6.7.*final protocol homogenization solution = **1x Homogenization solution Stable Master Mix.**

3x Homogenization solution Stable Master Mix: *3x HB, pH 6.6 – 100ml:* 66 mL of deionized / Milli-Q water was added to a 150 mL beaker together with a stir bar, and placed on a stir plate and put on a low stir. The following volumes of reagents were added to the beaker, stopping the stirring while pipetting:

Reagent	**Final Conc.**	**Fold Dilution (x)**	**Vol for 100 mL (µl)** *(divide volumes by 1000 to get mL)*
2.5 M Sucrose	0.75 M	3.33	30000
5 M NaCl	30 mM (0.03 M)	166.67	600
0.5 M $MgSO_4$	3 mM (0.003 M)	166.67	600
0.5 M KH_2PO_4	3 mM (0.003 M)	166.67	600
0.001 M $CaCl_2$	1500 nM (0.0000015 M)	66666.67	1.5
Total:	-	-	31801.5

The pH of the solution was measured at 4°C. The pH of the solution was adjusted to pH 6.6 with cold 1 M HEPES (**less** than 930 µl to avoid overshooting (>pH 6.65)), keeping record of the volume added. Once the pH of the solutions was correct, the necessary volume (<2 ml) of deionized / Milli-Q water to raise the combined volume to 100 mL, was calculated and added. The solution was sterile-filtered before transferring it to an appropriately labeled container stored at 2-8^{o}C for a few weeks (see comment). *Comment: Used within 1-2 months from date of first use after sterilization* **(⚠CRITICAL)**, *and less if not sterile filtered.*

Gradients tested:

Sucrose:

All sucrose gradients were prepared as the below 2.1M sucrose cushion master mix:

1. Bottom layer: **2.1 M sucrose cushion, pH 7.4** supplemented with 1mM spermidine on day of use. Middle layer: **1.8 M sucrose cushion, pH 7.4** supplemented with 1mM spermidine on day of use.

2. Bottom layer: **2.1 M sucrose cushion, pH 7.4** supplemented with 1mM spermidine on day of use. Middle layer: **1.5 M sucrose cushion, pH 7.4** supplemented with 1mM spermidine on day of use.

3. Bottom layer: **2.1 M sucrose cushion, pH 7.4** supplemented with 1mM spermidine on day of use. Middle layer: **1.3 M sucrose cushion, pH 7.4** supplemented with 1mM spermidine on day of use.

2.1M sucrose cushion master mix – *100ml*: 15 mL of deionized / Milli-Q water was added to a 150 mL beaker together with a stir bar, and placed on a stir plate and put on a low stir. The following volumes of reagents were added to the beaker, stopping the stirring while pipetting:

Reagent	**Final Conc.**	**Fold Dilution (x)**	**Vol for 100 mL (µl)** *(divide volumes by 1000 to get mL)*
3 M Sucrose	2.1 M	1.43	70000
1 M KCl	60 mM (0.06 M)	16.67	6000
5 M NaCl	15 mM (0.015 M)	333.33	300
0.5 M EDTA	1 mM (0.001 M)	500.00	200
0.5 M EGTA	0.5 mM (0.0005 M)	1000.00	100
1 M Tris-HCl, pH 8.0	15 mM (0.015 M)	66.67	1500
Total:	-	-	78100

The pH of the solution was measured at 4°C (see comment). Once the pH of the solutions was correct, the necessary volume (<7 ml) of deionized / Milli-Q water to raise the combined volume to 100 mL was calculated and added. The solution was sterile-filtered before transferring it to 3 appropriately labeled containers in aliquots of 25 ml (and one reserve of <25 ml) stored at 2-8ºC for a few weeks. *Comment: pH decreases by 0.1 unit with each 10-fold dilution (in this case it should still be within it's effective pH range of 7.5 - 8.0).*

Iodixanol:

All Iodixanol gradients were prepared as described in the SAME DAY preparations below:

4. Top layer: **29v/v% Iodixanol**. Supplemented with 1mM $MgCl_2$ + 1xPIC. Middle layer (sample): **35v/v% Iodixanol**. Supplemented with 1mM $MgCl_2$ + 1xPIC. Bottom layer: **40v/v% Iodixanol**. Supplemented with 1mM $MgCl_2$ + 1xPIC.

5. Top layer (sample): **35v/v% Iodixanol**. Supplemented with 1mM $MgCl_2$ + 1xPIC. Middle layer: **29v/v% Iodixanol**. Supplemented with 1mM $MgCl_2$ + 1xPIC. Bottom layer: **40v/v% Iodixanol**. Supplemented with 1mM $MgCl_2$ + 1xPIC.

6. Top layer (sample): **25v/v% Iodixanol***. Supplemented with 1mM $MgCl_2$ + 1xPIC. Middle layer: **29v/v% Iodixanol***. Supplemented with 1mM $MgCl_2$ + 1xPIC. Bottom layer: **40v/v% Iodixanol***. Supplemented with 1mM $MgCl_2$ + 1xPIC. *final protocol gradients.

SAME DAY:

Solutions:

The following solutions were prepared in the order they are written for efficiency:

100x Protease inhibitor cocktail (100x PIC) – *0.5 ml:* 500 µl of deionized / Milli-Q water (see alternative solvent used for testing) was added to a 2 ml roundbottom LoBind Eppendorf tube on ice labelled "100x PIC". One cOmplete EDTA-free Protease inhibitor cocktail tablet (see note) was added to the tube (see comment), and the tube inverted until completely dissolved (~5 min). Vortexing was avoided after adding the tablet. The solution was stored on ice until use. *Note: cOmplete Protease Inhibitors come as tablets, where one tablet inhibit proteolytic activity in up to 50 ml extraction solution (Roche Diagnostics, 2004). If 500 µl is too much, one can use an ethanol sterilized scalpel to cut one tablet in two and use 1/2 in 250 µl water. If 250 µl is too much, one can cut the tablet in four* and use 1/4 in 125 µl water. *It is difficult to accurately cut one tablet into uneven numbers or in less than 1/4, thus uneven numbers should be avoided and 125 µl should be the minimum. Comment: A 1x final concentration of PIC will be present in all the below solutions but will not be included in any calculations as its exact composition is unknown. Being accountable for just a 1% dilution of all the molarities, it is assumed negligible.*

> ⚠***CRITICAL**: Normal cOmplete tablets (with EDTA) should be avoided as they are not recommended for inhibition when divalent cations are required (Roche Diagnostics, 2004). The cOmplete Mini, EDTA-free Protease inhibitor cocktail tablets should be avoided as dissolving them into a 100x solution is impossible.*

1x Unstable Homogenization Buffer, pH 6.7 (1x HB) – *12ml:* 8 mL of deionized / Milli-Q water was added to a 15ml Falcon tube on ice. 4 mL of 3x HB, pH 6.6 was added to the tube, and mixed by inversion. *The volume was given by ([Solute in 1x HB]*0.012 L)/[Solute in 3x HB]= 0.004 L, where the respective solutes are Sucrose, NaCl, MgSO4, KH2PO4, CaCl2 and HEPES. The final 1x concentrations are 0.25 M Sucrose, 0.01 M NaCl, 0.001 M MgSO4, 0.001 M KH2PO4, 500 nM CaCl2 and approx. 0.003 M HEPES.* 120 µl 100x PIC (see supplements used for testing) was added to the tube and mixed by inverting to obtain 1xPIC. 6 ml was removed and added to a second 15 ml tube, labelling both "1x HB". The solutions were stored on ice until use. *Comment: 1x Unstable HB (1 part of 4ml to 2 parts of 4ml, for a total of 3 parts of 4ml; a 1/3 dilution = 1:2 ratio)) will be used directly, resulting in experimental conditions of pH 6.7 (measured). The proteolytic inhibition effect on aspartic (acid) proteases might decrease when used in the acidic pH range. In that case one could include pepstatin along with the cOmplete, EDTA-free tablets. This was not done here as the pH of the extraction step was only slightly acidic, performed quickly at a maximum of 4°C, and any long-term storage of nuclei was in a supercooled stage at -15°C, where proteolytic activity is assumed to be minimal.*

1.72x HB – *3 ml*: 2.867 ml 3x HB (master mix) was mixed with 2.133 ml deionized / Mili-Q water in a 5ml SnapCap centrifuge tube. *The volume to add was given by ([Solute in 1.72x HB]*0.005 L)/[Solute in 3x HB]= 0,002867 L, where the respective solutes are Sucrose, NaCl, MgSO4, KH2PO4, CaCl2 and HEPES. The final 1.72x concentrations are 0.43 M Sucrose, 0.0172 M NaCl, 0.00172 M MgSO4, 0.00172 M KH2PO4, 860 nM CaCl2 and approx. 0.005 M HEPES.* 85.7µl 100x PIC was added to the tube and mixed by inversion. *The volume to add was given by the final 1x concentration of PIC in a 7/12 dilution: (12/7)(10µl/ml)(5ml) = 85.7µl.* 3 ml was transferred to a new 5 ml tube labelled "1.72x HB" (see comment) and stored on ice until use. *Comment: 1.72x HB (roughly a 4:3 ratio of 700µl parts) will be used directly in a 7:5 ratio of 100µl parts. The final ratio of 4:8=1:2 results in experimental conditions of pH 6.7 (measured).*

40% IOD - 2x *8 ml*: The bottle with OptiPrep 60% (w/v) Iodixanol (stock) was shaken well before the bottle was held upside down, and the rubber cap was penetrated with a graduated syringe. 5.4 ml Iodixanol was withdrawn and transferred to two 15 ml Falcon tubes labelled "40% IOD". 70µl was pipetted out from each tube to get a final volume of 5.33 ml. 2.67 ml 3x HB (master mix) was added to the tubes and mixed by inversion (see comment). *The resulting concentration was given by (60%*5.33 ml)/(5.33 ml + 2.67 ml) = 39.975% ≈ 40%.*

80µl 100x PIC solution was added to the 40% tubes and mixed by inversion. The tubes were stored on ice until use. *Comment: The molarity of the different solutes at this dilution are equal* to that of Unstable 1x HB (*after adding PIC). Because OptiPrep Iodixanol is a solution in water with no additives, its pH is that of water, and the change in pH would be the same as diluting 3x HB with water, resulting in a final pH of 6.7 (measured) at this 1/3 dilution.*

60% IOD – *3 ml*: The bottle with OptiPrep 60% (w/v) Iodixanol (stock) was shaken well before the bottle was held upside down, and the rubber cap was penetrated with a graduated syringe. 3 ml Iodixanol was withdrawn and transferred to a 5ml SnapCap centrifuge tube labelled "60% IOD". **6µl** 0.5M $MgCl_2$ was added to the tube and mixed by inversion. *The volume to add was given by ((0.0015 L)(0.001 mol/L))/(0.5 mol/L) = 3*10^{-6} L = 3 µl.* The tube was stored on ice until use.

29% IOD – *4.4 ml*: 3.190 ml 40% IOD was mixed with 1.210 ml 1x HB (unstable) in a 5ml SnapCap centrifuge tube labelled "29% IOD" to make 4.4 ml 29% (see comment). *The volume to add was given by (29%*4400 µl)/(40%) = 3190 µl*. The tube was stored on ice until use. *Comment: The molarity of the different solutes at this dilution are equal to that of Unstable 1x HB. A 1x concentration of PIC is maintained by both the 40% Iodixanol gradient and the Unstable 1x HB.*

Alternative solvent used for testing:

Instead of dissolving ½ cOmplete proteinase inhibitor cocktail tablet (see note above) in 250µl dH2O to prepare a 100x solution to mix with the solutions used for homogenization, ½ tablet was instead dissolved in thawed 250µl aliquots of 500mM ATP, giving 1x PIC and 5mM ATP.

Supplements used for testing:

Homogenization buffer number **1** was supplemented with 0.5mM spermidine, 0.15mM spermine and 1xPIC before use. Number **2** was supplemented with 1xPIC before use. Number **3**, **4**, and **5** were supplemented with 1mM spermine, 1mM spermidine and 1xPIC before use. Number **6** was supplemented with 1xPIC, OR with 1mM spermine, 1mM spermidine and 1xPIC before use. Number **7** and **8** were supplemented with 0.4mM spermine, 0.2mM spermidine and 1xPIC before use. Number **9** was supplemented with 1mM GSH (glutathione)

and 1xPIC, OR 5mM ATP in 1xPIC (see preparation of 1xPIC above), OR not supplemented before use, i.e. without 1xPIC.

PROTOCOL:

The following **nuclei isolation protocol** can be used for **two** independent nuclei isolations (n=2) in parallel.

Start:

The following steps were carried out on ice or in a cold room at 4°C if not stated otherwise:

2.5 ml 1x HB (unstable) was added in two pre-chilled Homogenizer Dounce sets with a working capacity of 7 ml. Using sterile tweezers, 50 mg, alternatively 70 mg (testing), of frozen tissue (usually 2-3 tissue lumps of 20-30 mg) kept in -80ºC was added into each douncer.

> **! CAUTION:** It is extremely important that all items are kept very cold during direct tissue handling (tweezers, tared weighing boat etc.). It might also be necessary to wear extra hand protection when collecting tissue from -80ºC.

Using a sterile and chilled loose 'A' pestle (see note 1#), the tissue was homogenized using 2-3 **gentle** strokes or until the suspension was cloudy with few visible tissue fragments. 2-4 **gentle** strokes with the tight 'B' pestle was used to make a uniform suspension with no visible fragments. The homogenate from each douncer was transferred to two separate 5ml SnapCap centrifuge tubes labelled "S1" and "S2" using a p1000 pipette tip. The tubes were centrifuged for 5 min at 300 RCF (4ºC). In the meantime, the high (gradient 1) and low (gradient 2) molarity sucrose gradients **OR** 40% IOD (gradient 1) and 29% IOD (gradient 2) solutions were shaken (Iodixanol tends to settle into a continuous gradient after some time). 1 ml of gradient 2 was dispersed at the bottom of two pre-chilled 5ml SnapCap centrifuge tubes labelled "Grad 1" and "Grad 2". 2 ml of gradient 1 was slowly layered underneath the gradient 2 layer (see tip 1#), creating a clearly defined interface. After centrifugation, without disturbing the pellet, as much supernatant as possible (containing cytoplasmic debris and RNA) was removed from S1 and S2 (the remaining volume at the bottom was some ~30-50 µl). The nuclei pellets were gently resuspended by mixing 500 µl of 1x HB when sucrose gradients were used **OR** 500 µl of Pure IOD (see note 2#) when using Iodixanol gradients, directly with the nuclei/debris pellet in each tube using a p1000 tip. Then enough 1.72x HB was added to raise the total volume to 1200 µl (700 µl subtracting the volume of the pellet),

and mixed gently until the nuclei in S1 and S2 were fully resuspended without clumps (see note 3#). For each resuspension, the entire S1/S2 sample was drawn with a p1000 tip and dispensed slowly (see tip 2#) when the tip was placed straight onto the highest point where the surface has reached the tube wall in the tilted Grad 1/2 tubes. Again, a clearly defined interface was created. The Grad 1 and Grad 2 tubes were gently placed in a pre-chilled swinging bucket centrifuge to avoid disturbing the gradients and centrifuged for 75 minutes at 3220 RCF at 4 °C with the brake off (to avoid collapse of the gradient layers due to abrupt deacceleration). After centrifugation, the top layer (see note #4) in each tube were carefully aspirated and discarded. Between 700-900 µl of the (former) gradient 2 layer was collected with minimal debris using a p1000 pipette tip and transferred to pre-chilled 2 ml LoBind Eppendorf tubes labelled by date and "NUC 1"/"NUC 2".

Notes:

Note 1#: The Dounce Tissue grinder sets are designed based on the principle that the nucleus is relatively more resistant, compared to cells, to tissue dissociation processes. It comes with two pestles with varying clearance; a loose (71.12-119.38 µm) pestle for initial sample reduction and a tight (20.32-55.88µm) pestle to mechanically disrupt the cytoplasmic membrane of the large (>20µm) cells in the tissue, and release the smaller (<20 µm) nuclei while retaining the integrity of the nuclear membrane, to form the final homogenate (Kimble Chase Life Science & Research Products (n.d.)).

Note 2#: When the nuclei were mixed to 35% Iodixanol when testing gradient number 4 and 5, 700µl Pure IOD was used.

Note 3#: A 1x concentration of PIC is maintained by the extra PIC in the Unstable 1.72x HB. Because OptiPrep Iodixanol is a solution in water with no additives, its pH is that of water, and the change in pH would be the same as diluting Unstable 1.72x HB with water, resulting in a final pH of 6.7 (measured) at this effective 1/3 dilution.

Note 4#: For Iodixanol: after centrifugation, the former 25% layer should appear as a heterogeneous mix where debris are stratified into different bands. The former 29% layer should appear transparent or slightly milky between the bottom-most debris-band and the still intact gradient 1 interface. Most of the nuclei (~85%) would reside in the middle of this former 29% layer meaning that all of the debris-containing top layer can be gently aspirated down. There is a slight chance of loss by doing this as around 10% of the nuclei can be collected in the first 150 µl of the middle layer, but this is a tradeoff with regards to purity.

Tips:

Tip 1#: It is important to avoid any carry-over into the gradient 2 layer by wiping the side of the pipette tip with a *Kimwipe* and changing pipette tips between each drawing. As the interface raises, pull the pipette tip up so that the tip is always minimally submerged in the bottom layer. This will avoid excessive gradient 1 from the external surfaces of the pipette tip mixing with gradient 2 when slowly removing the tip after pipetting (known as "excessive volume displacement").

Tip 2#: The sample needs to be dispensed very slowly to **avoid** the liquid from running along the inside of the tube (as opposed to standard pipetting technique) as the liquid will gather momentum that makes it "fall" deeper into the uppermost gradient 2 layer, resulting in a mixing effect. During this step, it is also necessary to gradually withdraw the pipette tip up during pipetting for the same reason.

Density calculations for Homogenization solution 3 & 4:

Density is how much matter is contained within a volume, i.e., density equals mass per unit volume or density = mass/volume (D = M / V). Density of the highest commercially available concentration of Iodixanol, 60% OptiPrep, is 1.320 g/ml.

Homogenization solution 3

1#: *Density of the 25% Iodixanol nuclei suspension.*

As the 25% solution was made from mixing Unstable 1.72x HB and 60% Iodixanol we must first find the density of Unstable 1.72x HB. In other words, what is the final density achieved from mixing 500 µl of 60% Iodixanol directly with the nuclei/debris pellet and with Unstable 1.72x HB to a total volume of 1200 µl?

There are six masses*; the mass of the solutes (Sucrose, NaCl, MgCl2, CaCl2, HEPES) and the mass of the solvent (water). (*PIC is regarded negligible. See comment under Preparation of 100x PIC).

$$mass_{total} = mass_{Sucrose} + mass_{NaCl} + mass_{MgCl2} + mass_{CaCl2} + mass_{HEPES} + mass_{water}$$

One liter of water has a mass of one kilogram when measured at its maximal density (1 g/ml) at about 4 °C, the same temperature as the experimental setup. The mass of the solutes can be calculated from their molar mass, when we know their molarity (mol/L):

Molar mass of Sucrose ($C_{12}H_{22}O_{11}$) = 144.132 C (12*12.011) + 22.176 H (22*1.008) + 175.989 O (11*15.999) = 342.297. Mass of 0.43 moles (M = moles per liter) of the substance = **147.188 g**.

Molar mass of NaCl = 22.99 Na (1*22.99) + 35.453 Cl (1*35.453) = 58.443. Mass of 0.0172 moles of the substance = **1.005 g.**

Molar mass of MgCl2 = 24.305 Mg (1*24.305) + 70.906 Cl (2*35.453) = 95.211. Mass of 0.00172 moles of the substance = **0.164 g**.

Molar mass of CaCl2 = 40.078 Ca (1*40.078) + 70.906 Cl (2*35.453) = 110.984. Mass of 0.000000860 moles of the substance is **negligible**.

Molar mass of HEPES ($C_8H_{18}N_2O_4S$) = 96.088 C (8*12.011) + 18.144 H (18*1.008) + 28.014 N (2*14.007) + 63.996 O (4*15.999) + 32.066 S (1*32.066) = 238.308. Mass of approx. 0.0172 moles of the substance = **4.1 g**.

$mass_{total}$ = 147.188 g + 1.005 g + 0.164 g + 4.1 g + 1000 g = **1152.5 g**.
density = 1152.5 g/1000 mL = 1.1525 g/mL

The density of any Iodixanol gradient solution can be calculated using Eq. 1.

$$\rho_{solution} = \frac{(v_{Iodixanol} \times \rho_{Iodixanol}) + (v_{diluent} \times \rho_{diluent})}{v_{solution}} \qquad \text{Eq. 1}$$

Or equivalently

$$\rho_{solution} = \frac{m_{Iodixanol} + m_{diluent}}{v_{solution}}$$

Using Eq. 1, where v_Iodixanol = volume of OptiPrep Iodixanol = 0.500 ml; ρ_Iodixanol = density of OptiPrep Iodixanol = 1.320 g/ml*; v_diluent = volume of diluent = 0.700 ml; ρ_diluent = density of diluent = 1.1525 g/mL. **The addition of 0.001 moles of MgCl2 (3 µl in 1.5 ml WS) does not change the density at this level of accuracy.*

We get ρ_solution, nuc = Density of the 25% Iodixanol nuclei suspension *solvent* = **<u>1.22</u> g/ml.**

2#: *Density of the 35% Iodixanol nuclei suspension.*

What is the final density achieved from mixing 700 µl of 60% Iodixanol directly with the nuclei/debris pellet and with Unstable 1.72x HB to a total volume of 1200 µl?

Using Eq. 1, where v_Iodixanol = volume of OptiPrep Iodixanol = 0.700 ml; ρ_Iodixanol = density of OptiPrep Iodixanol = 1.320 g/ml; v_diluent = volume of diluent = 0.500 ml; ρ_diluent = density of diluent = 1.1525 g/mL, we get ρ_solution, nuc = Density of the 35% Iodixanol nuclei suspension *solvent* = **1.25 g/ml.**

Homogenization solution 4

1#: *Density of the 25% Iodixanol nuclei suspension.*

Molar mass of HEPES ($C_8H_{18}N_2O_4S$) = 96.088 C (8*12.011) + 18.144 H (18*1.008) + 28.014 N (2*14.007) + 63.996 O (4*15.999) + 32.066 S (1*32.066) = 238.308. Mass of approx. 0.005 moles of the substance = **1.2 g**.

$mass_{total}$ = 147.188 g + 1.005 g + 0.164 g + 1.2 g + 1000 g = **1149.6 g**.
density = 1149.6 g/1000 mL = 1.1496 g/mL

Using Eq. 1, where v_Iodixanol = volume of OptiPrep Iodixanol = 0.500 ml; ρ_Iodixanol = density of OptiPrep Iodixanol = 1.320 g/ml*; v_diluent = volume of diluent = 0.700 ml; ρ_diluent = density of diluent = 1.1496 g/mL, we get ρ_solution, nuc = Density of the 25% Iodixanol nuclei suspension *solvent* = **1.22 g/ml.**

2#: *Density of the 35% Iodixanol nuclei suspension.*

Using Eq. 1, where v_Iodixanol = volume of OptiPrep Iodixanol = 0.700 ml; ρ_Iodixanol = density of OptiPrep Iodixanol = 1.320 g/ml; v_diluent = volume of diluent = 0.500 ml; ρ_diluent = density of diluent = 1.1496 g/mL, we get ρ_solution, nuc = Density of the 35% Iodixanol nuclei suspension *solvent* = **1.25 g/ml.**

Density calculations for **gradient 6:**

1#: *Density of the 29% Iodixanol gradient.*

What is the final density achieved from mixing 1.595 ml 40% OptiPrep Iodixanol with 0.605 ml 1x HB?

Molar mass of MgSO4 = 24.305 Mg (1*24.305) + 32.066 S (1*32.066) + 63.996 O (4*15.999) = 120.367. Mass of 0.00172 moles of the substance = 0.207 g.

Molar mass of KH2PO4 = 39.098 K (1*39.098) + 2.016 H (2*1.008) + 30.974 P (1*30.974) + 63.996 O (4*15.999) = 136.084. Mass of 0.00172 moles of the substance = 0.234 g.

1x HB: Mass of 0.25 moles Sucrose, 0.01 moles NaCl, 0.001 moles MgSO4, 0.001 moles KH2PO4, 0.0000005 moles CaCl2, Approx. 0.003 moles HEPES and 1000 ml water sums to 1087.1 g. Density = 1.0871 g/ml.

Using Eq. 1, where v_Iodixanol = volume of 40% Iodixanol gradient = 1.595 ml; ρ_Iodixanol = density of 40% Iodixanol gradient= 1.3004 g/ml; v_diluent = volume of diluent = 0.605 ml; ρ_diluent = density of diluent = 1.0871 g/mL, we get ρ_solution, grad2 = Density of 29% Iodixanol gradient = **1.24 g/ml**.

2#: *Density of the 40% Iodixanol gradient.*

What is the final density achieved from mixing 5.33 ml 60% Iodixanol with 2.67 ml 3x HB?

3x HB: Mass of 0.75 moles Sucrose, 0.03 moles NaCl, 0.003 moles MgSO4, 0.003 moles KH2PO4, 0.000001 moles CaCl2, Approx. 0.009 moles HEPES and 1000 ml water sums to 1261.390 g. Density = 1.2614 g/ml.

Using Eq. 1, where v_Iodixanol = volume of OptiPrep Iodixanol = 5.33 ml; ρ_Iodixanol = density of OptiPrep Iodixanol = 1.320 g/ml; v_diluent = volume of diluent = 2.67 ml; ρ_diluent = density of diluent = 1.2614 g/mL, we get ρ_ solution, grad1 = Density of 40% Iodixanol gradient = **1.30 g/ml**.

APPENDIX E: QUALITY, YIELD AND PRECISION ASSESSMET PROTOCOL

SAME DAY:

Optional solutions:

1x Hoechst 33342 (fluorescent dye) [$C_{27}H_{28}N_6O \cdot 3HCl$. CAS No.: 875756-97-1. Molecular weight: 561.93 g/mol] – *500µl*: A suitable tube that could shield the solution from light was prepared. 500 µl deionized / Milli-Q water (see note) and 1 µl Hoechst stock (1 mg/ml) was added to the tube and mixed well. The solution was stored shielded from light on ice until use, or at 2-8ºC for a few weeks. *Note: Dilute in less water to get stronger signal.*

1x SYBR green (fluorescent dye) [$C_{32}H_{37}N_4S^+$. CAS No.: 163795-75-3. Molecular weight: 509.73 g/mol]: A suitable tube that could shield the solution from light was prepared. The total solution volume needed was calculated (usually 10 µl per sample multiplied by the number of parallels, plus 10% extra) and 9 volumes deionized / Milli-Q water and 1 volume

SYBR green stock was added to the tube and mixed well. The solution was stored shielded from light on ice until use, or at 2-8ºC for a few weeks.

PROTOCOL:

Start:

10 µl of the nuclei suspension (see note 1#) were collected and transferred to a 0.2 ml PCR tube, alternatively a 96-well PCR plate if many samples were counted. A single sample at a time was diluted 1:1 vol. with Trypan blue staining (see note 2#), alternatively, with either 1x Hoechst 33342 or 1x SYBR green (see note 3#), making sure that the fluorescent dye and sample was shielded from light at all times. Slightly less than 10 µl of (stained) nuclei suspension was loaded onto each side of a manual Thoma cell for counting, filling it completely without overflowing it (see note 4#). The slide was then placed under a bright-field microscope (in a dark room if the fluorescent dyes were used). The etched grid of the Thoma cell was quickly (see note 5#) located and the nuclei were inspected within 3-5 minutes (see note 6#) using 10×&20×/0.3, air objectives or 40×/0.5, air objective (see note 7#). When fluorescent dyes were used, the sample was only briefly subjected to full spectrum light to locate the grid before setting the correct position for the UV filter sets for SYBR green or Hoechst (see note 8#). Images were captured using an Axiocam 105 color, 60N-C 2/3¨ 0.5x, and analyzed later, using the ZEN Imaging Software "ZEN 3.0 (blue edition)". The nuclei yield and precision (if multiple isolations were performed) was calculated (see protocol calculations).

Notes:

Note 1#: It is recommended to repeat measurements to ensure accuracy by sample the nuclei suspension at least twice at different positions in the tube, mixing it with the dye and loading it in the Thoma cell. If there is longer than 10 minutes between each sampling, it is recommended to mix between.

Note 2#: Finding and documenting nuclei using only brightfield was difficult in my hands, and Trypan staining was used to assess quality. Trypan blue is a highly negatively charged dye which due to its relatively small size (~960 Daltons) can freely move into isolated nuclei not protected by the cytoplasmic membrane. Upon entry trypan blue stains positive intracellular proteins. When observed with bright-field microscopy, the nuclei acquire a darker bluish stain than their surroundings and are easily visible.

Note 3#: Trypan blue staining is not the ideal counting method for nuclei suspensions as it can stain debris from cytoplasm components or cell fragments. This could introduce random variability to the nuclei count, as debris can attach to otherwise high-quality nuclei and give impression of a large debris fragment, and thus omitted in the counting. For samples with a lot of debris, DNA staining fluorescent dyes may help distinguish nuclei from debris for more accurate quantification. Two such dyes were used in this thesis: SYBR Green with excitation peak = 498 nm/emission peak = 522 nm, and Hoechst 33342 with excitation peak = 352 nm/emission peak = 454 nm. The reason for not using only SYBR Green (most common) was that glutaraldehyde was used to fix nuclei in some tests. Glutaraldehyde induces a strong fluorescence by itself with fluorescence (emission) in the region 520-600 nm (Collins & Goldsmith, 1981) thus overlapping with SYBR Green. Hoechst 33342 was therefore used for glutaraldehyde treated samples. While fluorescent dyes do not stain debris, it often collapses nuclei and cannot be used to evaluate integrity, as compromised nuclei could be stained equally well.

Note 4#: Although the Thoma cell contains a fixed volume, the space between the counting chamber and the cover glass can increase slightly if you overflow it. This can result in underestimating the sample volume and thus overestimating the nuclei concentration.

Note 5#: A problem with evaluating nuclei morphology within the first 1-2 minutes after staining, is that not all nuclei have settled within the counting grid in the Thoma cell in this time. The same problem occurs after 10 minutes where a lot of the nuclei have already drifted out of the counting grid due to evaporation of liquid around the edges of the cover slide, creating a drift. Sometimes contamination with debris can get stained and drift on top of or under nuclei, or the staining dye itself produce grains that can get attached to the surface of nuclei, giving the impression of nucleoli. An example of this and drifting nuclei is given in **Figure E1**. In cases where grains or debris are prominent in a nuclei sample, nuclei should be evaluated multiple times to be able to distinguish nucleoli from debris. In addition, depending on how focus is established, it may or may not be possible to observe nucleoli in spherical nuclei (**Fig. E1.D & E**). It is also not all nuclei that contain nucleoli due to different stages of growth or death. Therefore, it is necessary to adjust the focus of the viewing pane for the entire Thoma cell and perform counting of the number of nuclei containing nucleoli to be able to draw some general conclusion on the presence/absence of nucleoli in the sample.

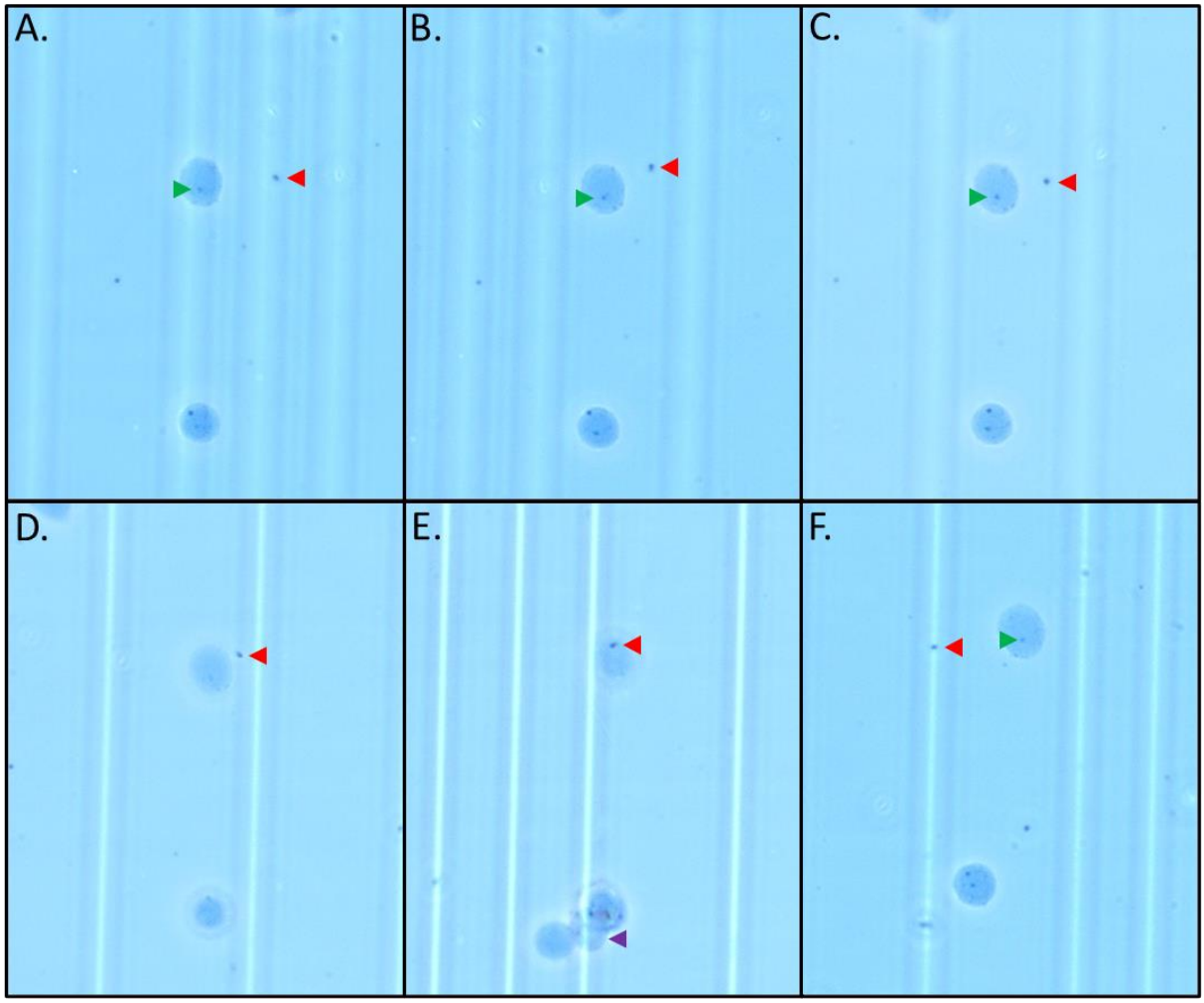

Figure E1 | Timelapse of the drift of two Trypan blue stained nuclei. *Microscopy images taken approx. every minute at 20X.* ***Green arrowhead*** *indicates nucleoli.* ***Purple arrowhead*** *indicates two nuclei not drifting and thus passed by the timelapsed nuclei.* ***Red arrowhead*** *indicates an impurity in focus. Being only slightly stronger in color, the impurity could be interchanged with a true nucleoli when it cohere in* ***E****, before detaching in* ***F****.*

Note 6#: The dilution with Trypan blue will induce a hypo-osmotic environment that will lead to a gradual swelling of the nuclei, in turn disturbing the morphology, such as dissolving nucleoli (Hancock, 2004) if the duration of the assessment/documentation is extended over several minutes. However, due to the empirical observation that the staining is extremely rapid, and that the swelling occurs with an inherited slowness, the documentation can still be representative if performed within 3-5 minutes from adding the dye, which is also when nuclei have stopped moving into the grid. If performed sufficiently fast, a centrally located nucleoli should be visible in many nuclei of good quality, disappearing after 10-15 minutes. This characteristic can also be used as a hypo-osmotic test.

Note 7#: Capturing images at 40× magnification was not achieved in my hands.

Note 8#: SYBR Green can be excited with 495 nm laser paired with a 525/50 nm bandpass filter* (Fs 38), while Hoechst 33342 can be excited with 395 nm laser paired with a 445/50 nm bandpass filter* (Fs 49). *By turning on the brightfield lamp with the green filter in place, the field of view should be green if it's a bandpass filter, and yellow-white if a long-pass filter (as blue has been filtered). The Axio Vert A1 microscope (used in this thesis) has a four-position mount for LED Filter Sets; Neutral-density filter (0.06, d=32x2), Fs 38 (consisting of filters EX BP 470/40, **BS FT 495**, EM BP 525/50), Fs 43 (EX BP 545/25, **BS FT 570**, EM BP 605/70) and Fs 49 (EX G 365, **BS FT 395**, EM BP 445/50) inserted in Reflector Module FL EC P&C (reflection is avoided through tilted mount for the emission (EM) bandpass (BP) filters). Bleaching occurs rapidly even with the correct filter, but slower than under full spectrum light.

Specific protocol calculations:

Yield: When the sample is under the coverslip, the nuclei suspension reaches a height of 0.1 mm and the volume can be calculated as: 1 mm x 1 mm x 0.1 mm = 0.1 mm^3 = 10^{-4} ml = 0.1 µl.

When counted N number of nuclei in one large 1 mm^2 square (that is, in 16 medium squares), the sample concentration can be calculated as: concentration in nuclei/ml = N x 10^4 (same as N x 10 nuc/µl)

If the sample has been diluted before loading (e.g. with a dye) this dilution must be taken into account. Taking the concentration-dilution factor (f) from our 1:1 dilution with Trypan blue (or others), we have: N x 10^4 x f nuc/ml, where f=2.

Precision: The dispersion of the nuclei yields around the mean, i.e. standard deviation (σ) was calculated using the following formula:

$$Standard\ deviation = \sigma = \sqrt{\frac{\Sigma(x - \bar{x})^2}{n - 1}}$$

Where x = the individual total nuclei count, $\overline{x}$ = the mean of all the counts, n = the number of data points (in the population).

DNA concentration: The total genomic content in one nuclei were calculated as follows:

The molecular weights of individual nucleotides are: 313.23 (dA), 304.21 (dT), 329.23 (dG) and 289.20 (dC), giving an AT-pair a weight of of 617.44, and a GC-pair a weight of 618.43. These weights exclude the water molecule removed during polymerization.

The total length of the Atlantic salmon (haploid) genome is 2 966 873 538 bp (Lien et al., 2016), of which 1 649 581 687 bp=A+T and 1 317 291 851 bp = G+C. The mass of each set of chromosomes equals the moles of dsDNA times the molecular weight of the dsDNA (mass of dsDNA = moles dsDNA (mol) x molecular weight of dsDNA)

Avogadro's number of molecules is one mole:

$$N_A = 6.0221408 * 10^{23} * \frac{1}{mol}$$

For simplicity, we regard the nuclei as containing two single copies (diploid) of 2 966 873 538 bp genomic DNA. So, the number of moles is:

$$n_{DNA} = \frac{2}{N_A} = 3.32 * 10^{-24} mol$$

Molecular weight of dsDNA = (number of base pairs of dsDNA x average molecular weight of a base pair) + n x 36.04 g/mol. The 36.04 g/mol accounts for the 2 -OH and 2 -H added back to the ends, and n is the number of chromosomes.

$$\begin{aligned} MW_{set_{chr}} = {} & (1\,317\,291\,851\ x\ 618.43) + (1\,649\,581\,687\ x\ 617.44) \\ & + 29\ x\ 36.04\ g/mol = 1.833170517x10^{12}\ g/mol\ (Daltons) \\ & = 183317051700.00\ g/mol. \end{aligned}$$

$$\begin{aligned} Mass_{DNA} &= 3.32 * 10^{-24} mol * 1.833170517 * 10^{12} \frac{\mathrm{g}}{\mathrm{mol}} = 6.086 * 10^{-12}\mathrm{g} \\ &= 6.086 * 10^{-3}\mathrm{ng} \end{aligned}$$

Example: For a sample of 2M nuclei, this corresponds to 12172 ng DNA in one sample. If the sample was 700µl, this corresponds to a DNA concentration of 0.012172 mg/0.7 ml = 0.017 mg/ml.

APPENDIX F: HIGH-SALT TREATMENT PROTOCOL

PREPARATIONS:

High-salt treatment solutions:

15% (w/v) Triton X-100 Permeabilization solution - *10ml:* 8 mL of deionized / Milli-Q water was added to a 15ml Falcon centrifuge tube. 4 mL of 3x HB, pH 6.6 was added to the tube and mixed by inversion to obtain 1x HB. *The volume to add was given by ([Solute in 1x HB]*0.012 L)/[Solute in 3x HB]= 0.004 L, where the respective solutes are Sucrose, NaCl, MgSO4, KH2PO4, CaCl2 and HEPES. The final 1x concentrations are 0.25 M Sucrose, 0.01 M NaCl, 0.001 M MgSO4, 0.001 M KH2PO4, 500 nM CaCl2 and approx. 0.003 M HEPES.* 1.5g of the full-strength Triton X-100 solution was dripped into another 15ml Falcon centrifuge tube (see comment). 8 ml of the obtained 1x HB above was added to the Triton X-100 tube. The tube was then put on an end-over-end mixer for minimum 30 minutes. After mixing, the volume was raised to the 10 ml mark with the 1x HB and mixed by inversion for 5 more minutes. The solution was stored at 2-8ºC for months. *Comment: Triton X-100 is very viscous, and a 15% TX-100 stock solution is made to make it easier to handle when diluting to working concentration.*

> ⚠**CRITICAL**: Some of the downstream processes are sensitive to hydrogen peroxide (e.g. the Fenton reaction), and the tube needs to be sealed properly to avoid excessive exposure to air as any ethylene oxide polymer can form trace peroxides on exposure to oxygen. Old bottles of Triton X-100 that have been opened many times should be avoided for the same reason. Avoid freezing.

Quencher-free high-salt solution – *50 ml:* 10 ml 3x HB, pH 6.6 was added to a 50 ml graduated beaker together with a stir bar, and placed on a stir plate and put on a low stir. 40 ml 5M NaCl was added to the beaker. *The volume to add was given by ((0.05 L)(4 mol/L))/(5 mol/L) = 0.04 L = 40 ml.* The solution was transferred to 9 appropriately labeled 5 ml tubes in aliquots of 5 ml stored at 2-8 ºC for months.

PROTOCOL:

Start:

For High-salt treatment: 15% Triton X-100 Permeabilization solution were gently mixed with the nuclei suspensions to a final concentration of 0.5% (see calculation 1#) before incubating for 15 minutes on ice. Quencher-free high-salt solution was added in a 1:1 volume ratio, mixed by gentle inversion and allowed to stay for 5 minutes before being directly processed with Hydroxyl Radical Footprinting.

Calculation:

1#: Based on a starting volume of 700 µl the volume to add was given by:

*(0.5%*700+X µl)/(15%)= X*, where *0.5% = 5/1000 = 1/200. 15% = 15/100 = 3/20.*

→ *((1/200)*700+X)/(3/20)= X*

→ *((1/200)*700+X = X*(3/20)*

→ *a(b+c)=ab+ac: (1/200)*700+(1/200)*X = X*(3/20)*

→ **200: (7/2)*200 + (1/200X)*200 = X*(3/20)*200*

→ *700 + X = 30X*

→ *X = 30X-700*

→ -30X: *X-30X = 30X-700-30X*

→ *-29X = -700*

→ *X = 700/29 = 24.1µl*

APPENDIX G: HYDROXYL RADICAL FOOTPRINTING PROTOCOL

PREPARATIONS:

HRF quenching solution – *10 ml*: 1 mL of deionized / Milli-Q water was added to a 10ml volumetric flask. The flask was placed on a weight and 3.0g (~2.5ml) of 100% Glycerol was added dropwise with a single use pipette (see note) and twirled. 2.867 ml 3x HB was added to a 15ml Falcon centrifuge tube. 2.133 ml deionized / Milli-Q water was added to the latter tube and mixed by inversion. *The volume to add was given by ([Solute in 1.72x HB]*0.005 L)/[Solute in 3x HB]= 0,002867 L, where the respective solutes are Sucrose, NaCl, MgSO4, KH2PO4, CaCl2 and HEPES. The final 1.72x concentrations are 0.43 M Sucrose, 0.0172 M NaCl, 0.00172 M MgSO4, 0.00172 M KH2PO4, 860 nM CaCl2 and approx. 0.005 M HEPES.* The obtained 1.72x HB above was used to raise the volume in the glycerol-containing flask to the 10ml mark. The solution was transferred to an appropriately labeled container stored at 2-8ºC for a few weeks. *Note: When pipetting glycerol, use ethanol sterilized scissors to cut the end of a pipette to make pipetting easier.*

SAME DAY:

Solutions:

The following solutions were prepared in the order they are written for efficiency:

1x HRF Homogenization Buffer, pH 6.7 (1x HRF HB) – *12ml:* 8 mL of deionized / Milli-Q water was added to a 15ml Falcon tube on ice. 4 mL of 3x HB, pH 6.6 was added to the tube, and mixed by inversion. *The volume was given by ([Solute in 1x HB]*0.012 L)/[Solute in 3x HB]= 0.004 L, where the respective solutes are Sucrose, NaCl, MgSO4, KH2PO4, CaCl2 and HEPES. The final 1x concentrations are 0.25 M Sucrose, 0.01 M NaCl, 0.001 M MgSO4, 0.001 M KH2PO4, 500 nM CaCl2 and approx. 0.003 M HEPES.* The solution was stored on ice until use.

10 mM Sodium ascorbate [$C_6H_7NaO_6$. Synonyms: (+)-Sodium L-ascorbate, L(+)-Ascorbic acid sodium salt, Vitamin C sodium salt. CAS Number: 134-03-2. Molecular Weight: 198.11 g/mol] solution – 5 *ml:* 10 **mg** sodium ascorbate was weighed out in a tared weighing boat and rinsed into a 5ml SnapCap centrifuge tube labelled "SA" using 5 ml 1x HRF HB. *The amount to weigh was given by (0.01 mol/L)(0.005 L)(198.11 g/mol) = 0.0099g.* The solution was wrapped in aluminum foil and stored on ice until use.

⚠**CRITICAL:** The sodium ascorbate solution is light sensitive.

40mM Hydrogen peroxide [H_2O_2. CAS Number: 7722-84-1. Molecular Weight: 34.01 g/mol. Molarity: 9.8] solution – *0.5 ml:* 498µl 1x HRF HB was added to a 2 ml Eppendorf LoBind tube labelled "H2O2". 2 **µl** of 30% w/w H2O2 was pipetted into the tubed and mixed by inversion. *The volume to pipette was simply a dilution by a factor of ~250 (9.8/250=0.0392M).* The solution was stored on ice until use.

PROTOCOL:

Start:

Two tubes with 1× Fe(II)-EDTA stock solution was collected from the freezer to thaw. The nuclei suspensions were gently mixed with a p1000 pipette. To calculate the amount of HRF reactants to add for a 0.75X HRF reaction, the volume in each of the tubes were divided by 15 to get X (see calculation 0#). To each tube the following volumes were added quickly:

X * 1.5µl Fe(II)-EDTA

X * 1.5µl H2O2

X * 2µl Sodium Ascorbate

The tubes were mixed by gentle inversion before a quick spin down, and allowed to stay for 1h at 4°C. The HRF reaction was quenched by adding 2.5µl * Y (see calculation 2#) of the HRF quenching solution (6 w/v% glycerol final conc.) (see comment) to each tube and mixed by inversion (see calculation 3#).

Comment:

If subsequent electrophoresis was performed, 30% w/v Glycerol Sample loading solution, Tris-Glycine for SDS-PAGE, **OR** Lithium for BN-AGE, was used instead to avoid dilution of the sample before loading the gel as they contain CBB.

Protocol specific calculations:

Example calculations for a tube with 700µl starting volume:

0#: X = 700/15=46.67

1#: 700 + X*5 = 933.33µl

2#: Y = #1/10 = 93.33

3#: 2#*2.5 = 233.33µl.

APPENDIX H: SDS-PAGE PROTOCOL

PREPARATIONS:

Electrophoresis loading solution:

30% w/v Glycerol Sample loading solution Tris-Glycine – *10ml:* 1 mL of deionized / Milli-Q water was added to a 10ml volumetric flask. The flask was placed on a weight and 3.0g (~2.5ml) of 100% Glycerol was added dropwise with a single use pipette (see note) and twirled. The following volumes of reagents was added to the flask:

Reagent	**Final Conc.**	**Fold Dilution (x)**	**Vol for 10 mL (µl)** *(divide volumes by 1000 to get mL)*
CBB 10%	0.5%	20	500
Tris 2M	25mM (0.025M)	80	125

Glycine 2M	19.2mM (0.0192M)	104.17	96
Total:	-	-	721

The volume was raised with 2ml deionized / Milli-Q water and twirled, repeating until the 10ml mark. The solution was transferred to an appropriately labeled container stored at 2-8ºC for a few weeks. *Note: When pipetting glycerol, use ethanol sterilized scissors to cut the end of a pipette to make pipetting easier.*

PROTOCOL:

Start:

From untreated, high-salt treated, frozen OR supercooled nuclei subjected to 0.75X HRF for 1h at 4ºC and quenched with 30% w/v Glycerol Sample loading solution Tris-Glycine containing CBB:

The stained lysates were filtered through 0.22µm low-binding Durapore PVDF membranes (2-ml Ultrafree®-CL) by centrifuging the samples at 250 RCF for 6 minutes. The largest filtered volume was collected in a tube labelled filtrate (FIL) and the smaller volume retained by the membrane was collected in a tube labelled retentate (RET).

10µl of the samples were loaded in a precast 15-well (15 µl), 4–15% Mini-PROTEAN® TGX Stain-Free™ Protein Gel (see comment 1#). In addition to the samples, 2µl Precision Plus Protein™ Kaleidoscope™ Prestained Protein Standards were included in one well (see comment 2#). The loaded polyacrylamide gel was placed in a Mini-PROTEAN Electrophoresis Cell and the SDS-PAGE was run at 300V, for 37min using 10x premixed Tris/Glycine/SDS electrophoresis buffer diluted with water to 1x (i.e. 25 mM Tris, 192 mM glycine, 0.1% SDS, pH 8.3) in the vertical electrophoresis chamber. After electrophoresis the gel was removed from the cast and examined with a ChemiDoc™ imaging system and analyzed with the built-in settings for the Stain-free system in the Image Lab™ software.

Comments:

1#: The normal sample loading scheme (provided in the kit) for Mini-PROTEAN® TGX Stain-Free™ Protein Gel was not followed. The reason for this was because the highly denaturing environment from the addition of 2x Laemmli sample buffer and β-mercaptoethanol to the samples are believed to significantly reduce the various non-covalent attractive forces, like ionic interactions, through which CBB is linked to the stained proteins. The same problem applies to heating the samples at 90-100ºC for 5 min before loading. By

omitting these steps, it is possible that some proteins will be in complexes resulting in size distributions not representative for the nuclear proteome. However, the purpose was to see if prior sample treatments resulted in any potential differences in size distributions of proteins in the FIL/RET, and these samples were loaded identical.

2#: This is a mixture of ten multicolor recombinant proteins with sizes ranging from 10–250 kD, which is the size range 90% of proteins in most organisms are in (Bio-Rad (A)).

APPENDIX I: BN-AGE PROTOCOL

PREPARATIONS:

Electrophoresis solutions tested:

Tris-Glycine electrophoresis running solution*, pH 7.0 – *2L:* 1.0 L deionized/Milli-Q water stored at 4°C was added to a 2.5 L graduated beaker. A large stir bar was added, and the beaker was put on low stirring. The following volumes of reagents was added to the beaker:

Reagent	**Final Conc.**	**Fold Dilution (x)**	**Vol for 2000 mL (µl)** *(divide volumes by 1000 to get mL)*
Tris 2M	25mM (0.025M)	80	25000
Glycine 2M	19.2mM (0.0192M)	104.17	19200
Total:	-	-	44200

The pH of the solution was measured at 4°C. The pH of the solution was adjusted to pH 7.0 (see comment) with cold undiluted HCl. Once the pH of the solutions was correct, the volume was raised to the 2.0 L mark with deionized / Milli-Q water. The solution was sterile-filtered before transferring it to an appropriately labeled container stored at 2-8ºC for a few weeks. **At pH 7.0 this solution will not have significant buffering capacity to prevent pH changes during electrophoresis, i.e., not a buffer.*

5 mM Lithium Acetate electrophoresis running solution, pH 6.6 – *2L:* 1.75 L deionized/Milli-Q water stored at 4°C was added to a 2.5 L graduated beaker. A large stir bar was added, and the beaker was put on low stirring. 31.9 mL Lithium Regeneration Buffer 6* stored at 4°C was added to the beaker while measuring the pH (close to 4°C) (see calculations). The pH was adjusted to pH 6.6 with cold undiluted glacial acetic acid (~500µl). This creates the following reaction: Acetic Acid + Lithium Hydroxide = Water + Lithium Acetate. Once the pH of the solution was correct, the volume was raised to the 2.0 L mark

with deionized / Milli-Q water. The solution was sterile-filtered before transferring it to an appropriately labeled container stored at 2-8ºC for a few weeks.* While Lithium hydroxide monohydrate is equally or better suited for the purpose, due to lack of availability it was necessary to use an alternative source for Lithium hydroxide in the form of *BIOCHROM Lithium Regeneration Buffer 6,* 1.3 w/w% $LiOH \cdot H_2O$ (Biochrom Ltd, 2020).

30% w/v Glycerol Sample loading solution Lithium – *10ml:* 1 mL of deionized / Milli-Q water was added to a 10ml volumetric flask. The flask was placed on a weight and 3.0g (~2.5ml) of 100% Glycerol was added dropwise with a single use pipette (see note) and twirled. 500µl CBB 10% was added to the flask. The volume was raised to the 10ml mark with 5 mM Lithium Acetate. The solution was transferred to an appropriately labeled container stored at 2-8 ºC for a few weeks. *Note: When pipetting glycerol, use ethanol sterilized scissors to cut the end of a pipette to make pipetting easier.*

Calculations:

Molar mass of Lithium Hydroxide Monohydrate ($LiOH \cdot H_2O$) = 6.941 Li (1*6.941) + 31.998 O (2*15.999) + 3.024 H (3*1.008) = **41.963**.

In 1000 g of solution, $LiOH \cdot H_2O$ is 13 g (1.3 w/w%) and H2O is 987 g (98.7 w/w%).

13(g)/41.963(g/mol) = **0.310 moles.**

From this we can get the molality, i.e., the amount of substance (in moles) divided by the mass (in kg) of the solvent:

0.310 moles/0.987g = **0.314 moles/kg solvent** (water), i.e., moles solute.

We want to get the molarity, i.e., the amount of substance (in moles) divided by the volume (in litres) of the solution, mol/L (M). The relative density of the BIOCHROM Lithium Regeneration Buffer 6 is 1.009g/mL (Biochrom Ltd, 2020). We can calculate the molarity as follows (assuming 1 kg of solvent (water)):

1. The total mass of $LiOH \cdot H_2O$ (solute) is given by: *(0.314 moles solute)*(41.963 g/mole) = 13.17 g $LiOH \cdot H_2O$.*

2. The total weight of the solution in grams is given by: *(1000 g solvent (water)) + (13.17 g $LiOH \cdot H_2O$) = 1013.17 g solution.*

3. The volume of the solution in liters is given by: *(1013.17 g)*(1mL/1.009 g (density)) = 1.004 mL = 1.004 L.*

4. The molarity is then calculated by: *(0.314 moles solute)/(1.004 L) =* ***0.313 M*** *$LiOH \cdot H_2O$.* This equals **313 mM Li^+**, since lithium hydroxide is a strong base and thus will dissociate completely in water: $LiOH \rightleftharpoons Li^+ + OH^-$

To dilute the solution to 5 mM (0.005 M), in 2L final volume, the amount to dilute is given by (0.005 mol/L *2 L)/0.313 mol/L = 0.0319 L = **31.9 mL**.

Agarose gel:

A 0.3% Agarose (AG) gel was prepared by weighing out 0.3g AG [Low EEO Agarose. Synonym(s): 3,6-Anhydro-α-L-galacto-β-D-galactan, Agarose LE. CAS No.: 9012-36-6] in a tared weighing boat. The AG was rinsed into an Erlenmeyer flask (150ml) with 100ml 5 mM Lithium Acetate electrophoresis running solution **OR** Tris-Glycine electrophoresis running solution (testing). The flask was weighed, and the agarose solution was pulse-microwaved until all the agarose was dissolved. The flask was weighted again, and the evaporated liquid was replaced with deionized water. When the solution had cooled to about 60°C, the solution was poured into a pre-assembled gel casting tray with a comb, ensuring that no bubbles were present. The gel was allowed to stay for 30 minutes in room temperature to set.

PROTOCOL:

Start:

From untreated and supercooled nuclei subjected to 0.75X HRF for 1h at 4°C and quenched with 30% w/v Glycerol Sample loading solution Lithium containing CBB: The stained lysates were filtered through 0.22µm low-binding Durapore PVDF membranes (2-ml Ultrafree®-CL) by centrifuging the samples at 250 RCF for 6 minutes. The largest filtered volume was collected in a tube labelled filtrate (FIL) and the smaller volume retained by the membrane was collected in a tube labelled retentate (RET). The comb was removed from the gel cast, and the 0.3% agarose gel was transferred to an electrophoresis chamber and 5 mM Lithium Acetate electrophoresis running solution **OR** Tris-Glycine electrophoresis running solution (for testing) was filled to barely submerge the gel. 5µl from each of the sample's FIL/RET fractions were loaded in individual wells. The electrophoresis was run at 300V for 45 minutes at room temperature. After electrophoresis the gel was examined with a ChemiDoc™ imaging system and analyzed with the built-in settings for CBB staining in the Image Lab™ software.

APPENDIX J: HYPO-OSMOTIC RELATIVE SIZE CHANGE

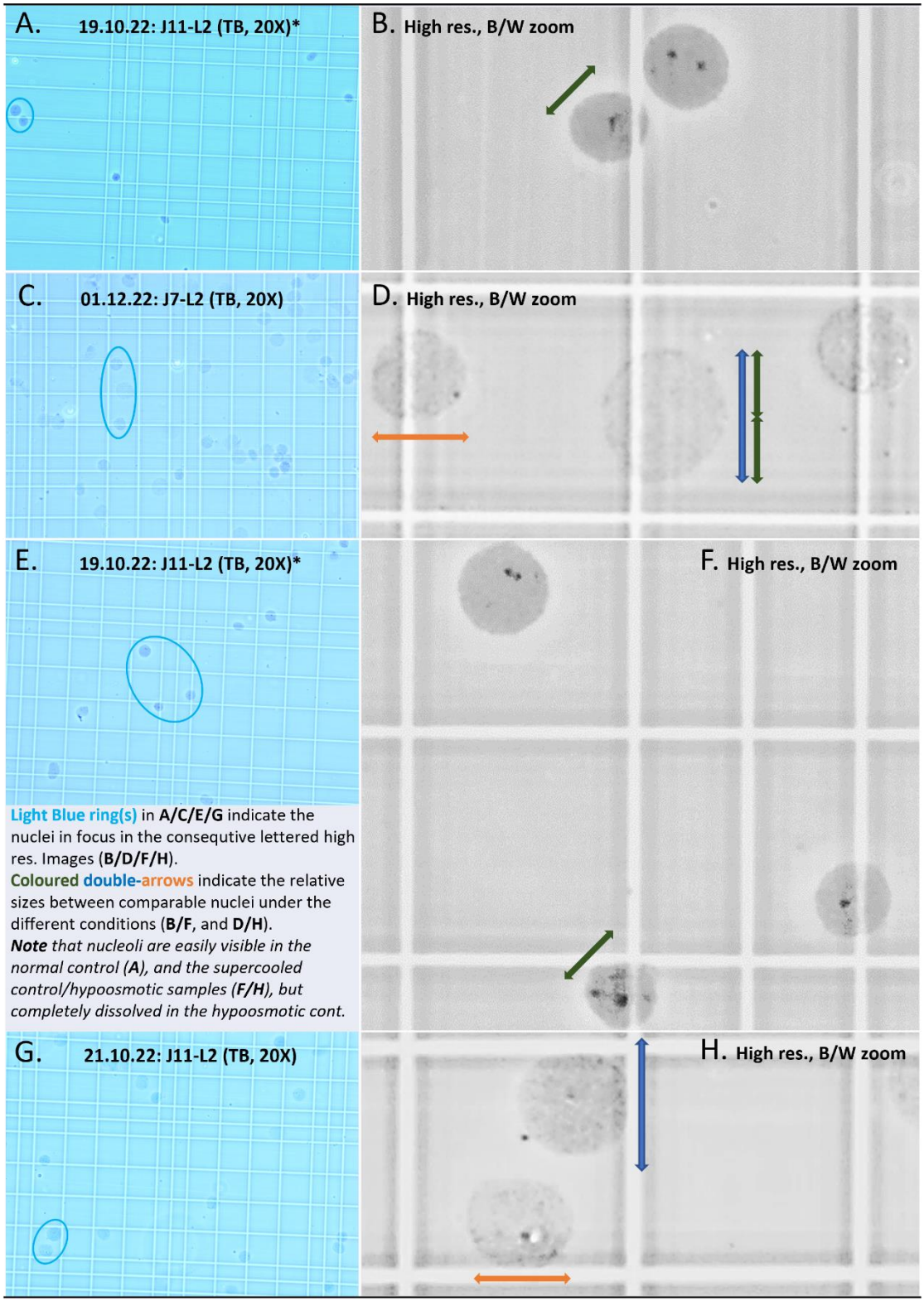

Figure J1 | Micrograph of Trypan blue stained nuclei isolated with the final protocol. **nuclei are still moving into the grid, thus the apparent yield is an underestimate.* ***A/B****: Untreated (UT) nuclei after <30 sec in dilute condition (normal control),* ***C/D****: UT nuclei after >15 min in dilute condition (hypoosmotic control),* ***E/F****: Supercooled (SC) nuclei after <30 sec in dil. Cond. (SC control),* ***G/H****: SC nuclei after >15min in dil. cond.*

APPENDIX K: GLUTARALDEHYDE FIXATION PATTERN

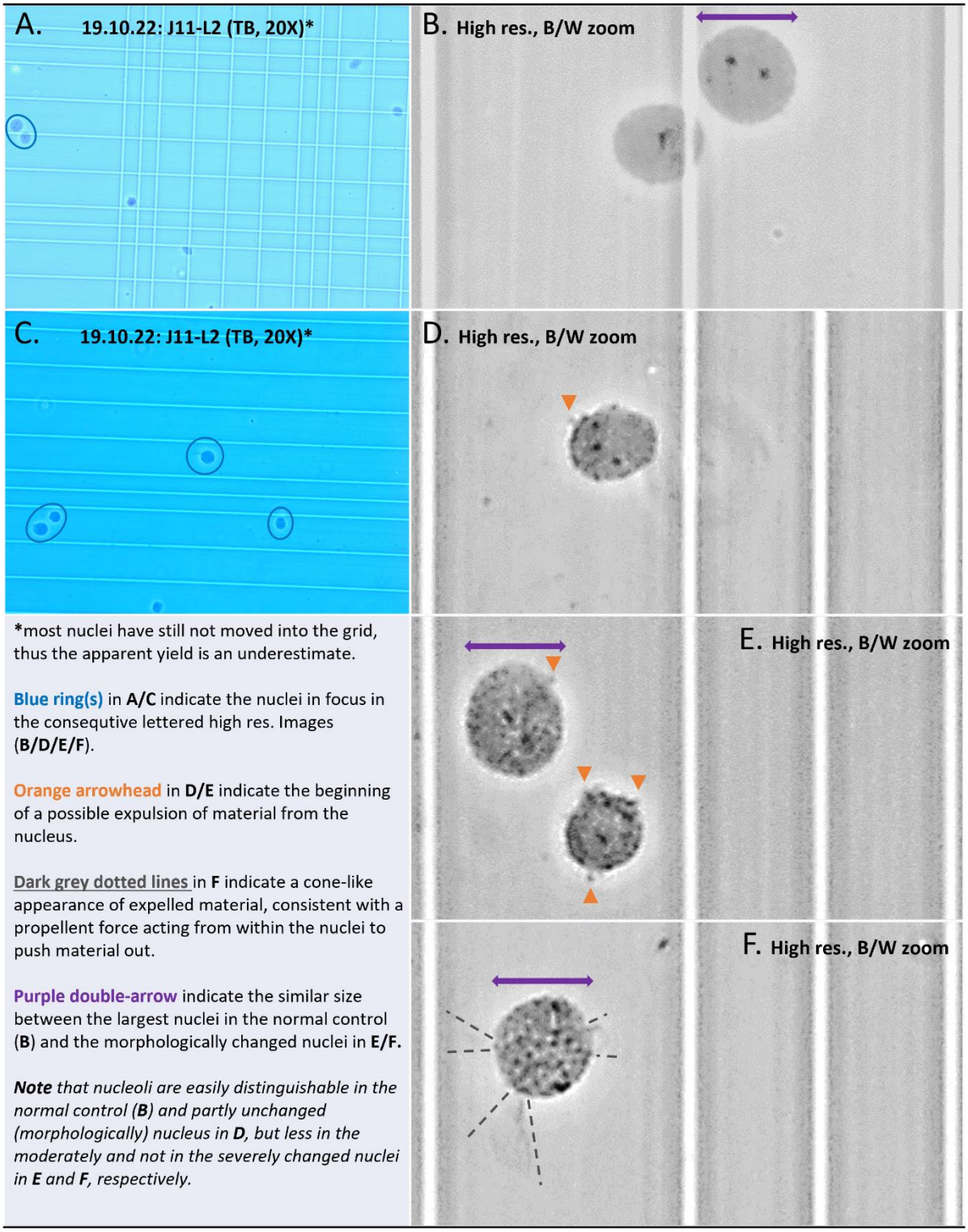

Figure K1 | Micrograph of Trypan blue stained nuclei isolated with the final protocol. A/B*: Untreated nuclei after <30 seconds in dilute condition (normal control),* ***C/D/E/F****: Nuclei treated with 0.3% glutaraldehyde for 1h 30min, pictures taken after <30 seconds in dilute condition.*

APPENDIX L: IMPROVEMENTS FOR FURTHER INVESTIGATIONS

In retrospective, several improvements to the experiments run in this thesis could be done, including redoing experiments to achieve more replicates of important results, together with more controls. Right before the submission of this manuscript, I was made aware of several tools that could be used to reduce subjectivity of many of observations and increase reproducibility of some of the in-lab parameters.

1. The self-made cooling chamber is probably difficult to reproduce exactly and could be a crucial parameter. In contrast, Thermo Scientific™ Mr. Frosty™ Freezing Containers are common in many labs dealing with cell preservation. Although a cooling rate of ~0.5°C/minute was found to be the most optimal and prevented ice formation in my tests, the standardized Mr. Frosty™ Freezing Containers report a rate of cooling very close to -1°C/minute (common for many cryopreservation procedures; Kratochvílová et al., 2018) which could be tested. In addition, they have a much larger capacity (12 to 18 tubes from 1 to 5 mL) than the 4 tubes up to 2 ml in the self-made cooling chamber of mine.
2. Trypan blue is commonly used to differentiate live and dead cells, not to explore nuclei integrity or shape/size of nucleoli. If one is interested in looking at effects on nucleoli, then a more appropriate stain for this could be Enzo Life Sciences' NUCLEOLAR-ID® Green detection kit.
3. Trough Galaxy (galaxyproject.org), a tool named CellProfiler can analyze nuclei pictures and detect both nucleoli and debris to give more objective quality, yield and purity assessments. Measure of the nuclei diameter or evaluation of the density of the chromatin inside the nuclei are likely also possible.

END

Thanks to everyone working at the Center for Integrative Genetics (CIGENE) for facilitating and making room for me in the laboratory to conduct the experiments in this thesis. I want to thank my supervisors, Dr. Marie-Odile Baudement and Associate professor Matthew Peter Kent for their support in the lab and feedback during the writing process. I would also like to direct a special thanks to Kristil Kindem Sundsaasen and Terese Andersstuen for invaluable help with locating and replenishing chemicals and equipment. You always made time for even the strangest chemical or material requests, and I appreciate that and your positive attitude.

Magnus B. Skulberg

Norges miljø- og biovitenskapelige universitet
Noregs miljø- og biovitskapelege universitet
Norwegian University of Life Sciences

Postboks 5003
NO-1432 Ås
Norway